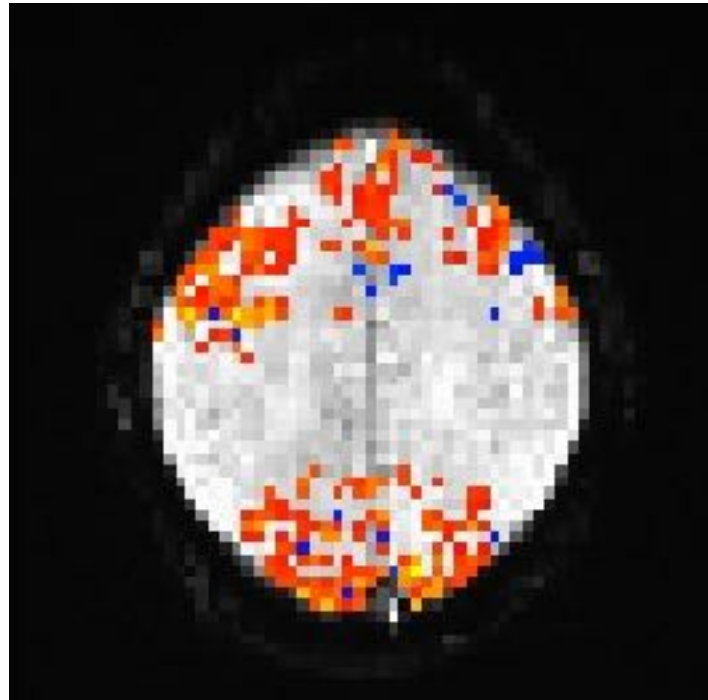


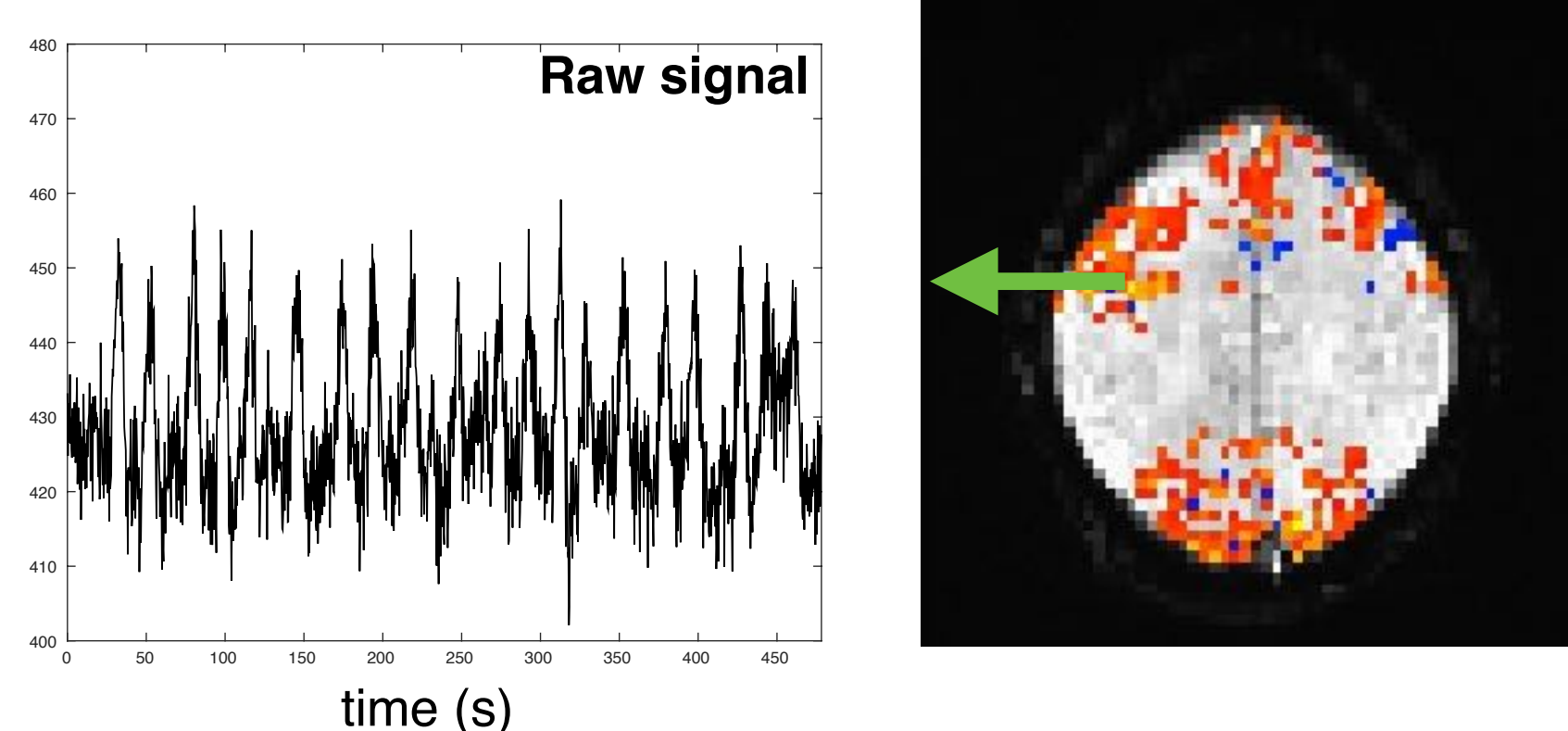
Overview of noise and denoising methods in BOLD fMRI

César Caballero Gaudes, PhD.
Basque Center of Cognition, Brain and Language
San Sebastian - Donostia, Spain
c.caballero@bcbl.eu

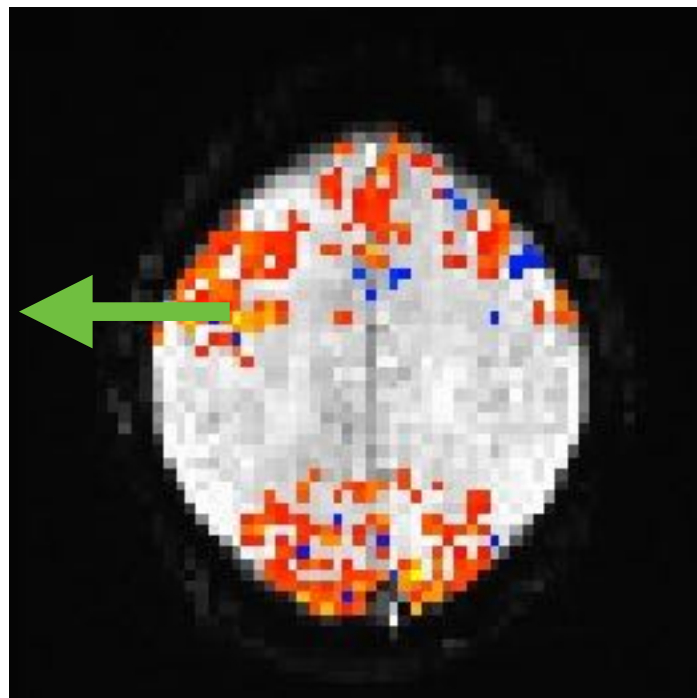
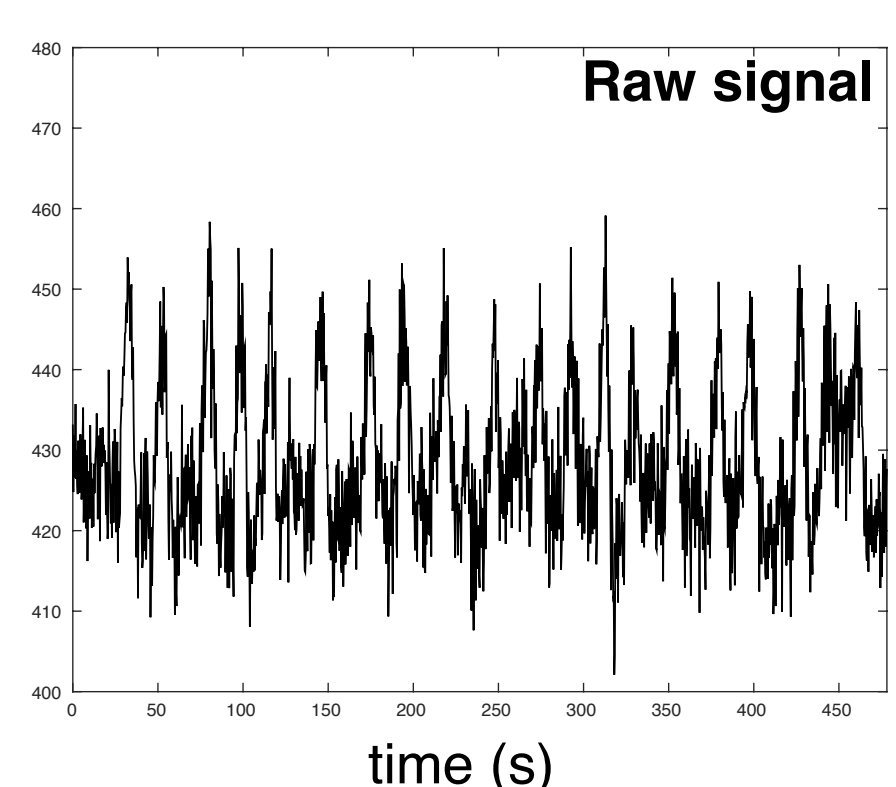
Introduction: Task-based fMRI



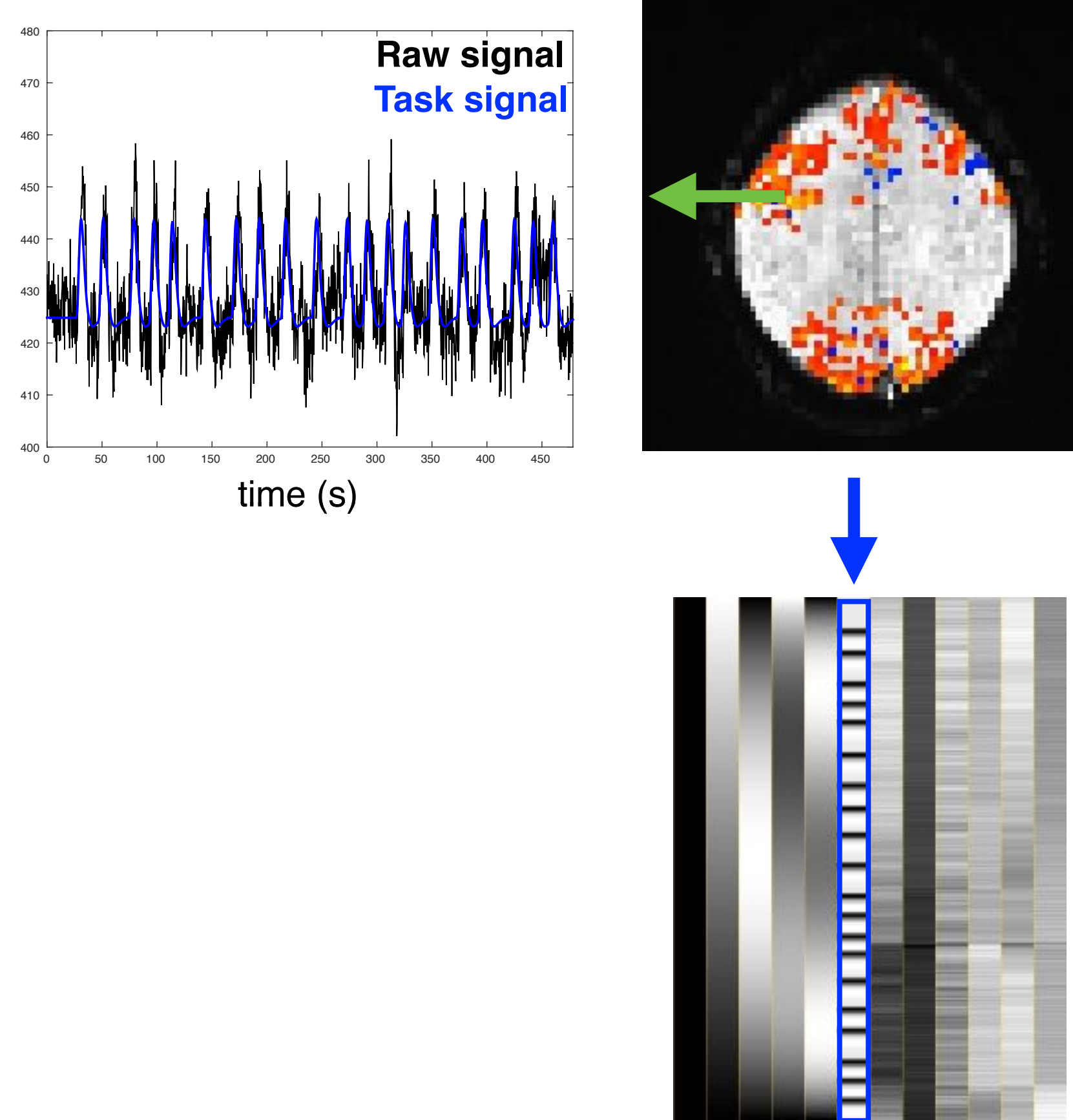
Introduction: Task-based fMRI



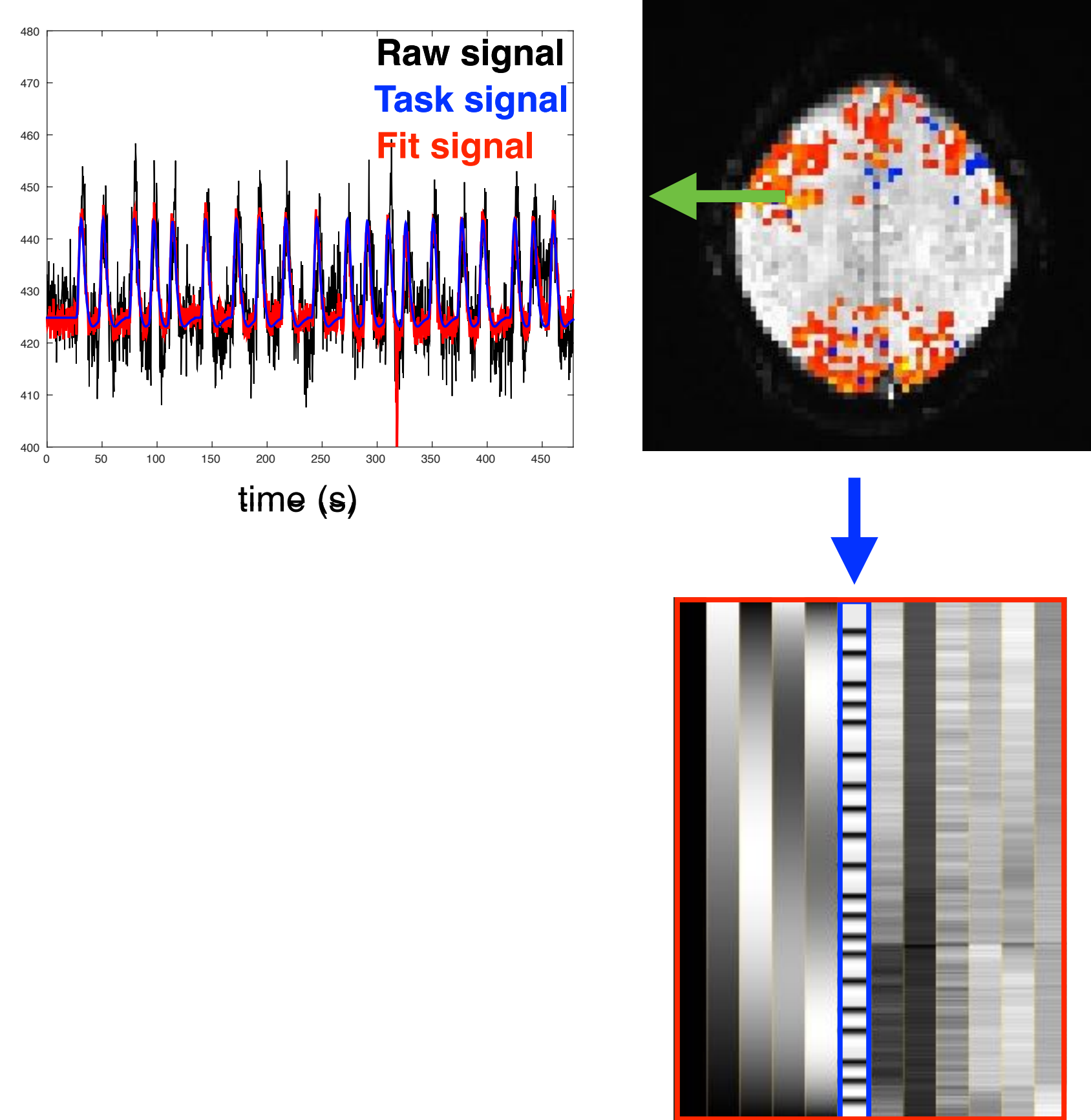
Introduction: Task-based fMRI



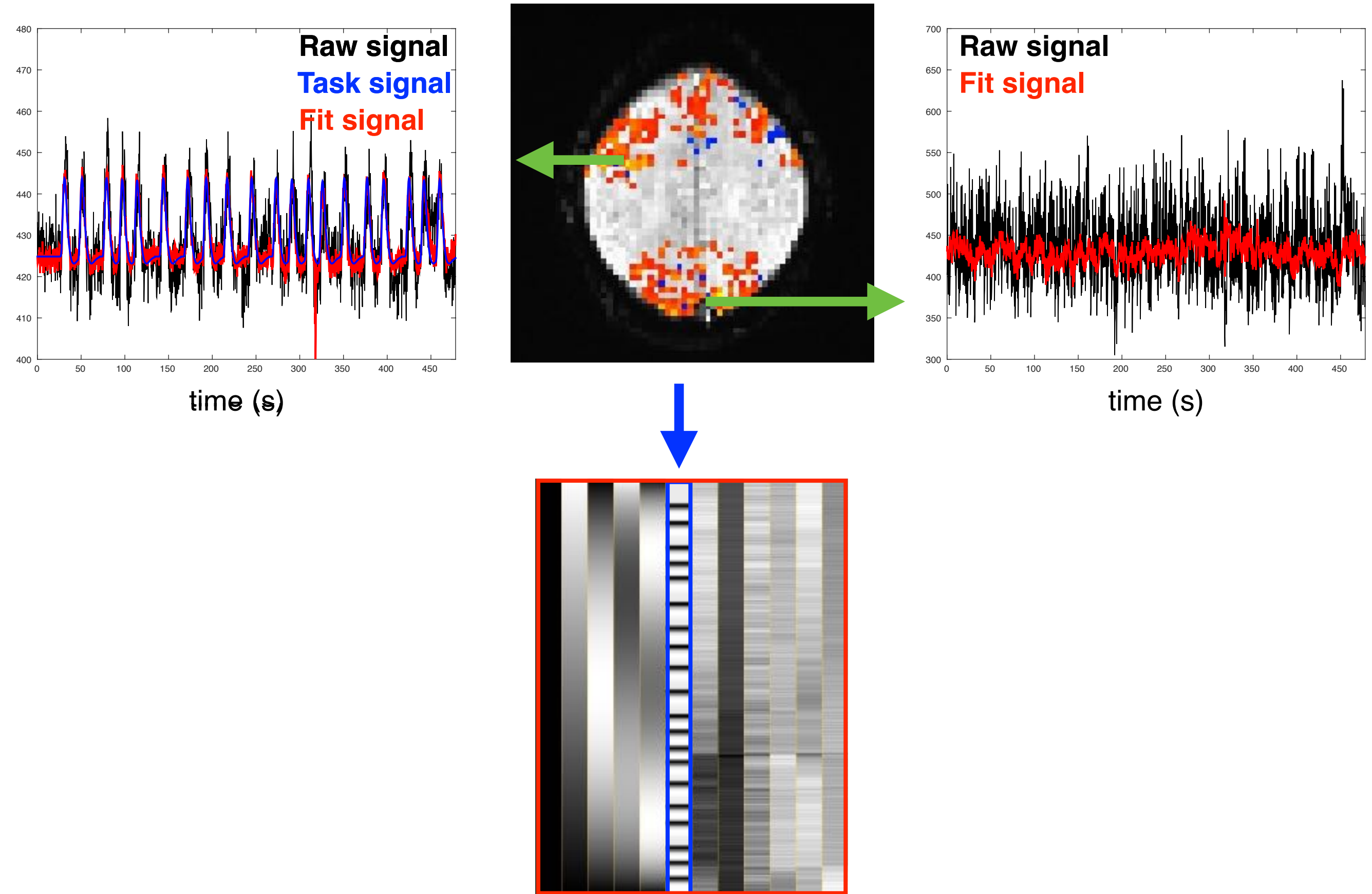
Introduction: Task-based fMRI



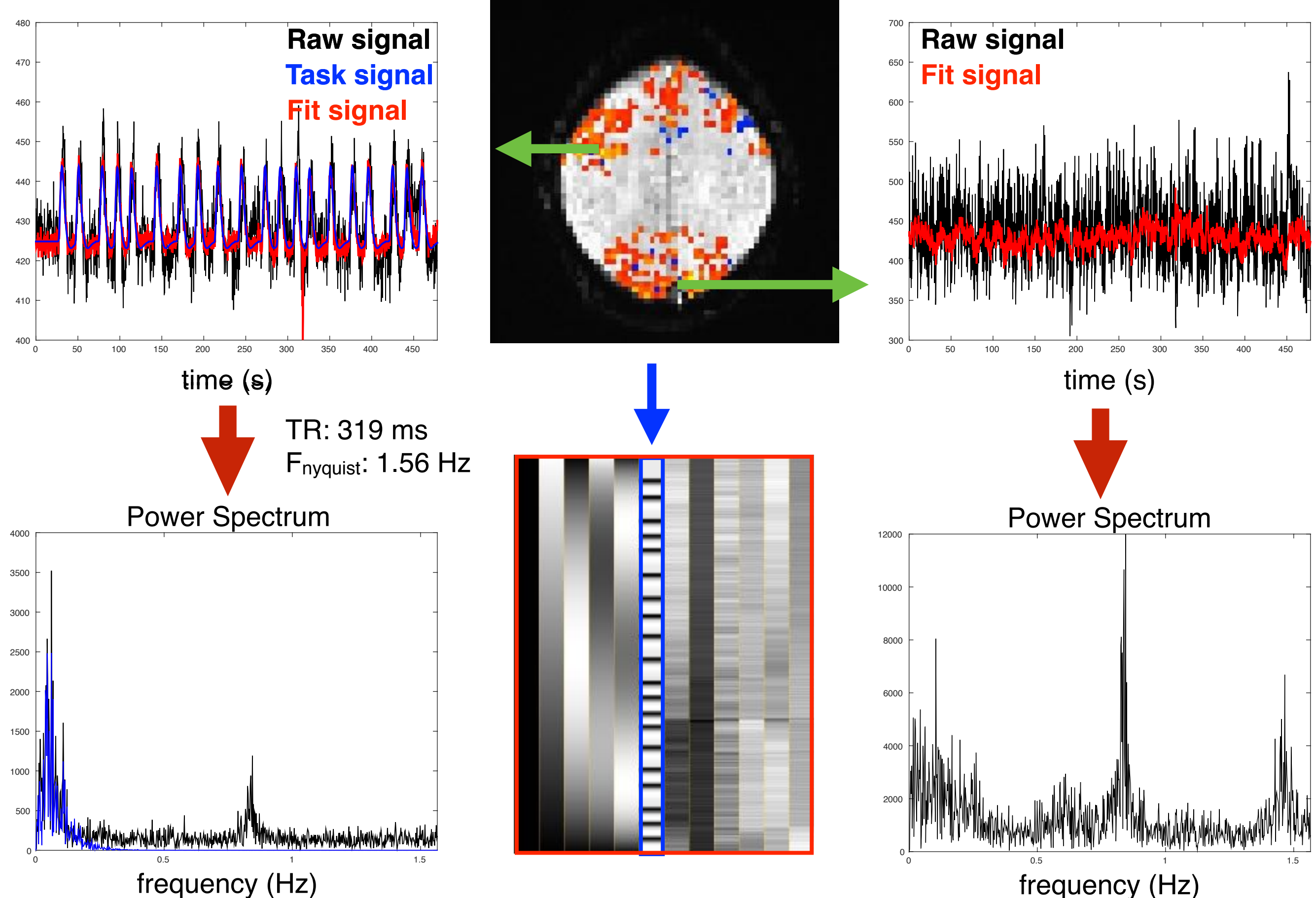
Introduction: Task-based fMRI



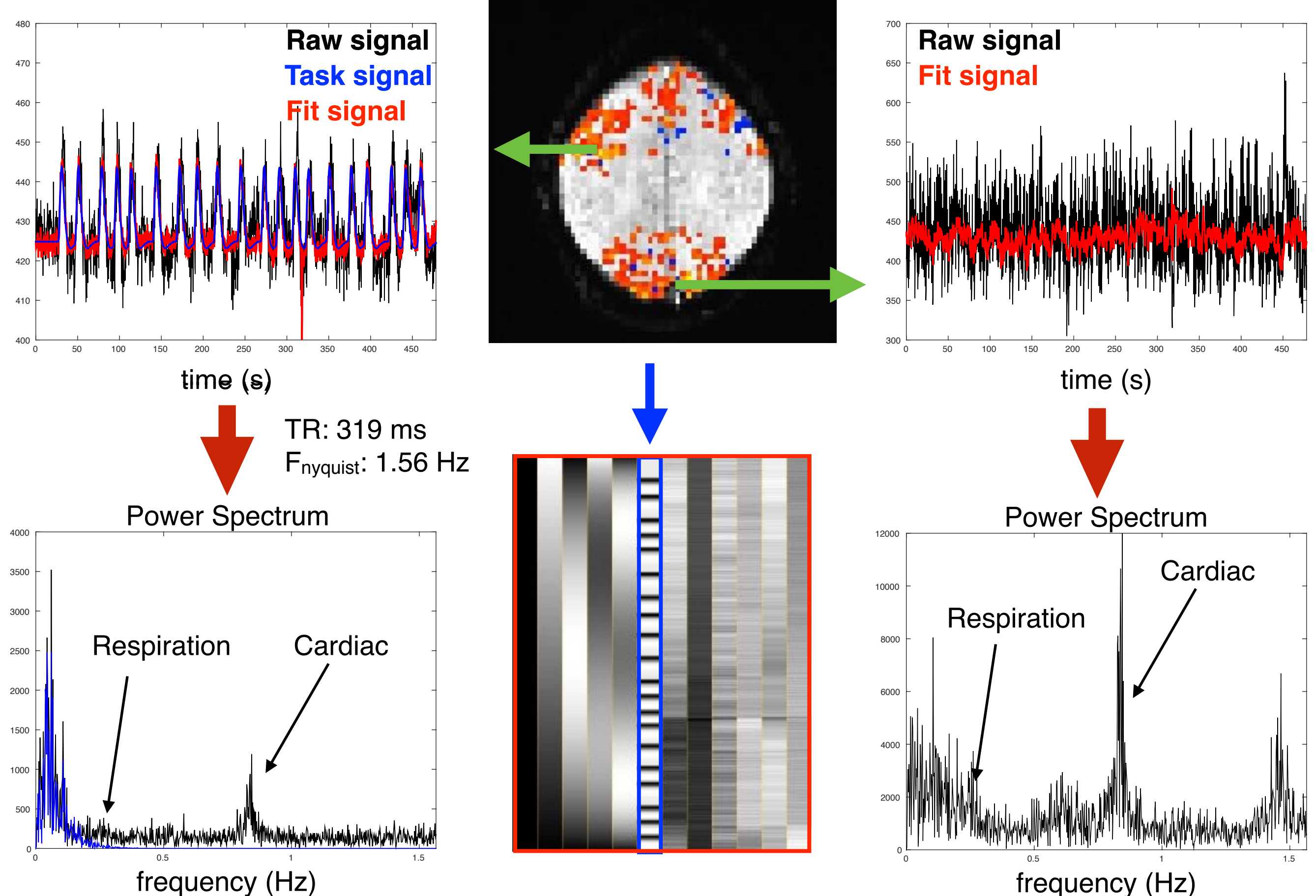
Introduction: Task-based fMRI



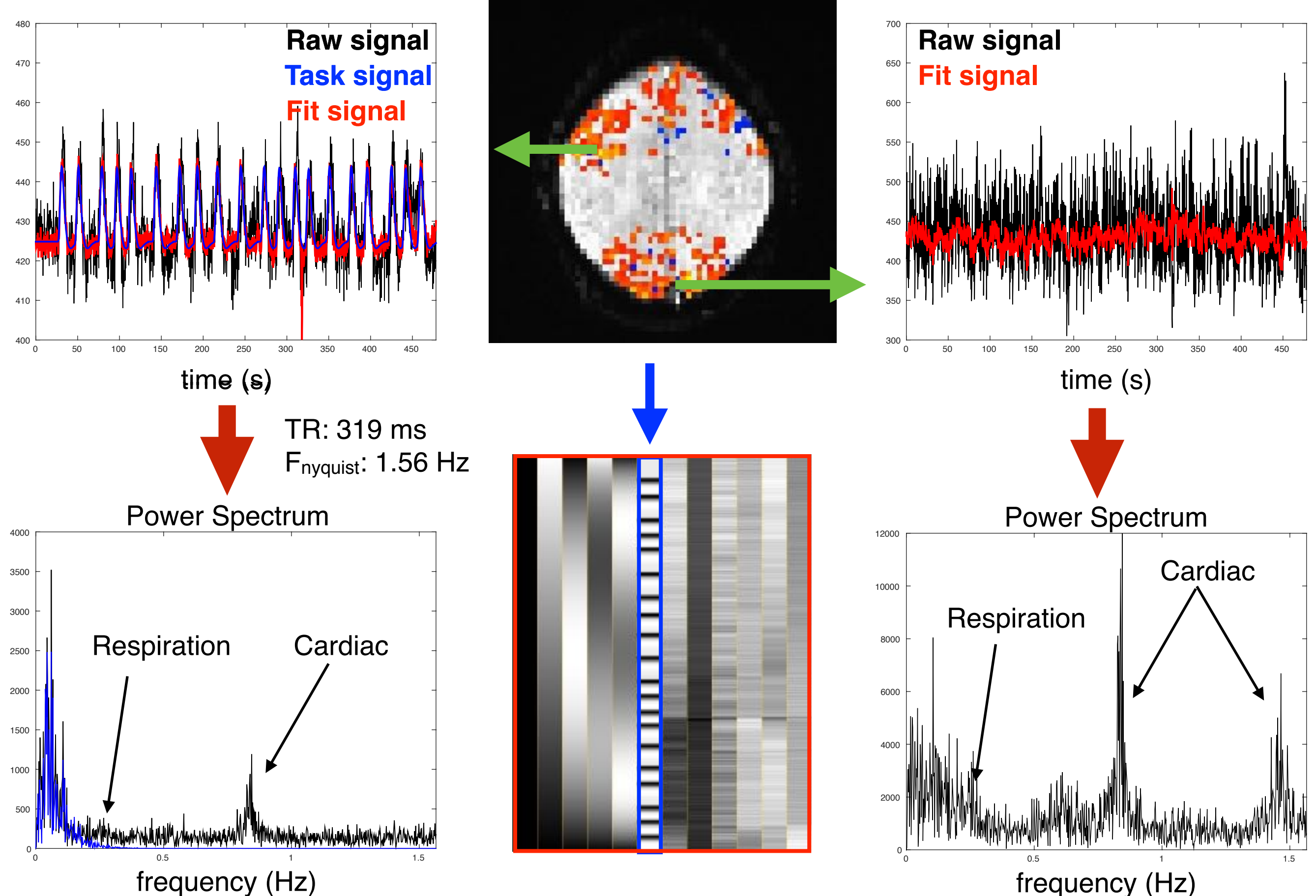
Introduction: Task-based fMRI



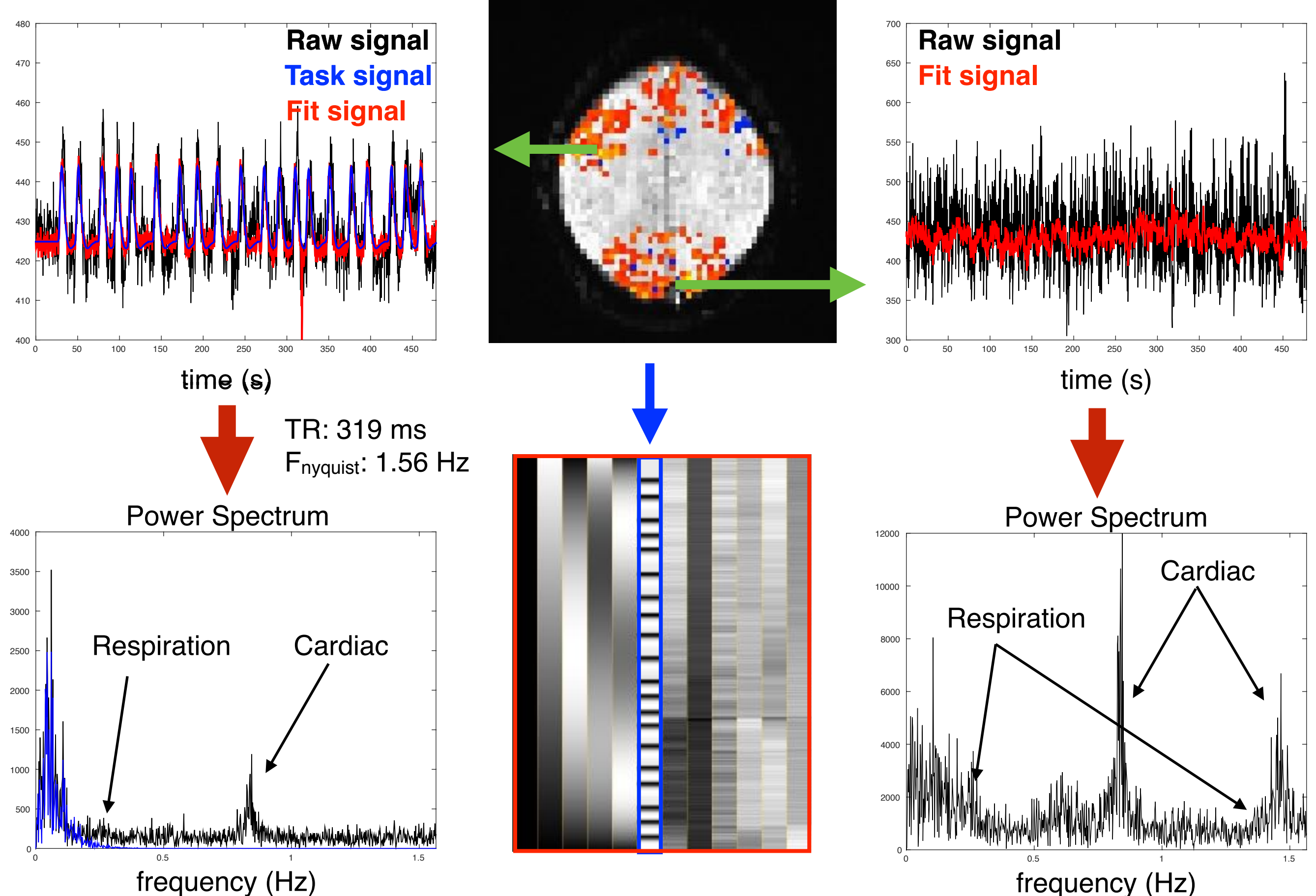
Introduction: Task-based fMRI



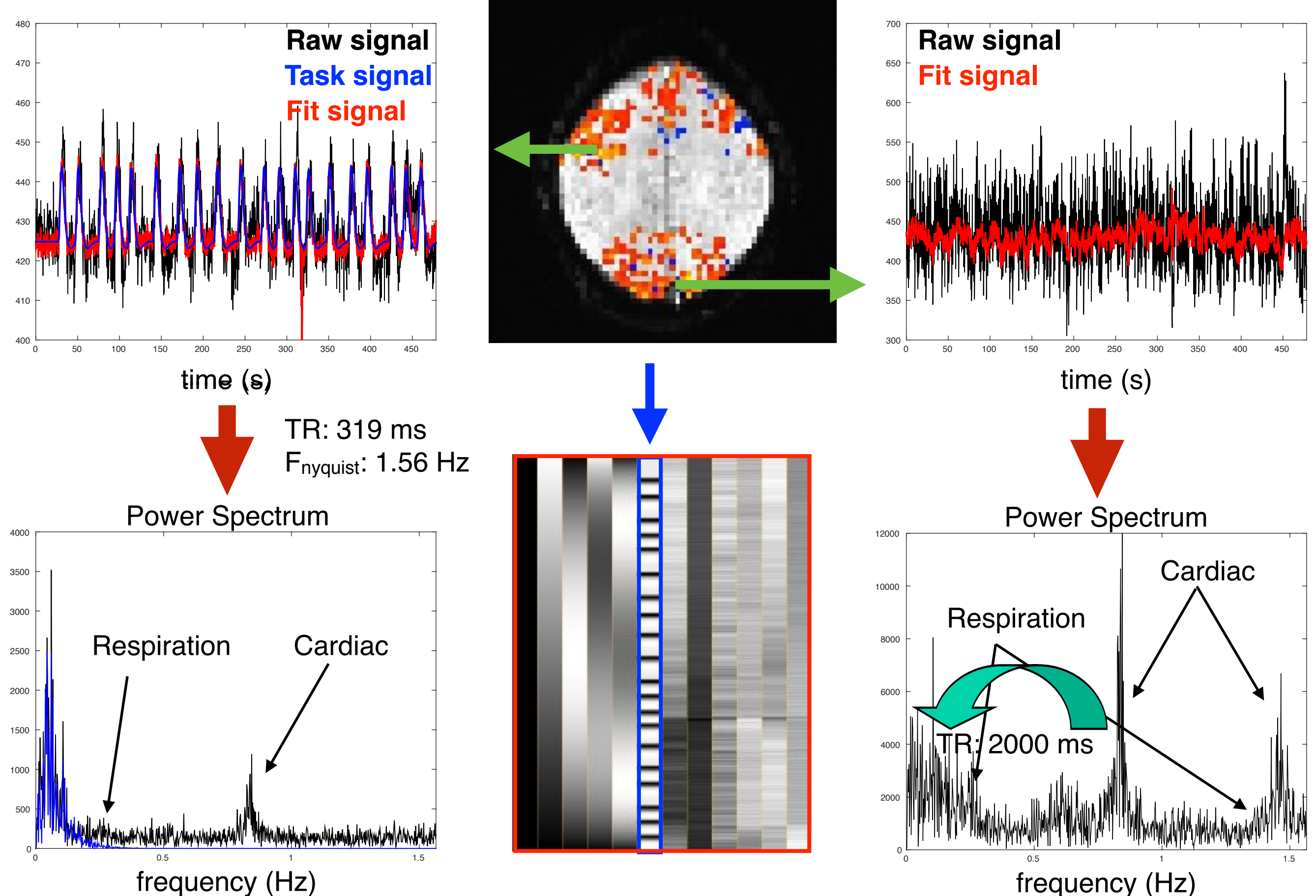
Introduction: Task-based fMRI



Introduction: Task-based fMRI

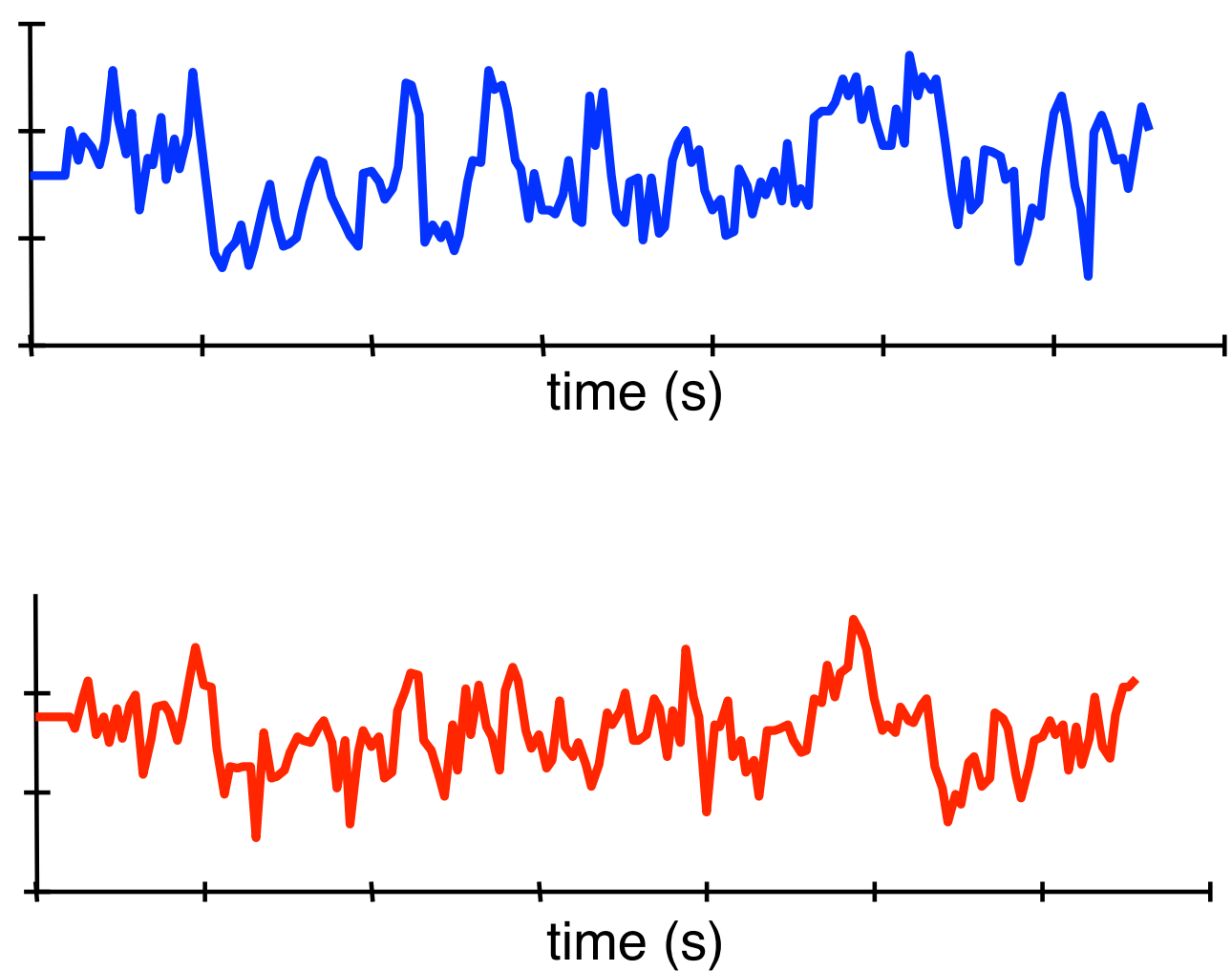
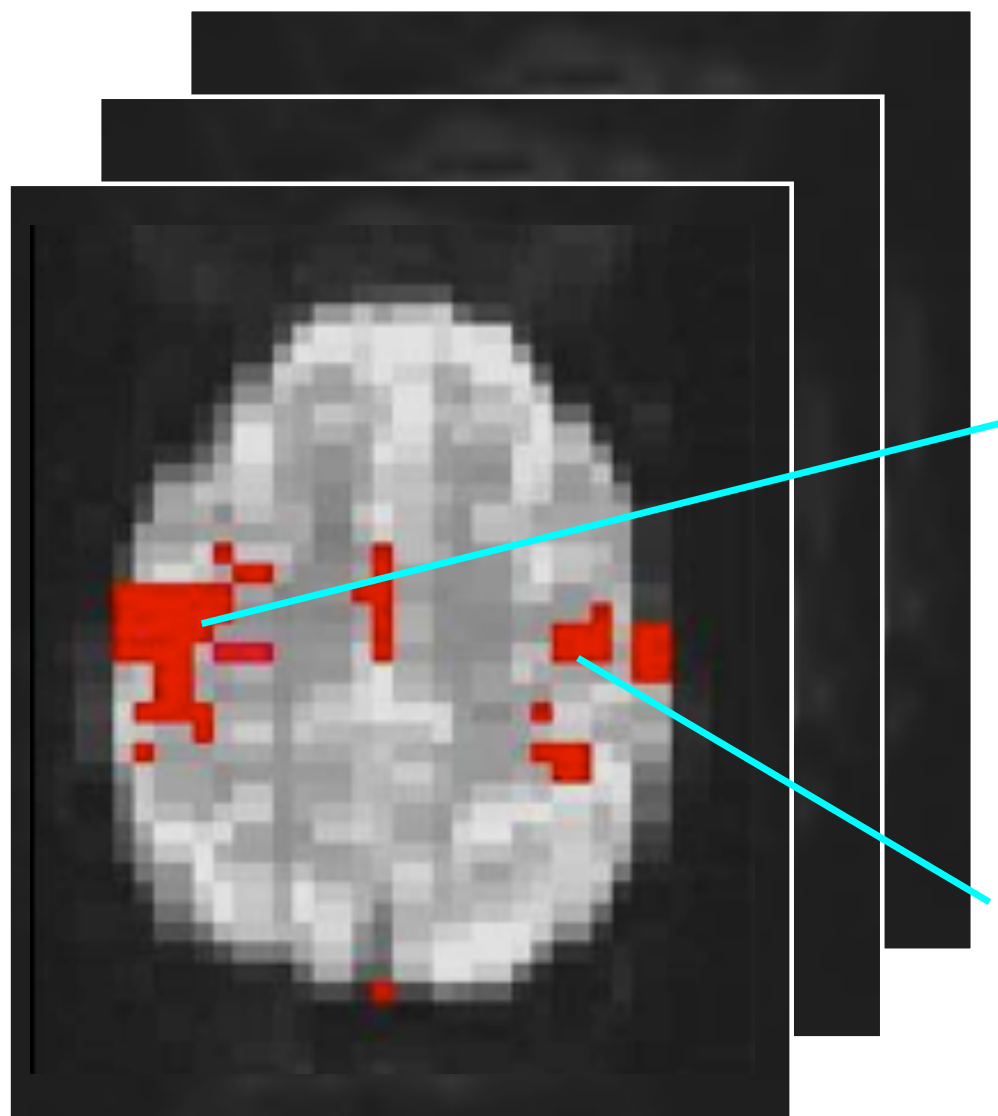


Introduction: Task-based fMRI



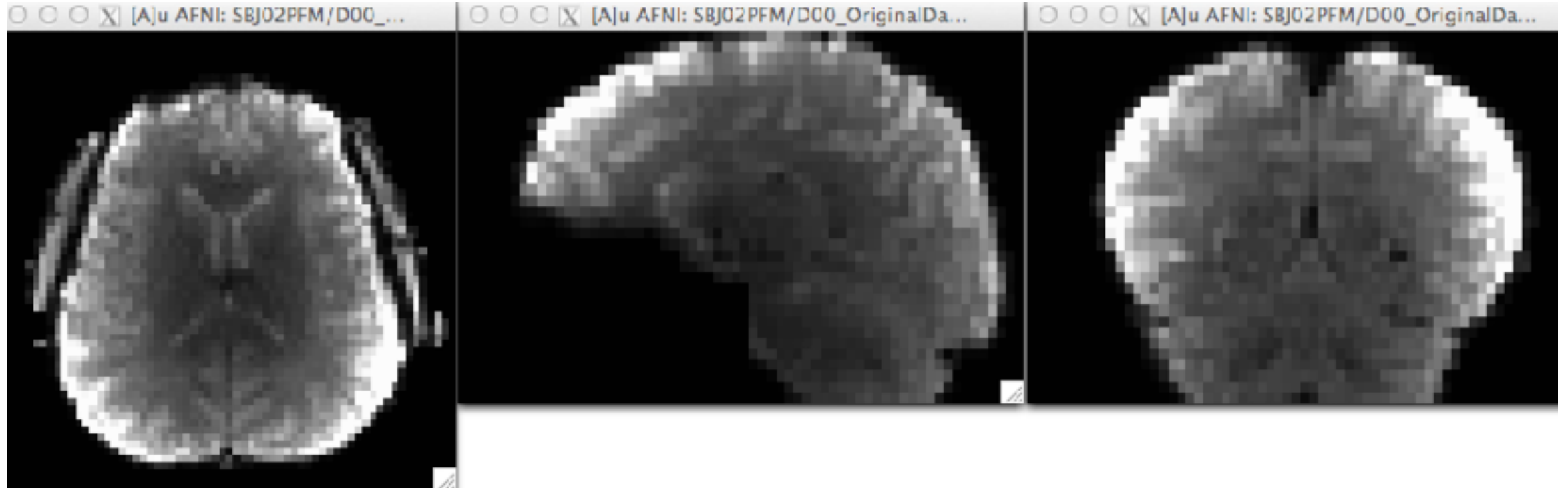
Introduction: Resting-state fMRI

- In resting-state fMRI, the reference signal is usually the time series of a voxel or region of interest.

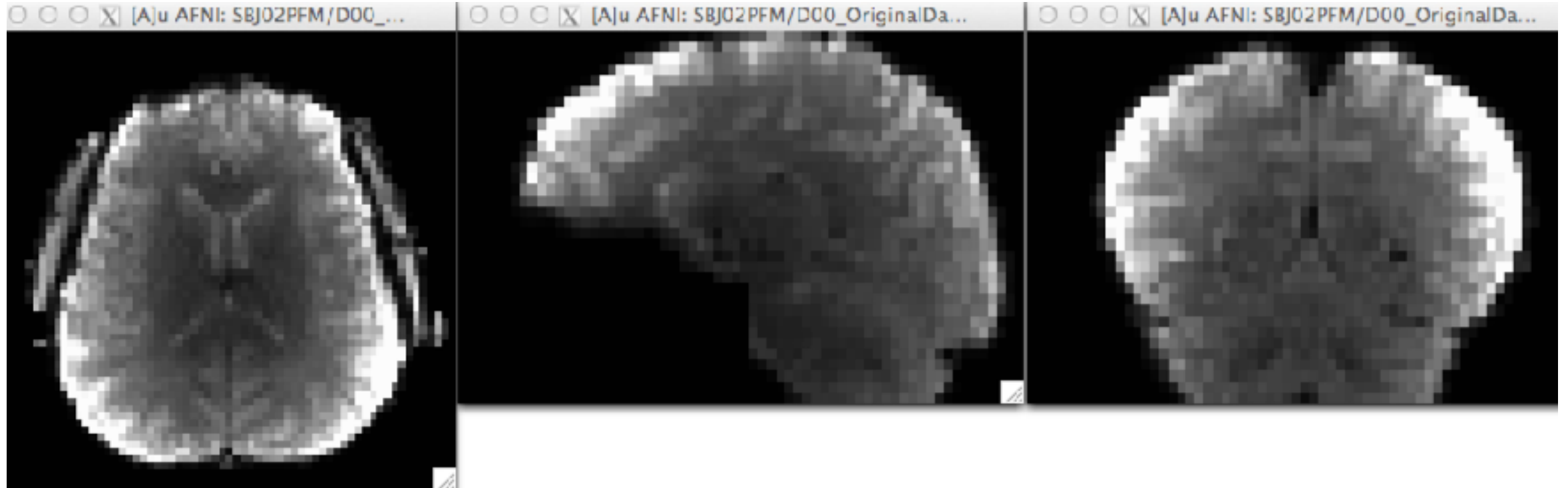


Sources of the BOLD fMRI signal

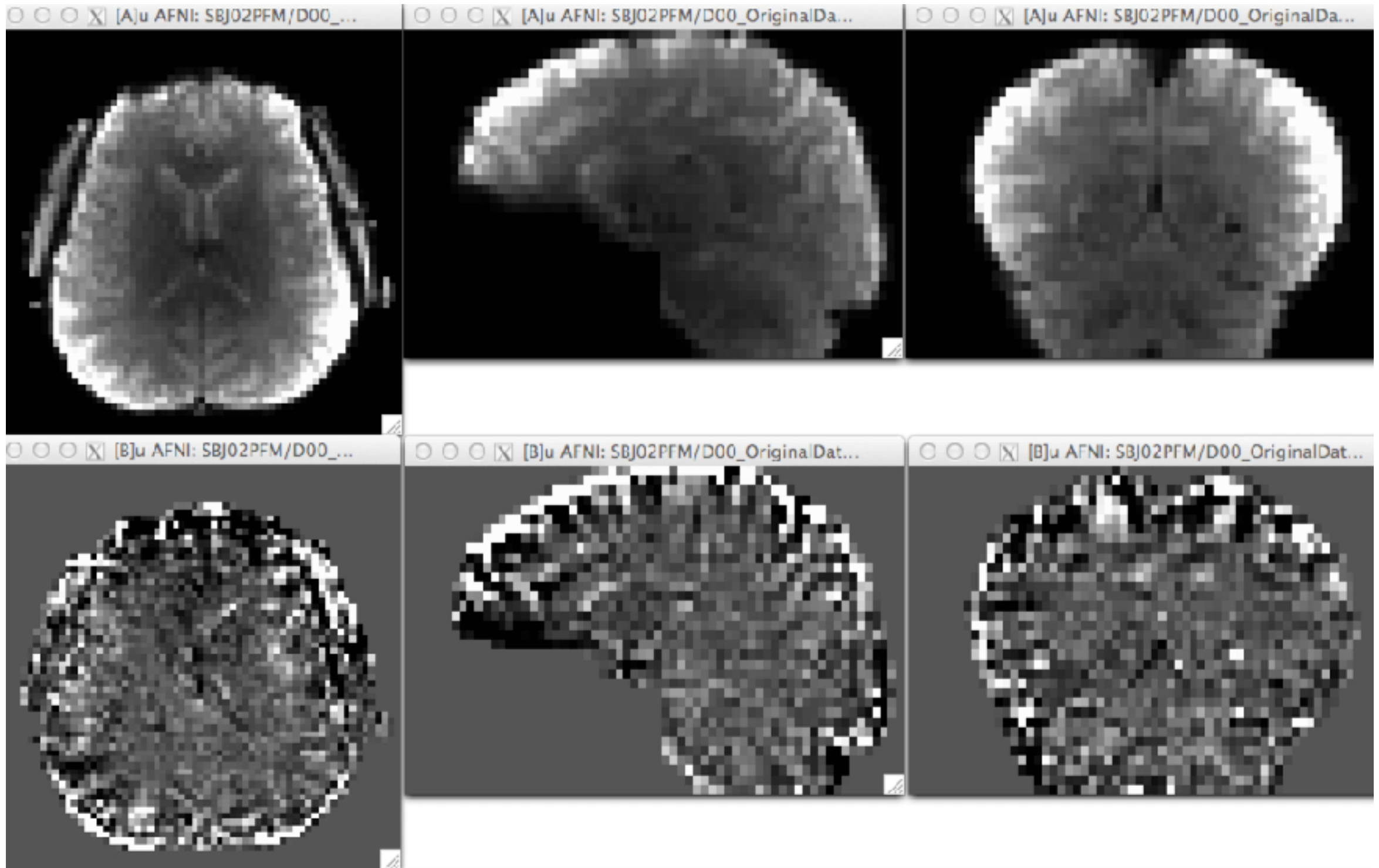
Sources of the fMRI signal: Motion-related fluctuations



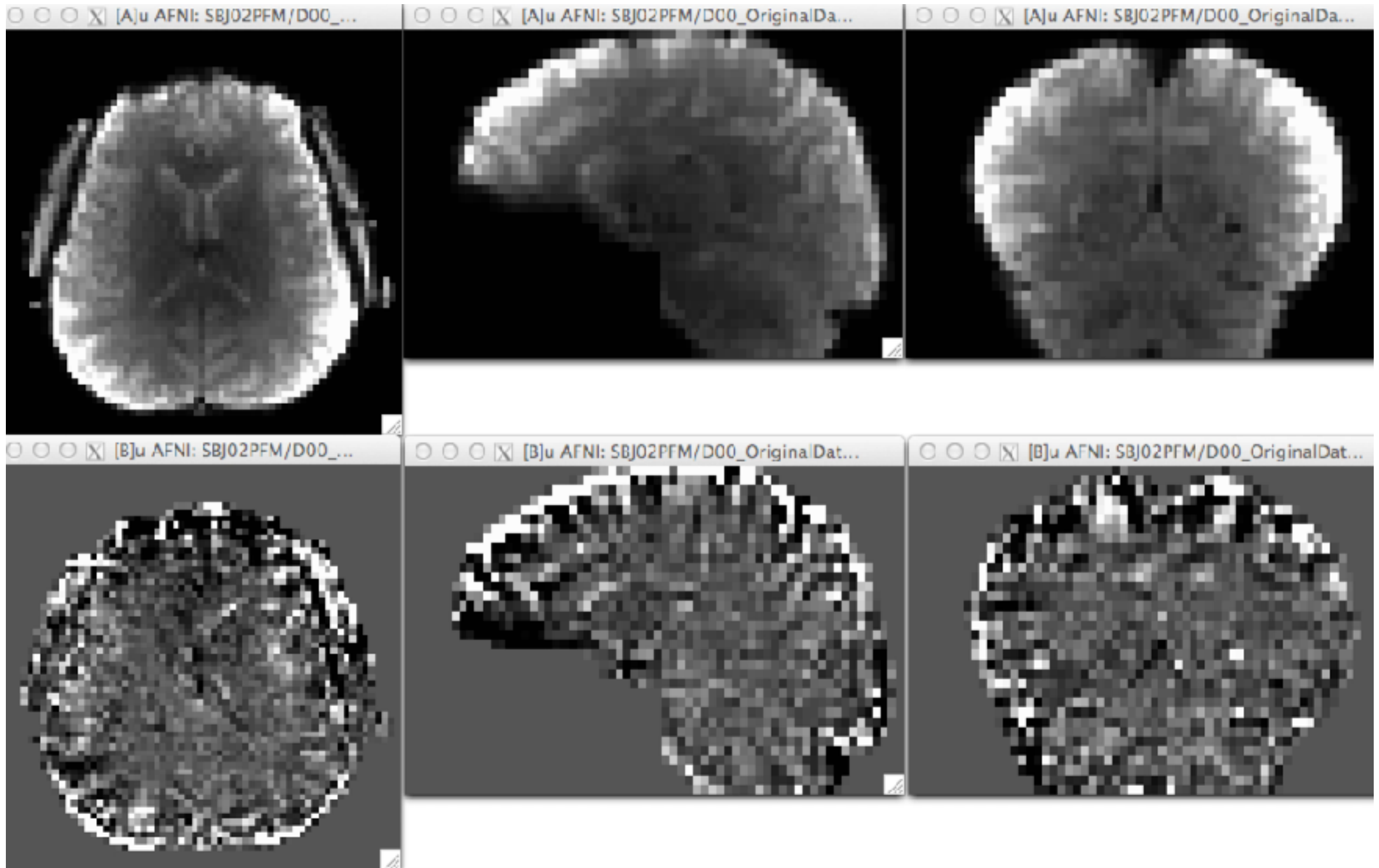
Sources of the fMRI signal: Motion-related fluctuations



Sources of the fMRI signal: Motion-related fluctuations

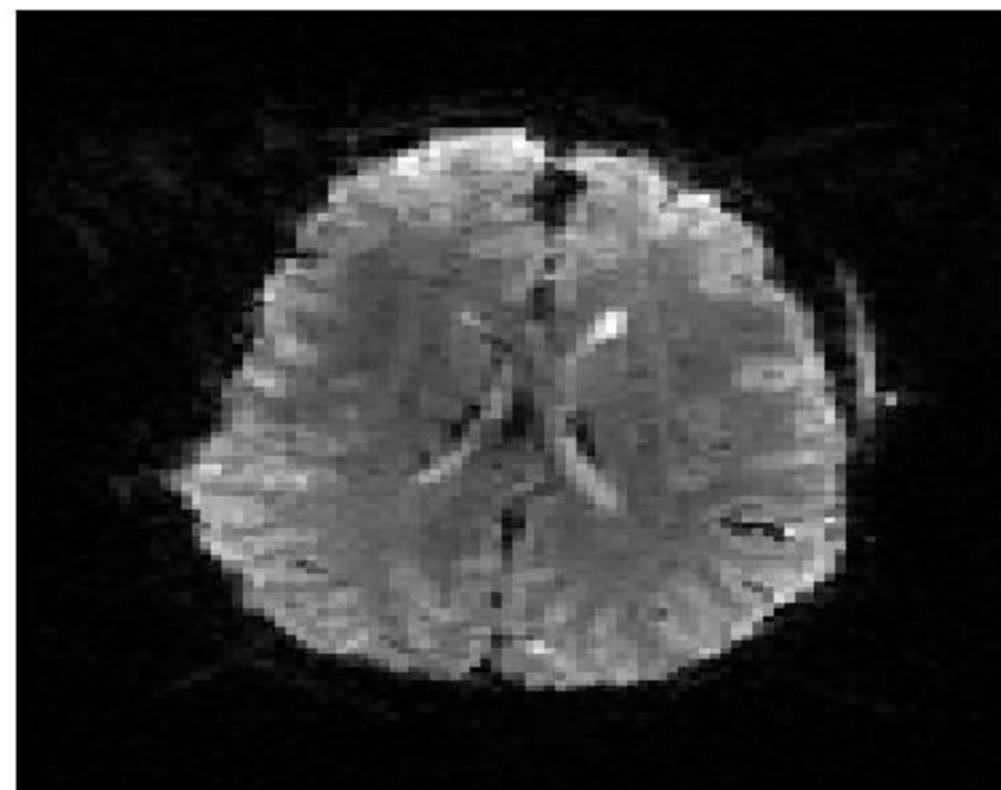


Sources of the fMRI signal: Motion-related fluctuations

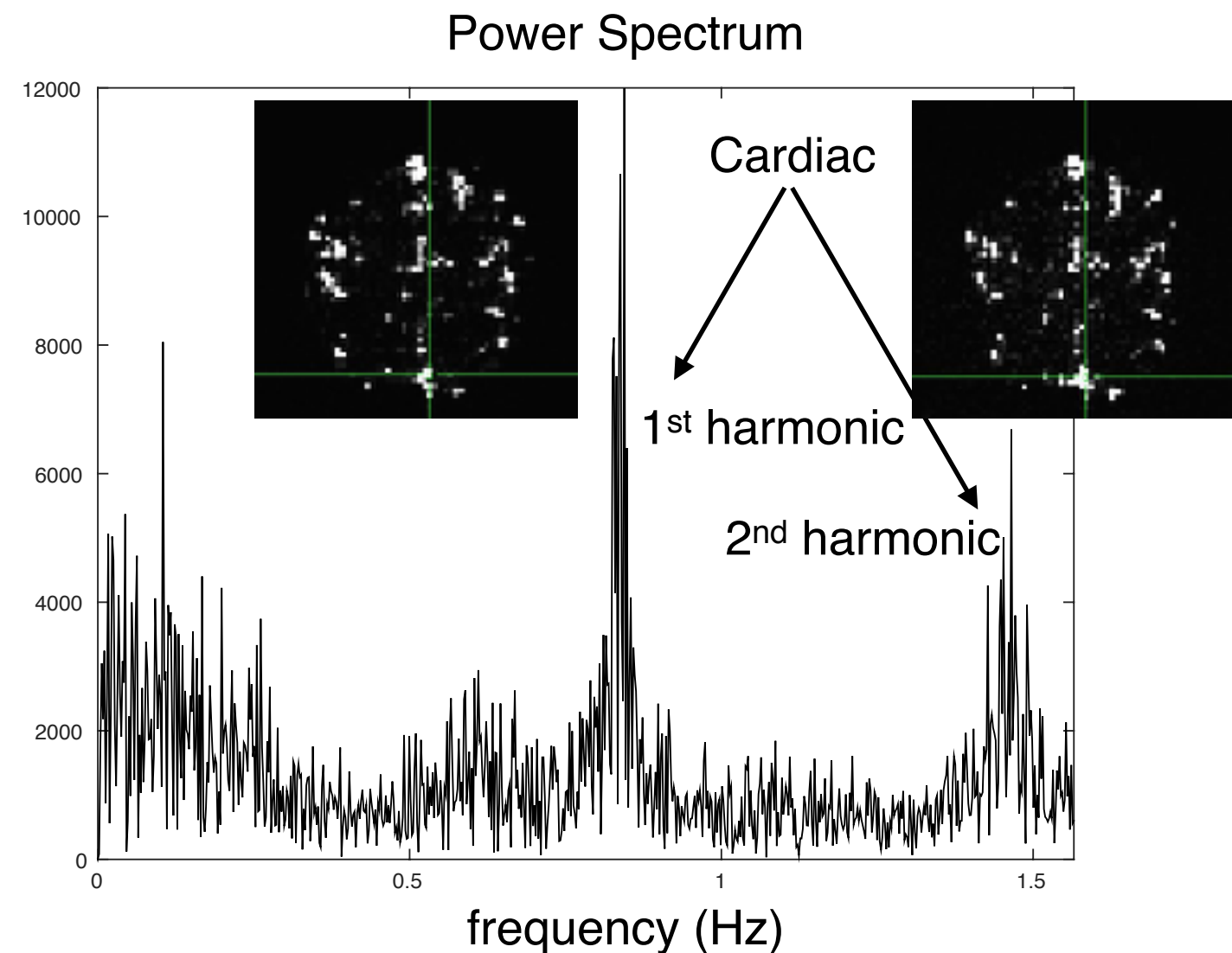


Cardiac Noise (approx. 0.8-1 Hz)

- Cardiac pulsability generates small movements in brain tissue as well as inflow effects in and around vessels. It is often localized in tissue regions close to:
 - Large arteries and draining veins (e.g. sagittal sinus or circle of Willis)
 - Edges of the brain, lateral ventricles and sulci.



Video courtesy of Catie Chang (NIH), TR: 100 ms

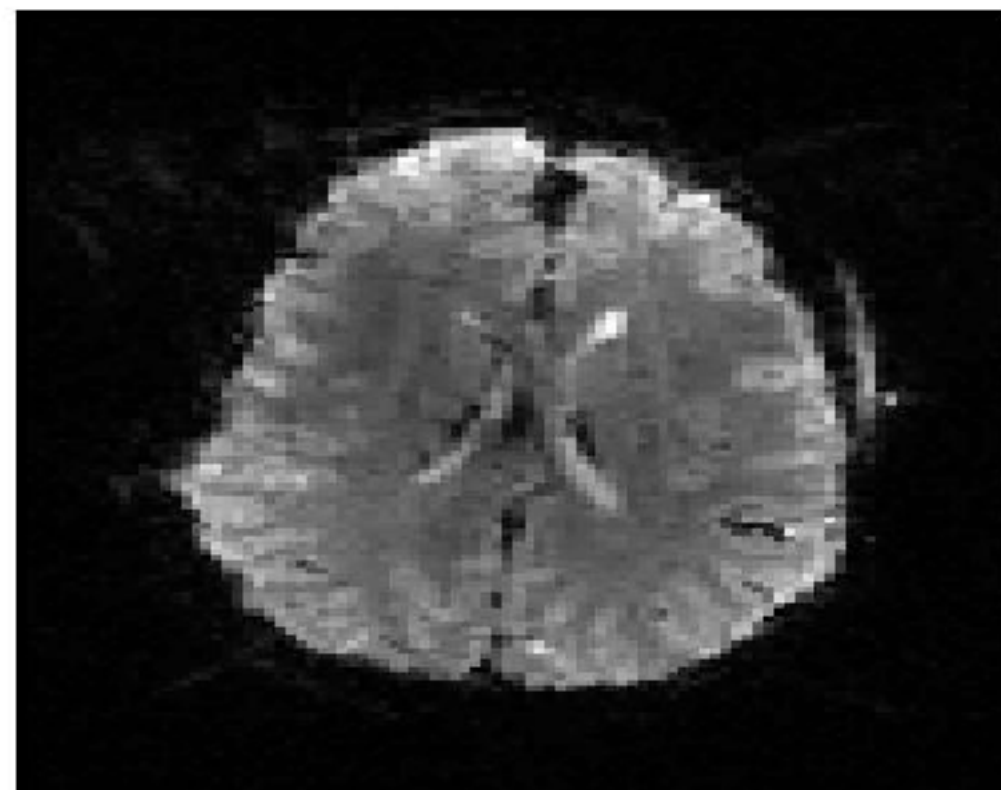


Dagli et al. (1999). Localization of cardiac-induce signal change in fMRI. Neuroimage 9:407-415

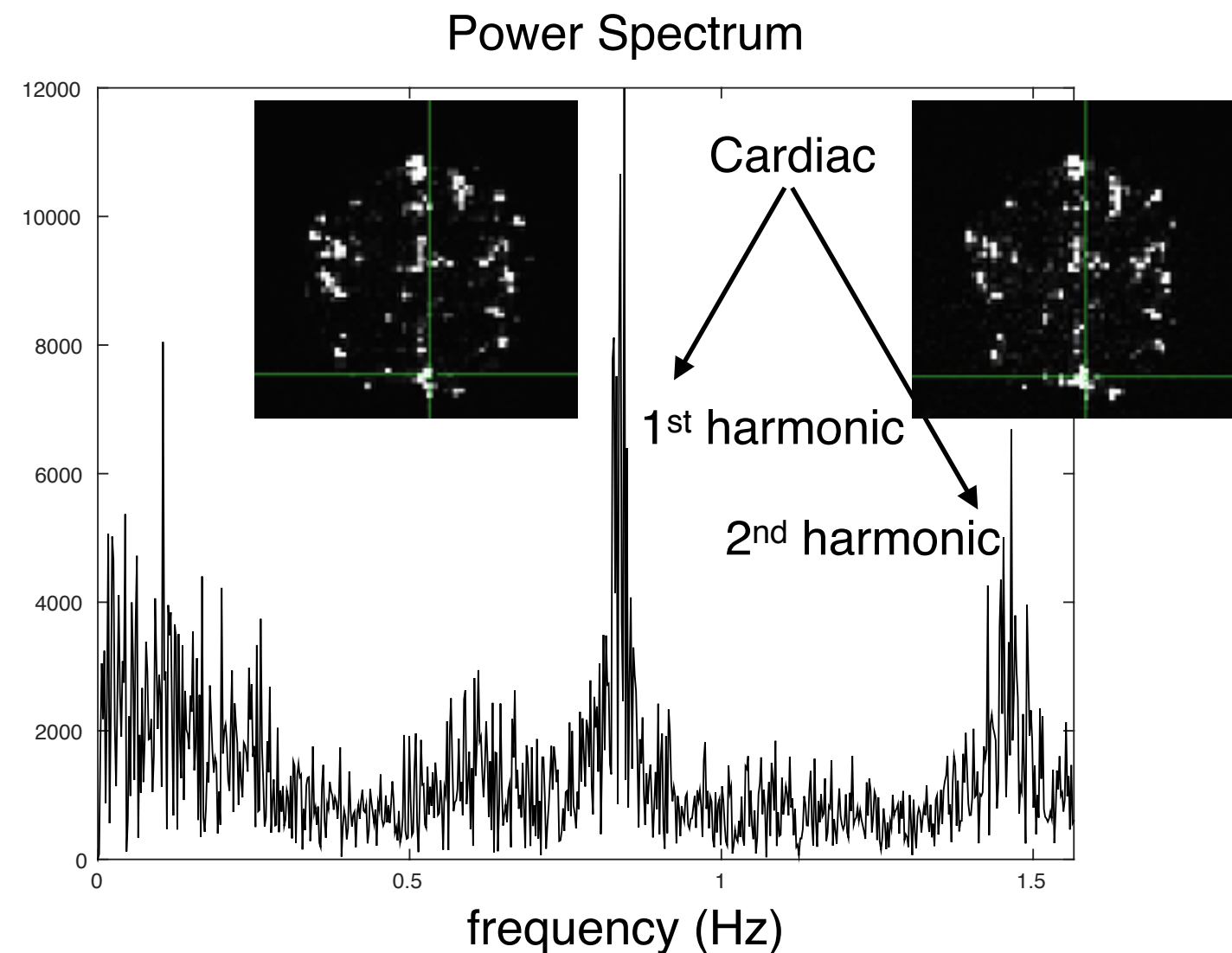
Bhattacharyya and Lowe (2004). Cardiac-induced physiological noise in tissue is a direct observation of cardiac-induced fluctuations. Magn Reson Imaging 22(4):9-13.

Cardiac Noise (approx. 0.8-1 Hz)

- Cardiac pulsability generates small movements in brain tissue as well as inflow effects in and around vessels. It is often localized in tissue regions close to:
 - Large arteries and draining veins (e.g. sagittal sinus or circle of Willis)
 - Edges of the brain, lateral ventricles and sulci.



Video courtesy of Catie Chang (NIH), TR: 100 ms

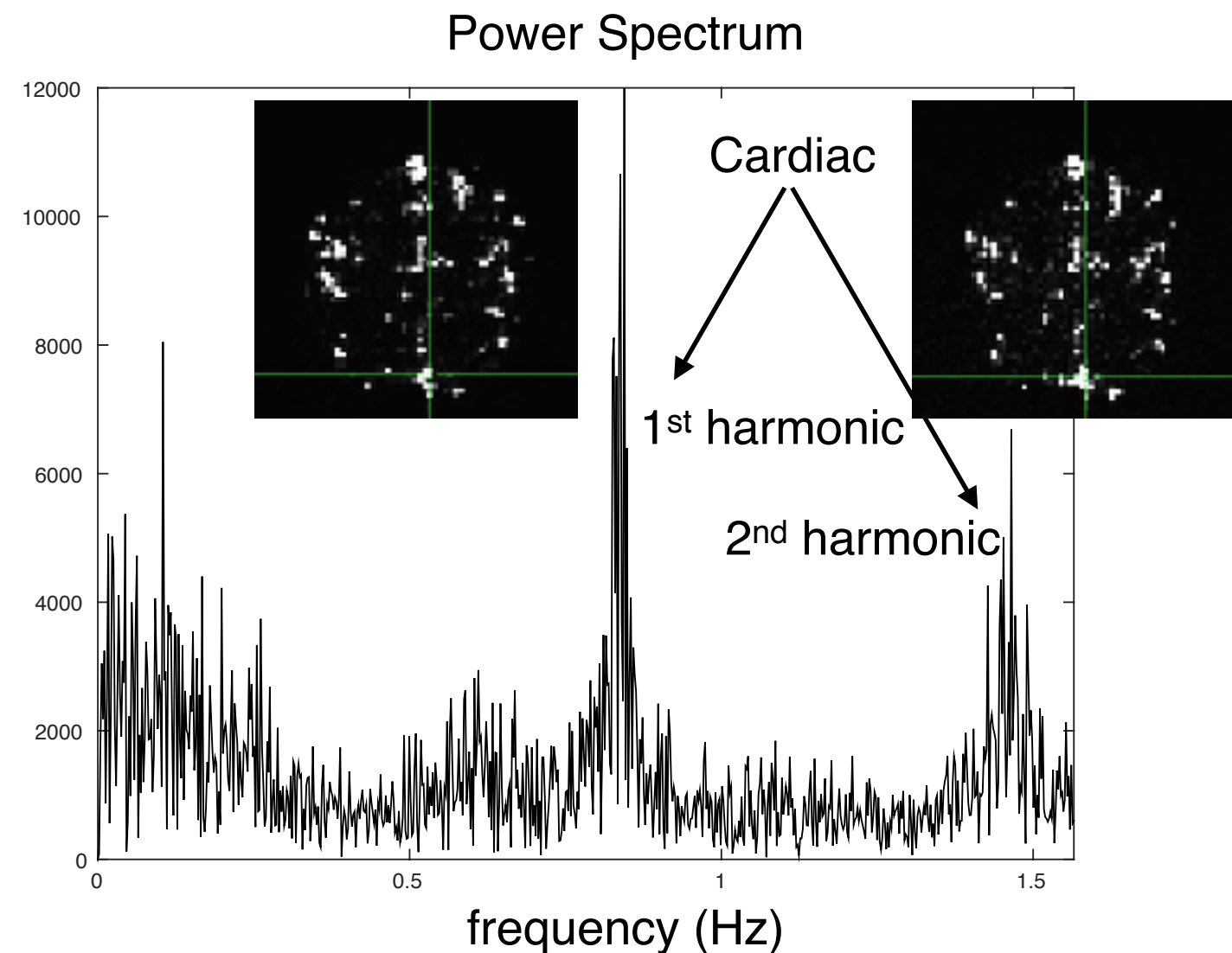
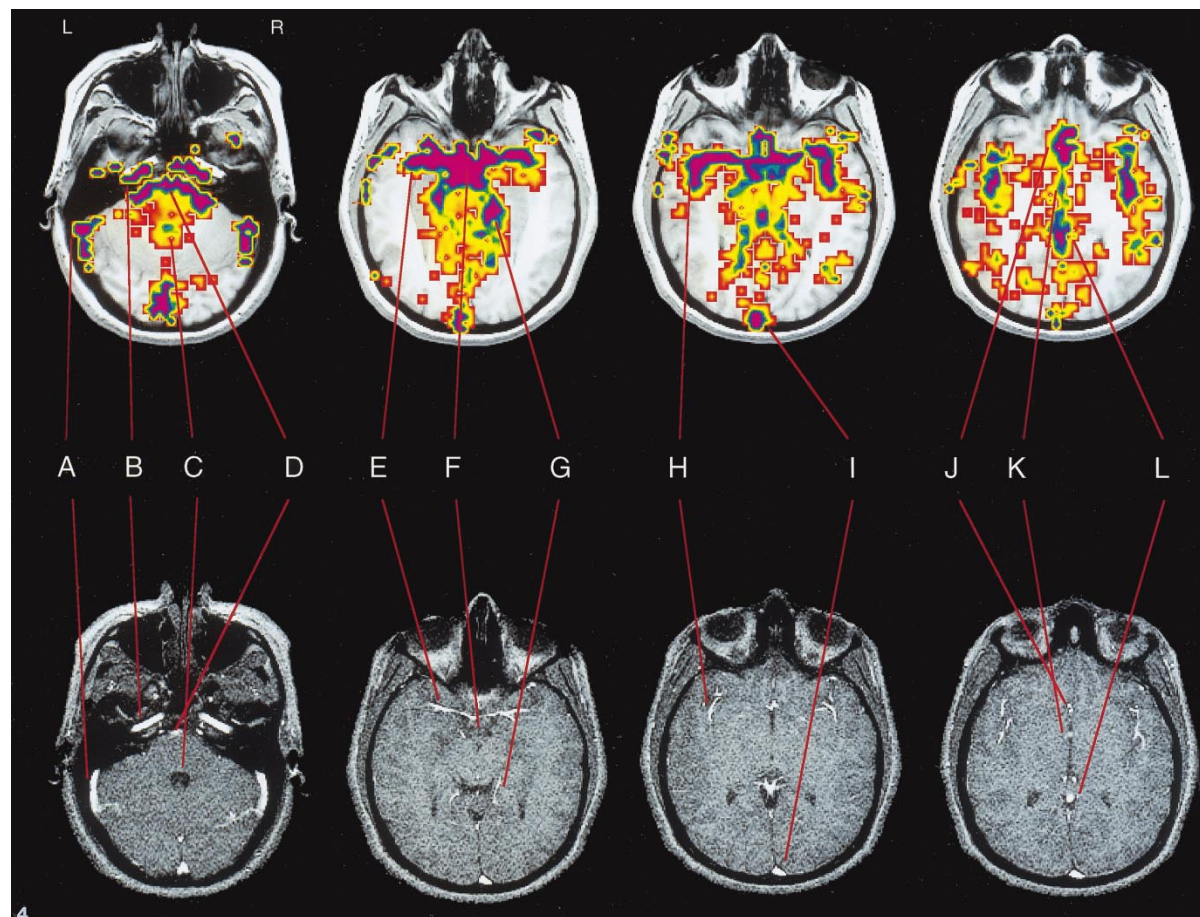


Dagli et al. (1999). Localization of cardiac-induce signal change in fMRI. Neuroimage 9:407-415

Bhattacharyya and Lowe (2004). Cardiac-induced physiological noise in tissue is a direct observation of cardiac-induced fluctuations. Magn Reson Imaging 22(4):9-13.

Cardiac Noise (approx. 0.8-1 Hz)

- Cardiac pulsability generates small movements in brain tissue as well as inflow effects in and around vessels. It is often localized in tissue regions close to:
 - Large arteries and draining veins (e.g. sagittal sinus or circle of Willis)
 - Edges of the brain, lateral ventricles and sulci.

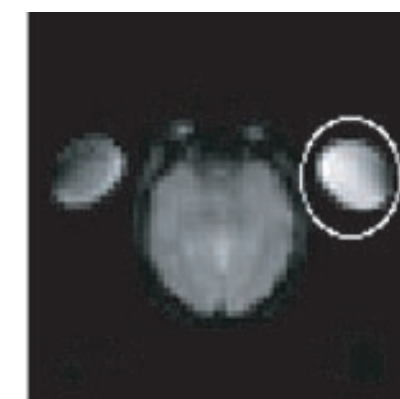
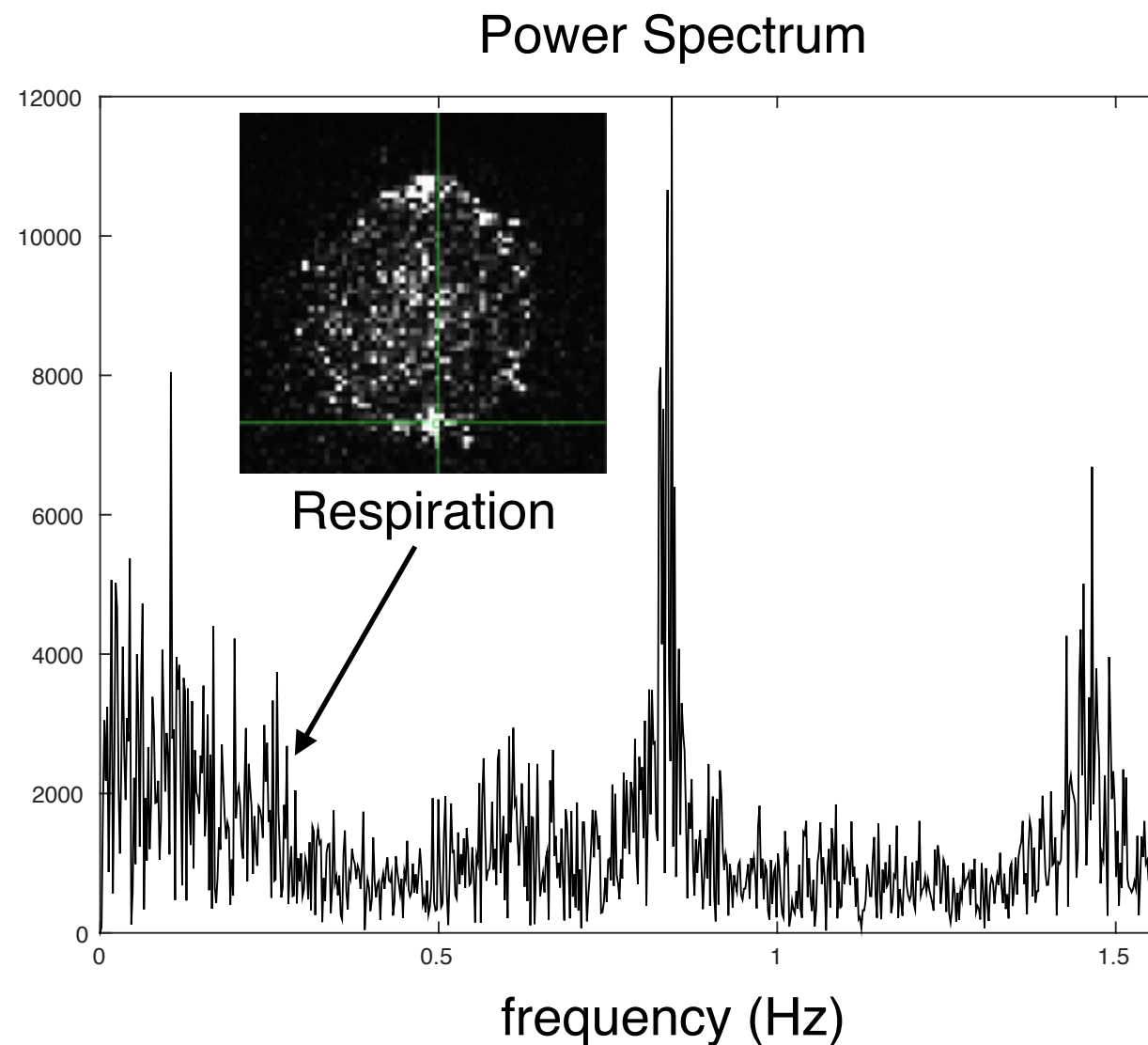


Dagli et al. (1999). Localization of cardiac-induce signal change in fMRI. Neuroimage 9:407-415

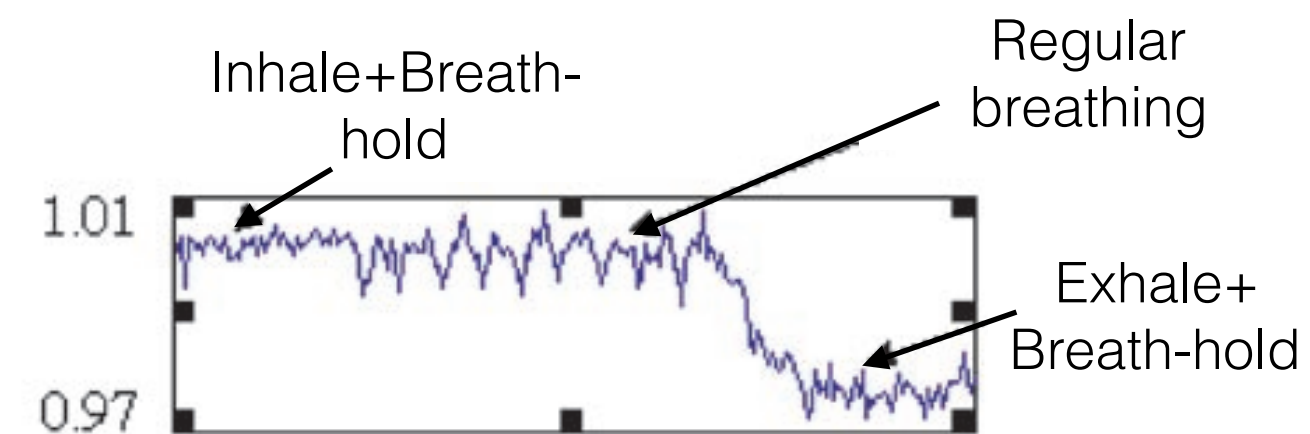
Bhattacharyya and Lowe (2004). Cardiac-induced physiological noise in tissue is a direct observation of cardiac-induced fluctuations. Magn Reson Imaging 22(4):9-13.

Respiratory Noise (approx. 0.2-0.4 Hz)

- Thoracic movements during breathing result in respiratory-dependent changes in the magnetic field in the head volume that produce a phase shift in the image. More spatially global effects.
- Small changes of the head also introduce spin history artefacts. Closely related to head movement artefacts and also cardiac pulsability.

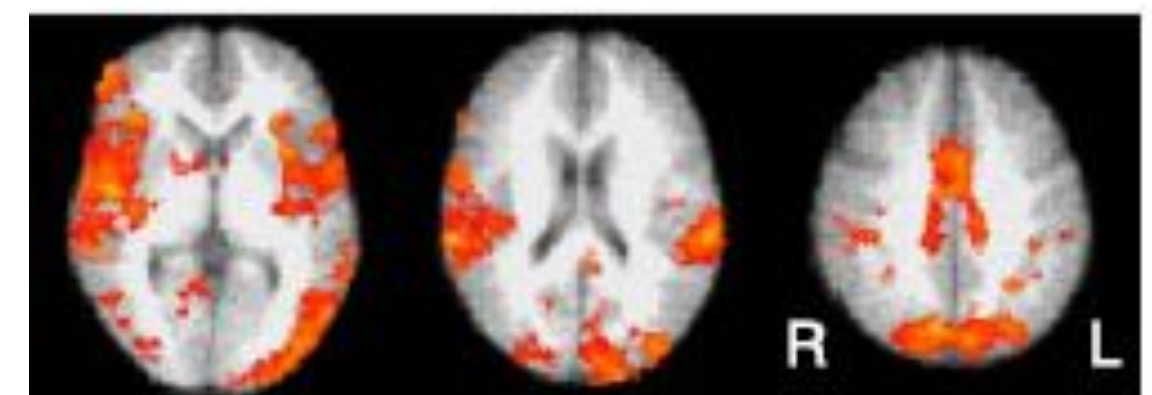
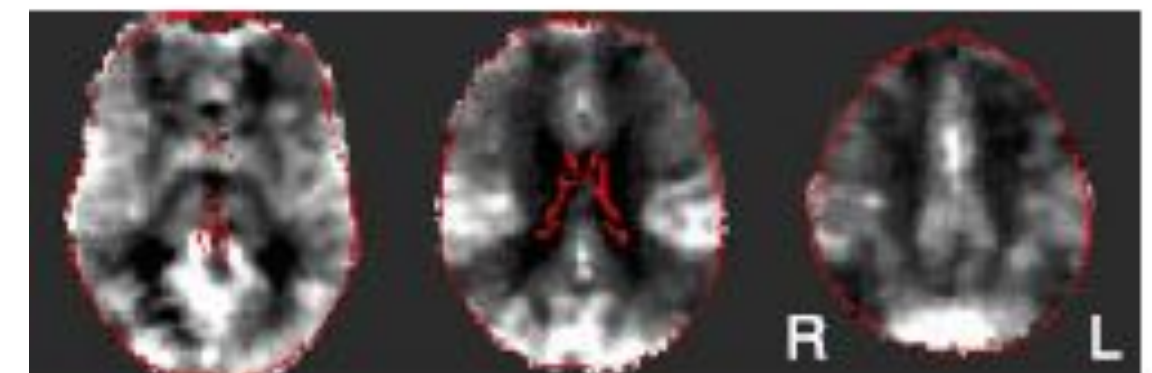
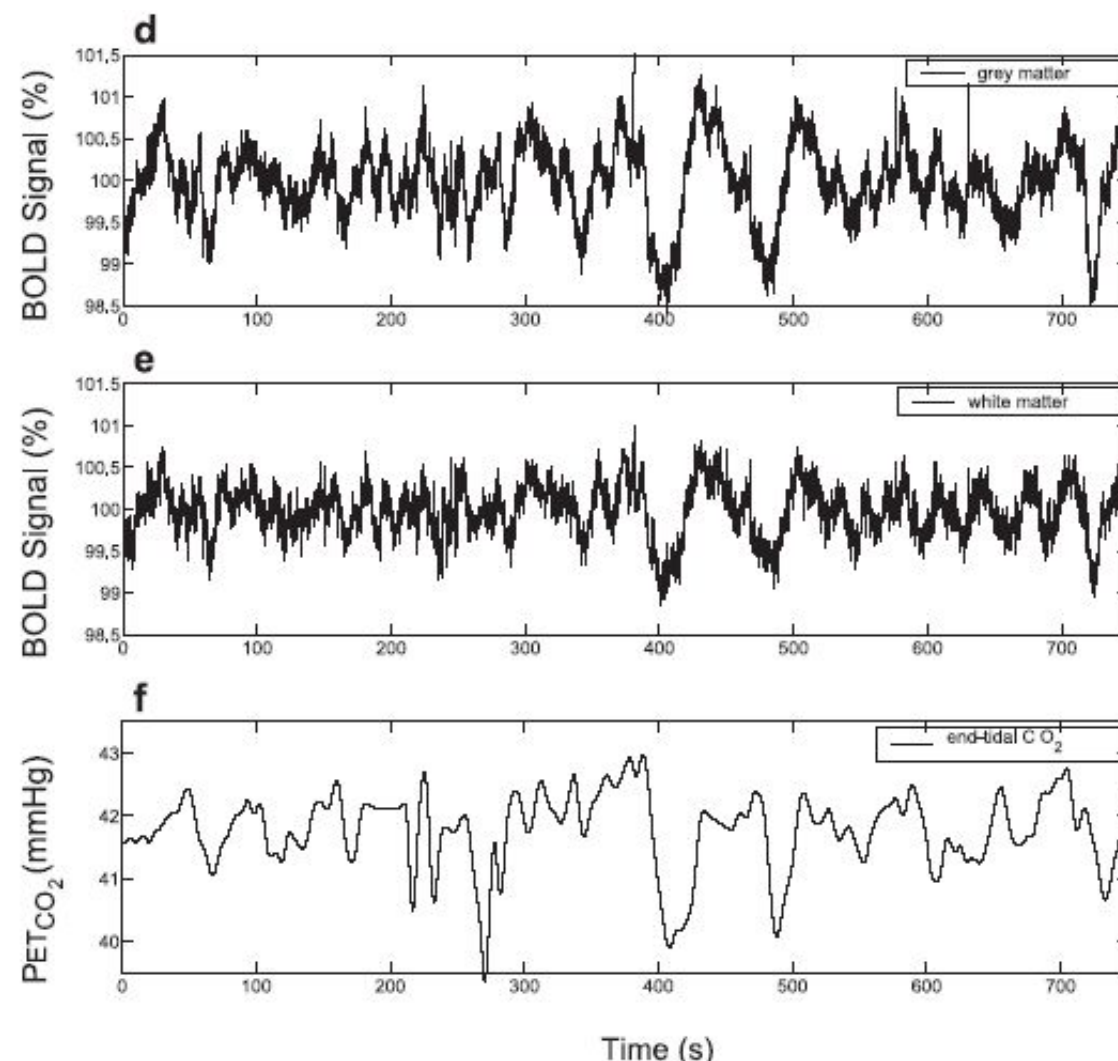


2 bottles of copper sulfate attached to the head coil



Low frequency physiological fluctuations (below 0.1 Hz)

- Variations in respiratory rate affect the fMRI signal by changing the oxygenation level and arterial level of CO₂, which is a potent cerebral vasodilator.



Wise et al. (2004). Resting fluctuation in arterial carbon dioxide induce significant low frequency fluctuations in BOLD signal. Neuroimage 21(4):1652-1664.

Sources of the fMRI signal: Draining veins

- Gradient-Echo (GE) Echo-Planar Imaging (EPI) typically used for BOLD fMRI has stronger contribution from macrovessels, mainly located in pial surface.
- BOLD contamination from macrovessels (large arteries, draining veins) are a serious impediment for high-resolution localization of neuronal activity in fMRI.

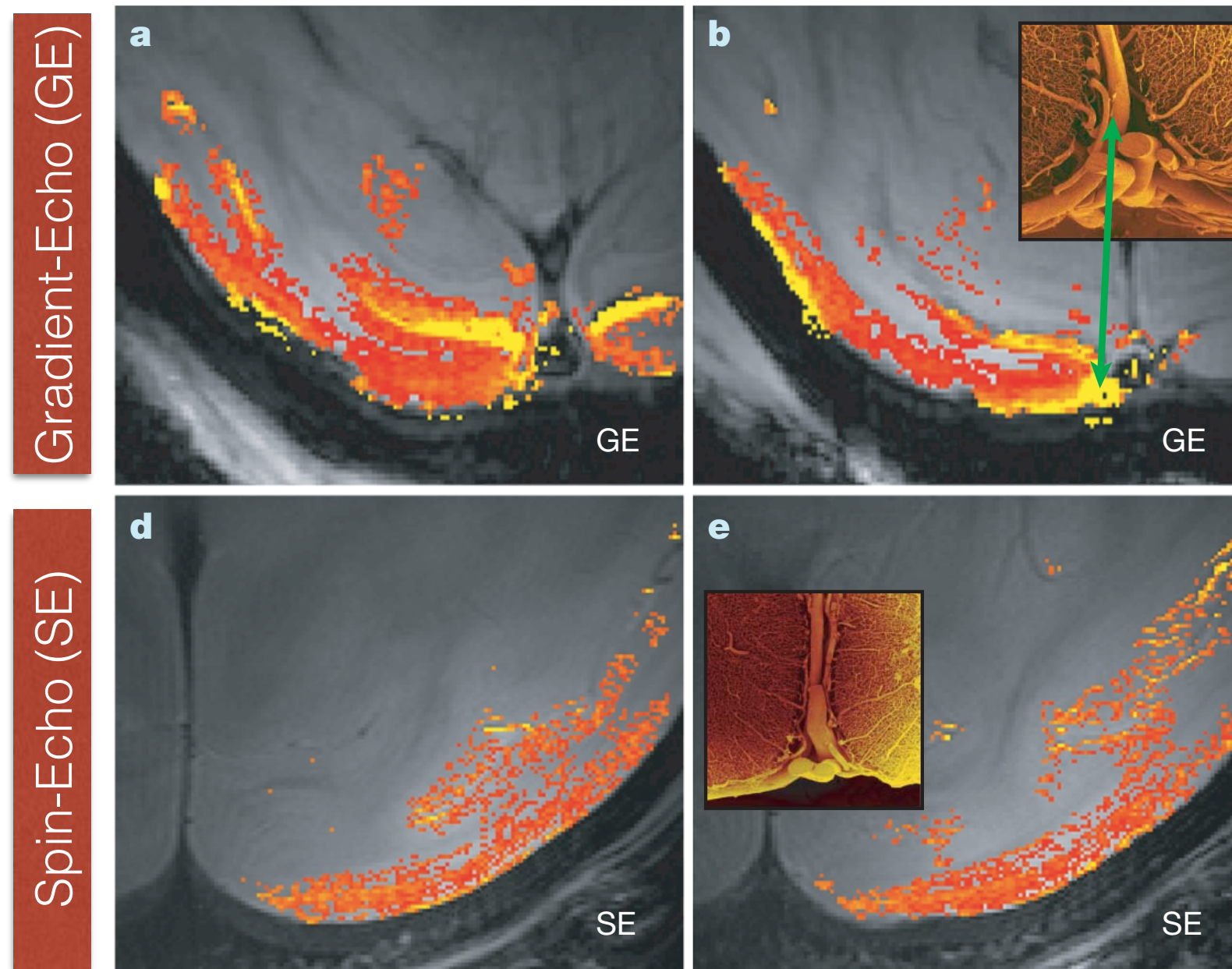
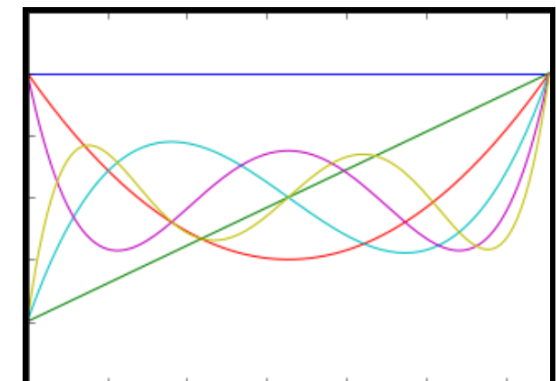
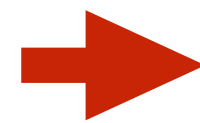
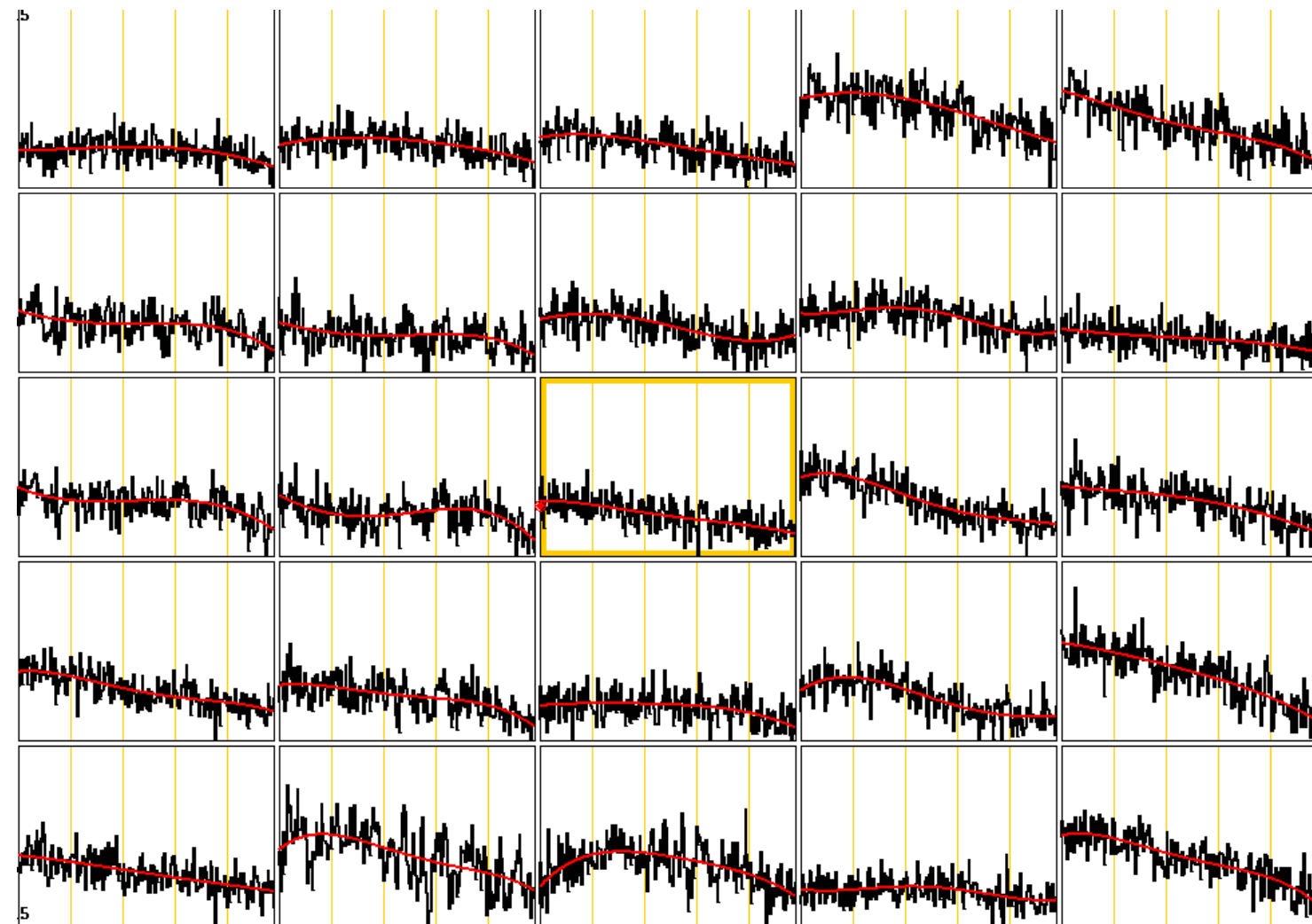


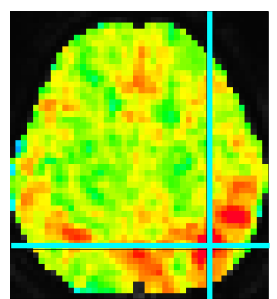
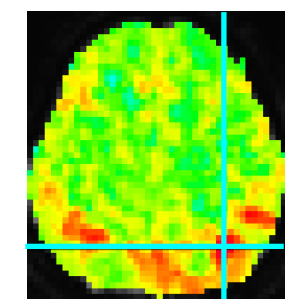
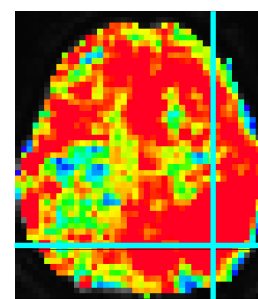
Figure adapted from Logothetis (2008)
What we can do and what we cannot
do with fMRI. Nature 453:869-878

Sources of the fMRI signal: Low frequency drifts

- Low frequency fluctuations in the signal (< 0.01 Hz) related to very slow head displacements, scanner-related drifts (e.g. heating), etc.
- Different for each voxel (even neighbouring voxels)
- Usually eliminated via filtering (detrending), e.g. high pass filtering

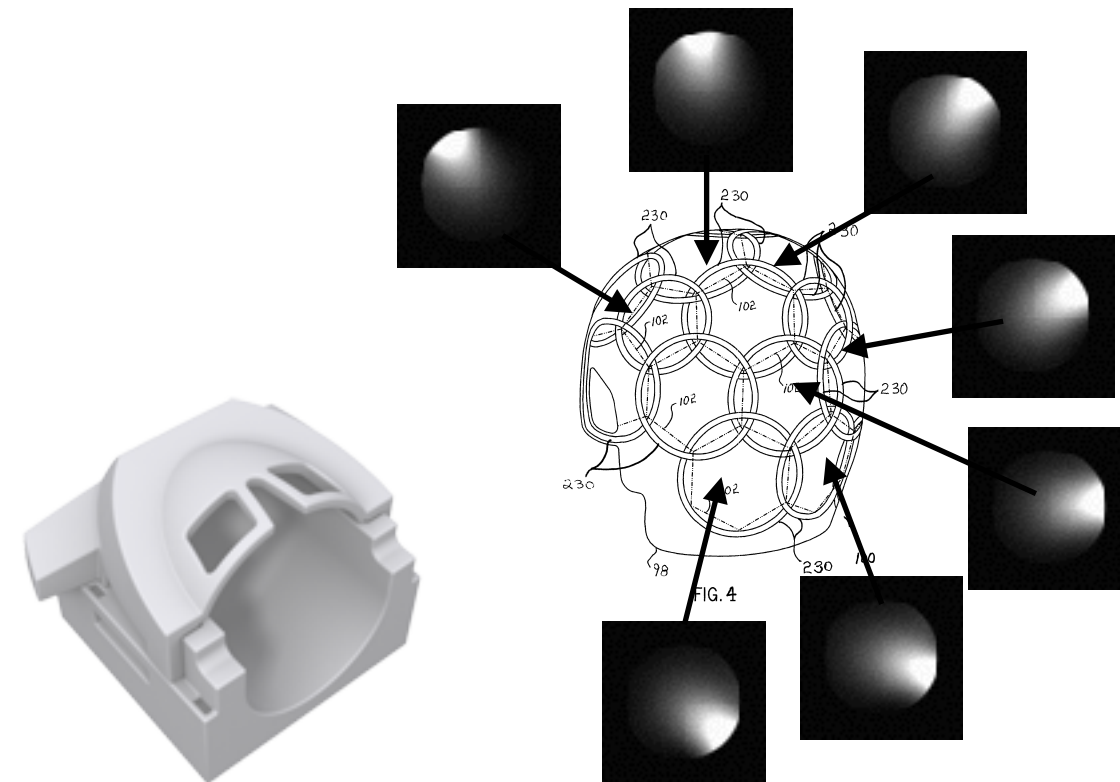


Functional Connectivity Maps (@InstaCorr)



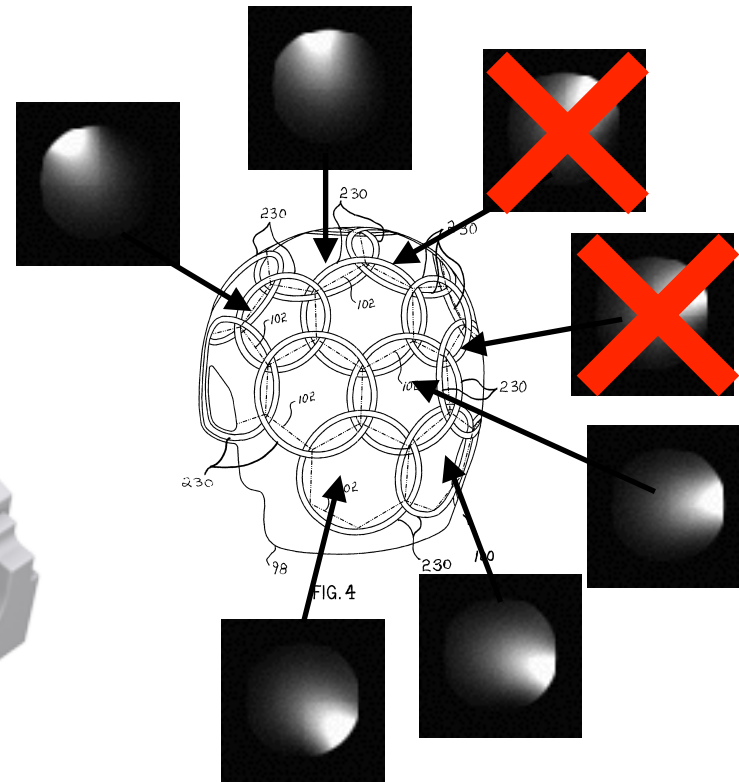
Sources of the fMRI signal: Hardware-related instabilities

- Nowadays, most MRI scanners use multichannel receiver coils for data acquisition

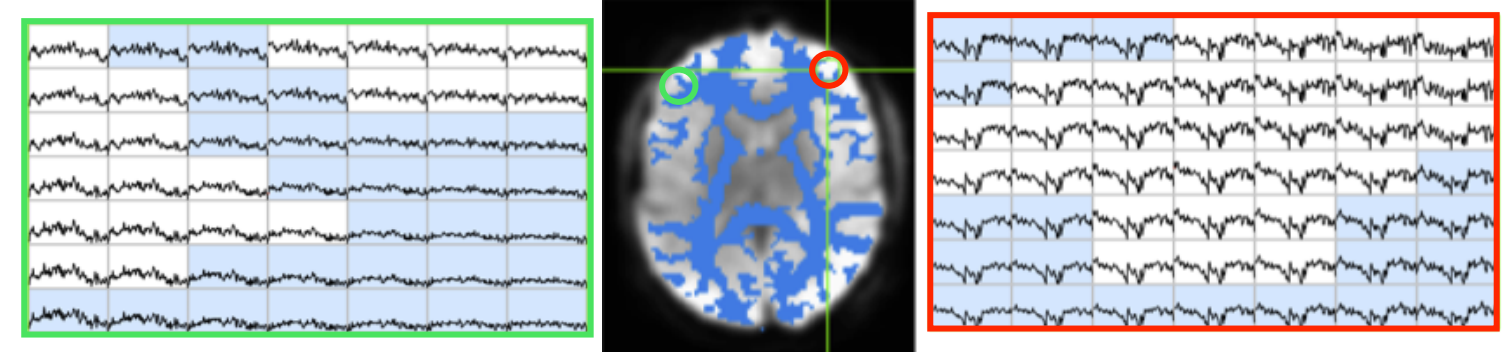
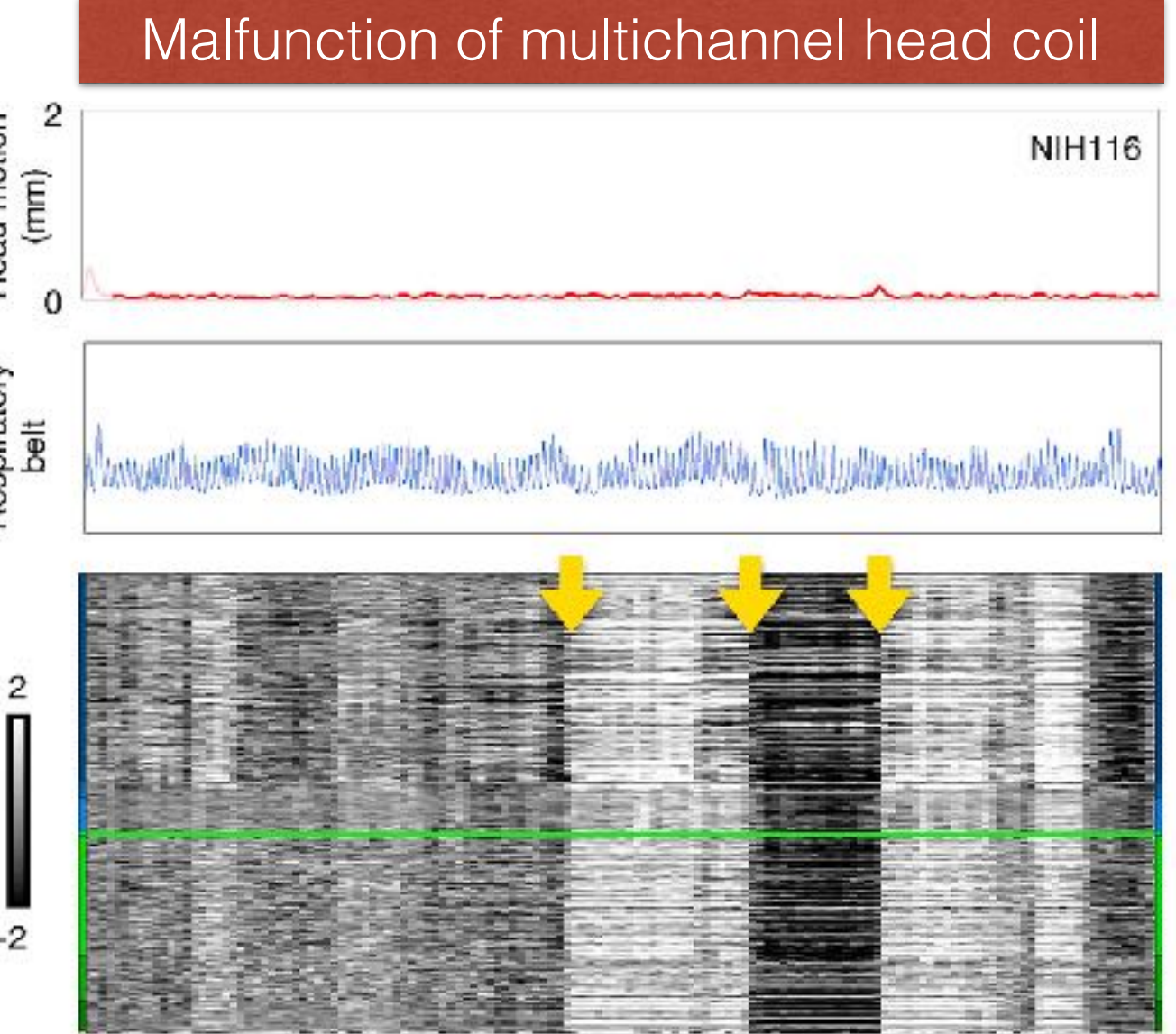
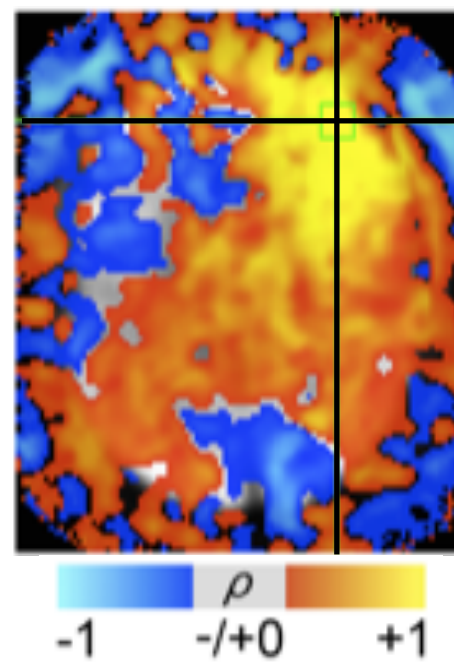


Sources of the fMRI signal: Hardware-related instabilities

- Nowadays, most MRI scanners use multichannel receiver coils for data acquisition



Functional
Connectivity Map
(@InstaCorr)

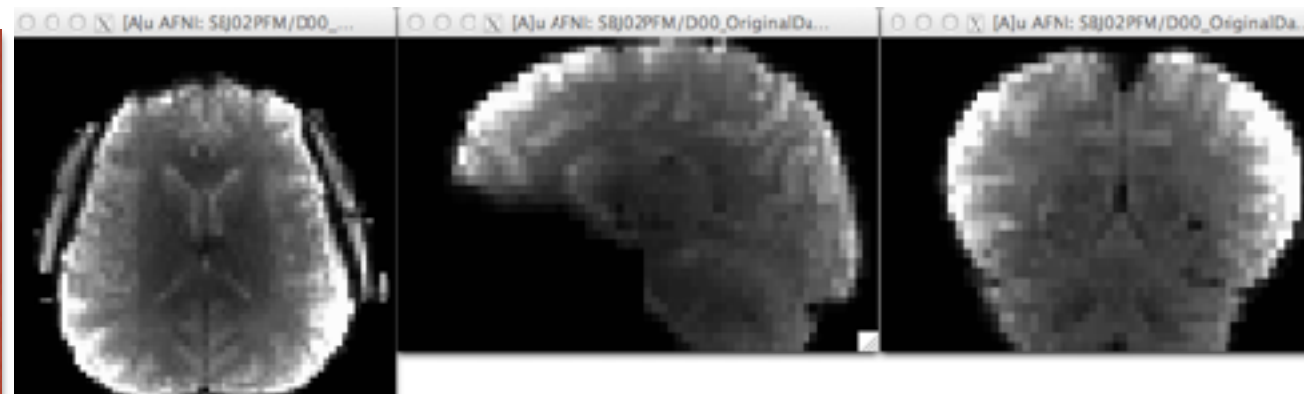


Methods for denoising the BOLD fMRI signal

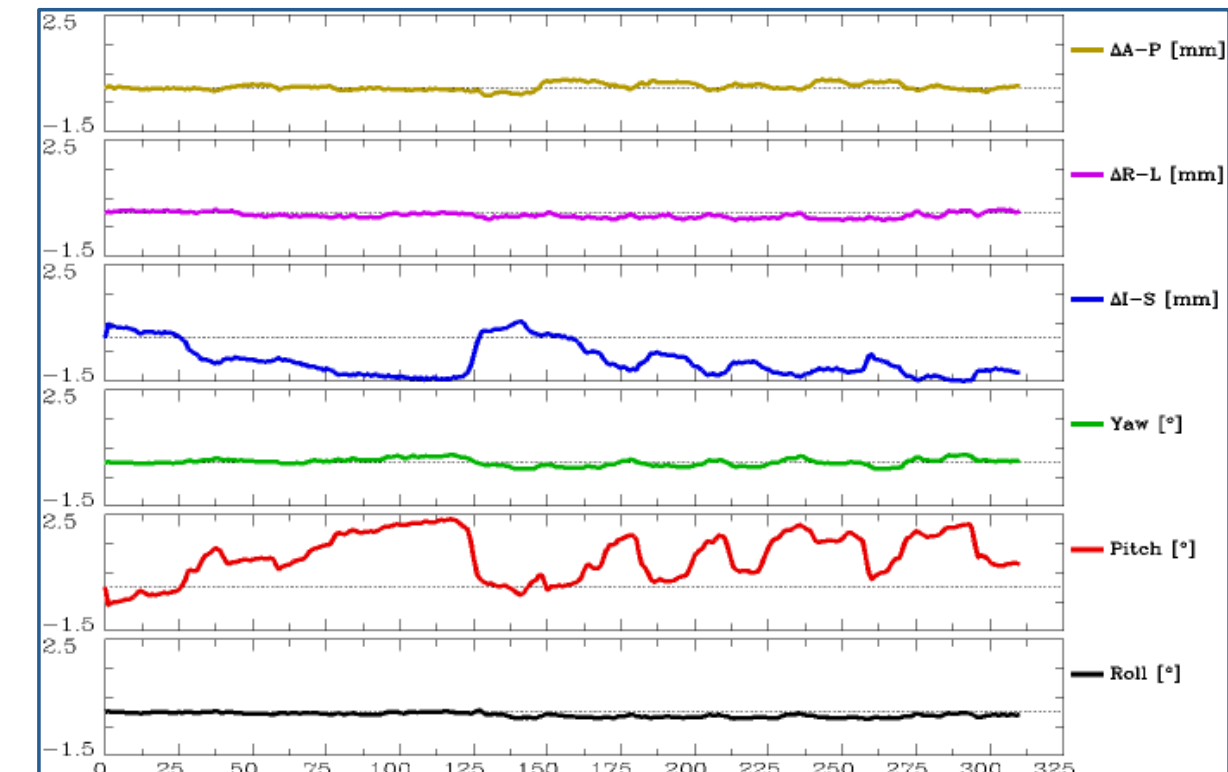
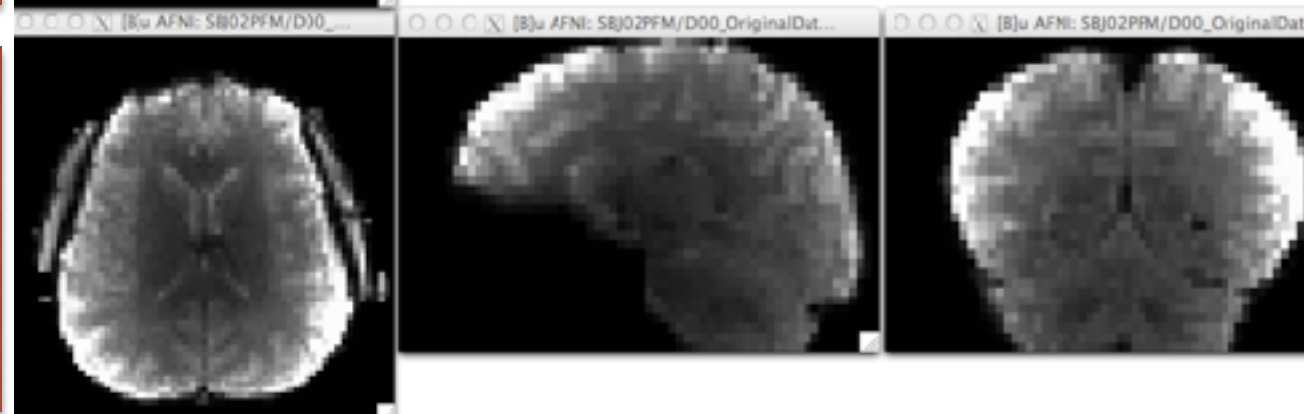
Compensation of motion effects: Volumetric realignment

- Translation ($\Delta x, \Delta y, \Delta z$) and rotation (yaw, pitch roll) to reference image

BEFORE CORRECTION



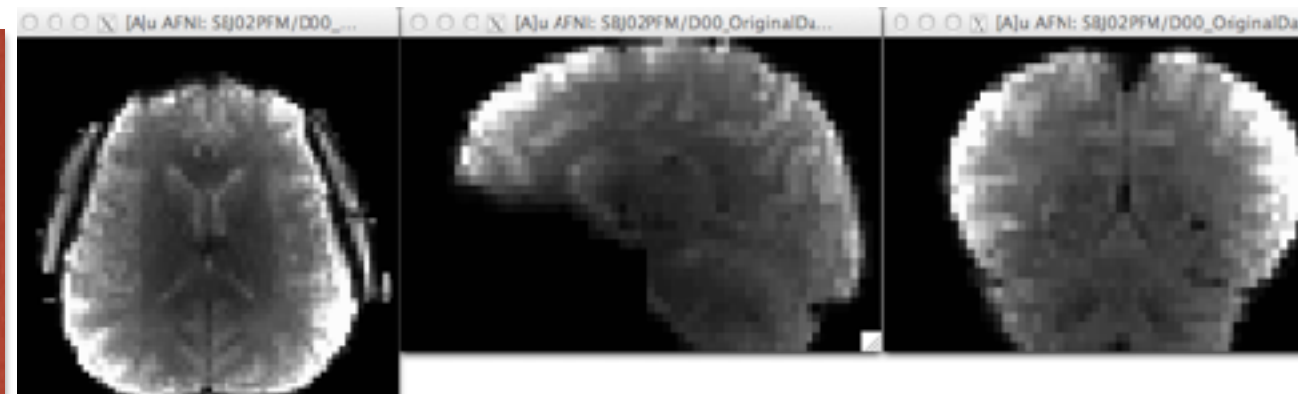
AFTER CORRECTION



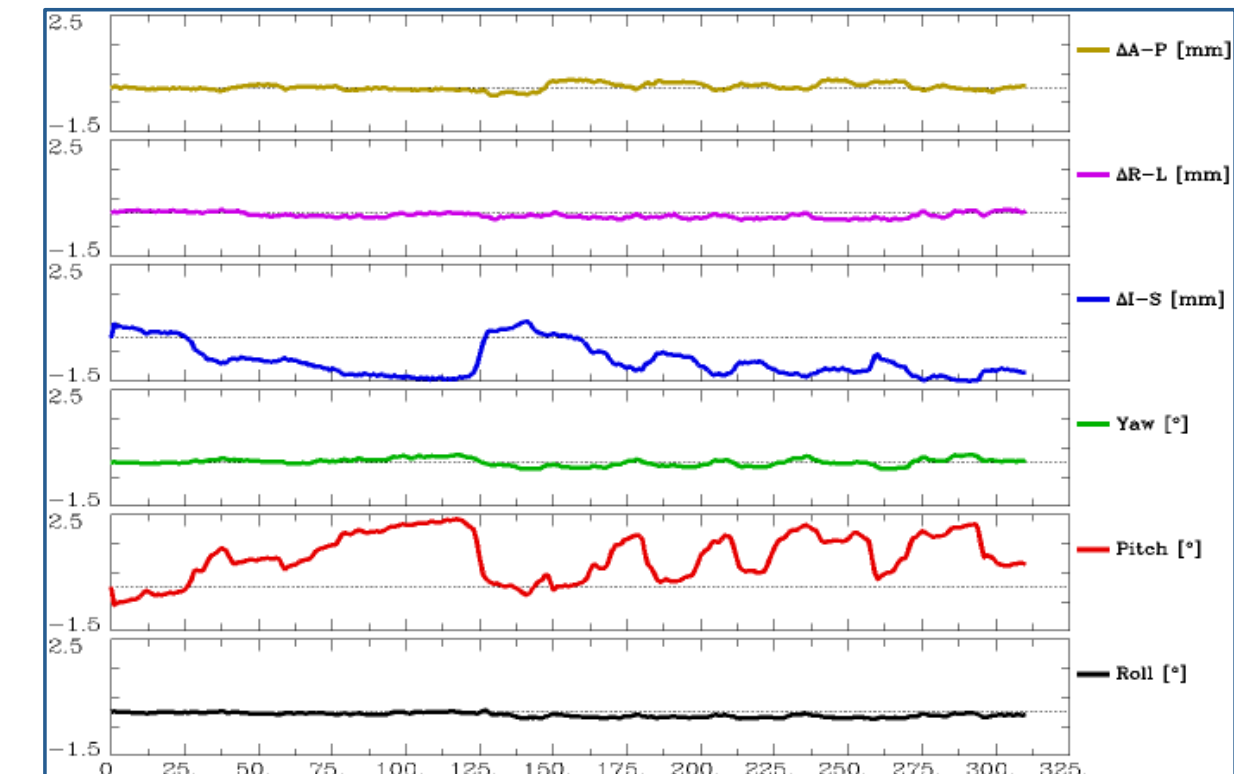
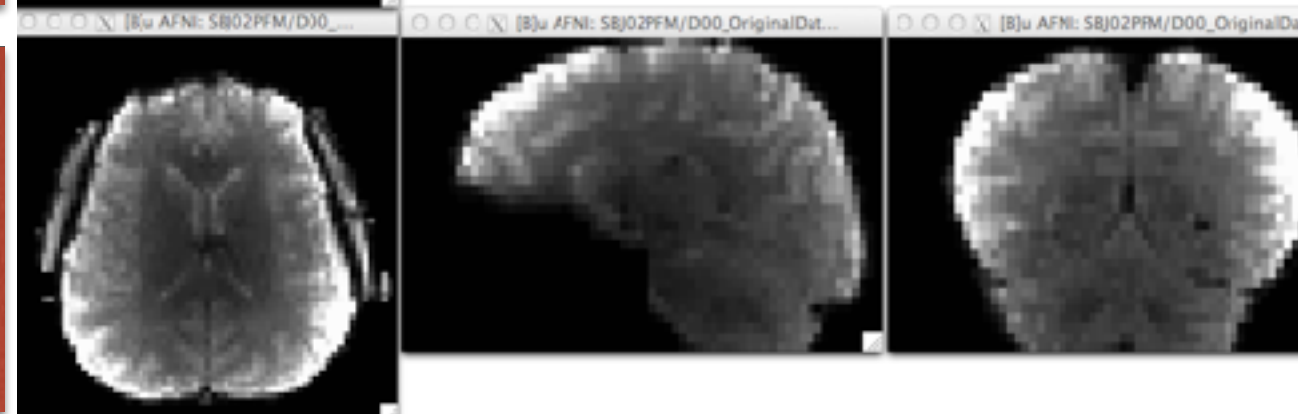
Compensation of motion effects: Volumetric realignment

- Translation ($\Delta x, \Delta y, \Delta z$) and rotation (yaw, pitch roll) to reference image

BEFORE CORRECTION



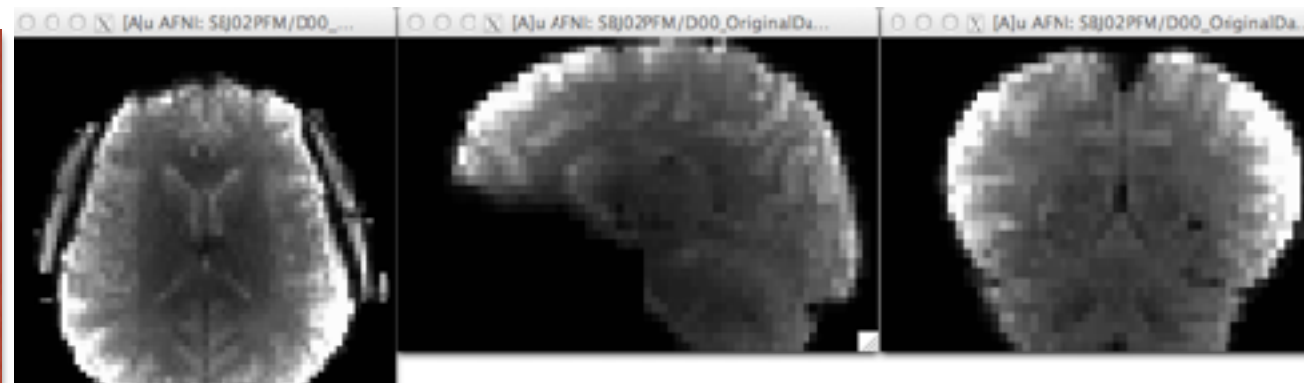
AFTER CORRECTION



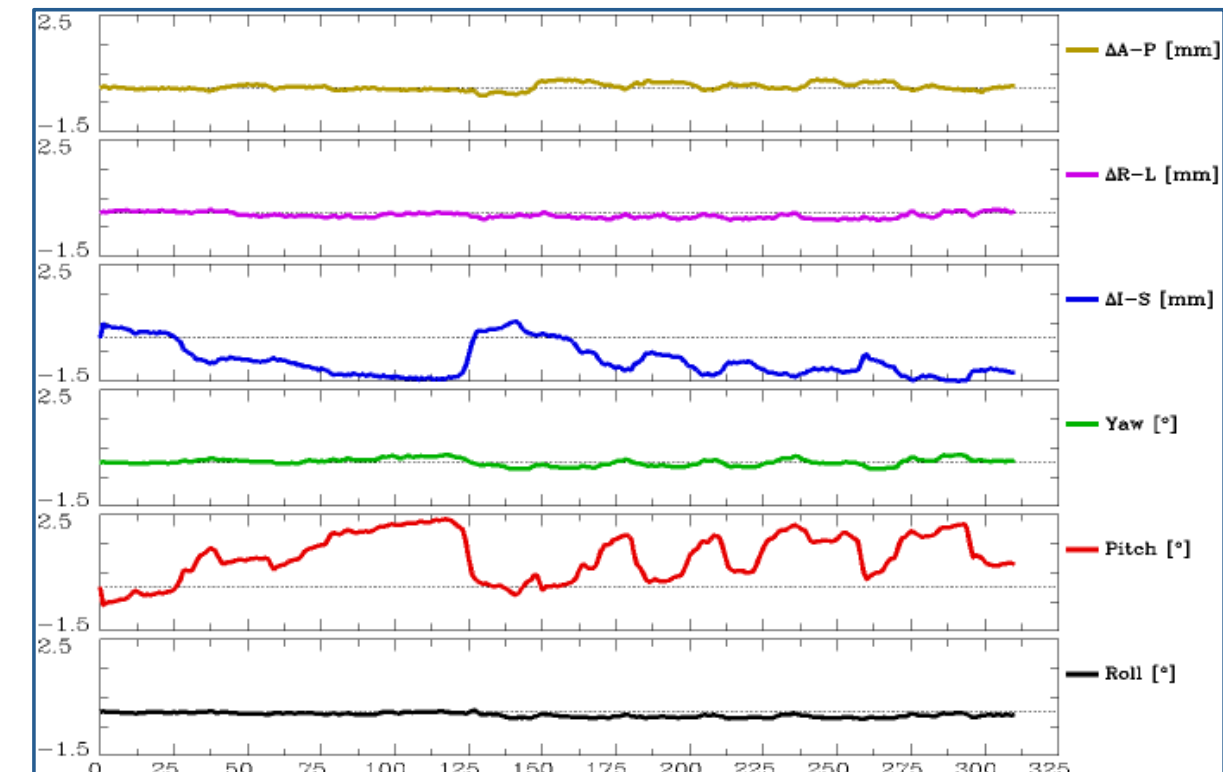
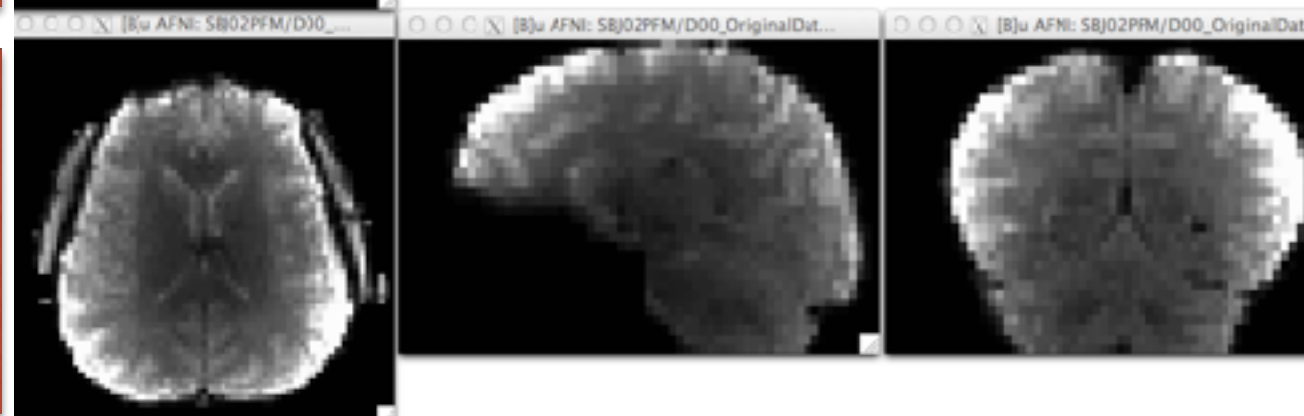
Compensation of motion effects: Volumetric realignment

- Translation ($\Delta x, \Delta y, \Delta z$) and rotation (yaw, pitch roll) to reference image

BEFORE CORRECTION



AFTER CORRECTION

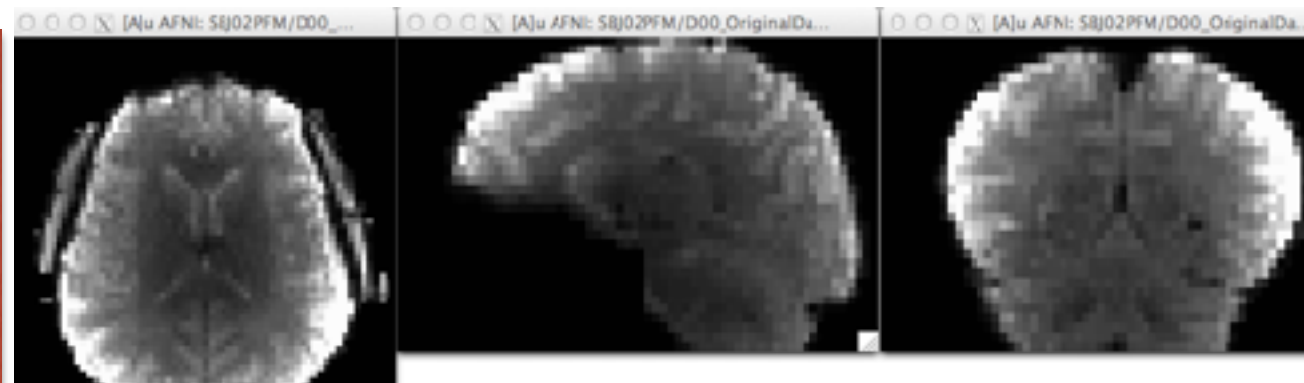


- Realignment does not fully compensate for motion-related signal changes. It cannot correct the data as if motion had never occurred.

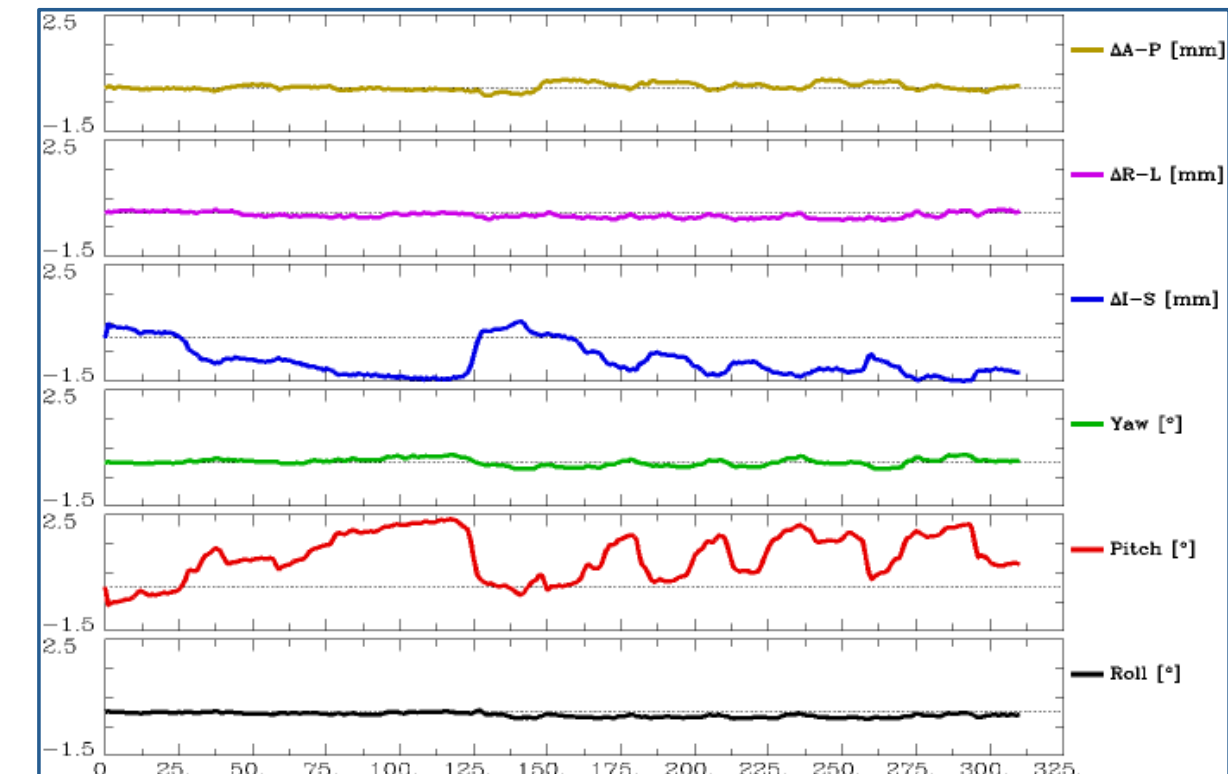
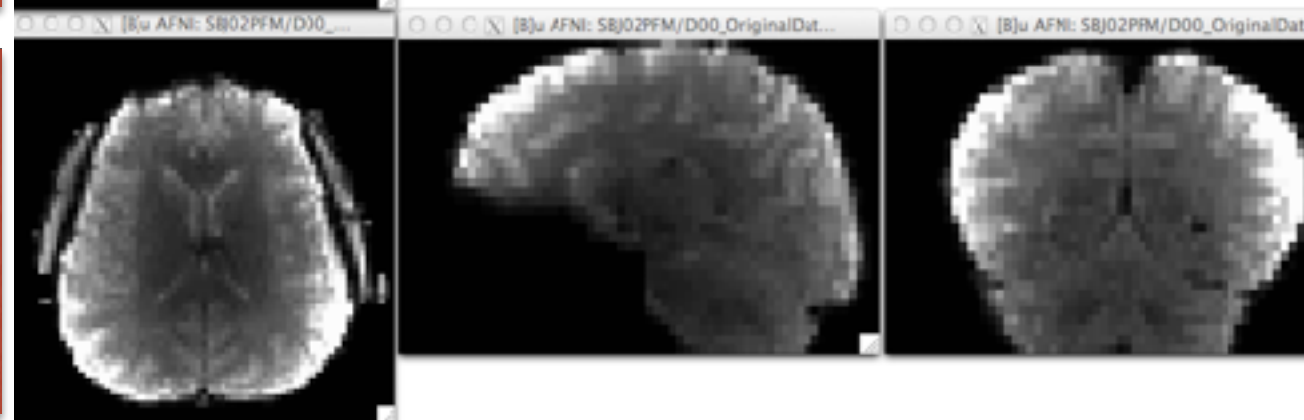
Compensation of motion effects: Volumetric realignment

- Translation ($\Delta x, \Delta y, \Delta z$) and rotation (yaw, pitch roll) to reference image

BEFORE CORRECTION



AFTER CORRECTION

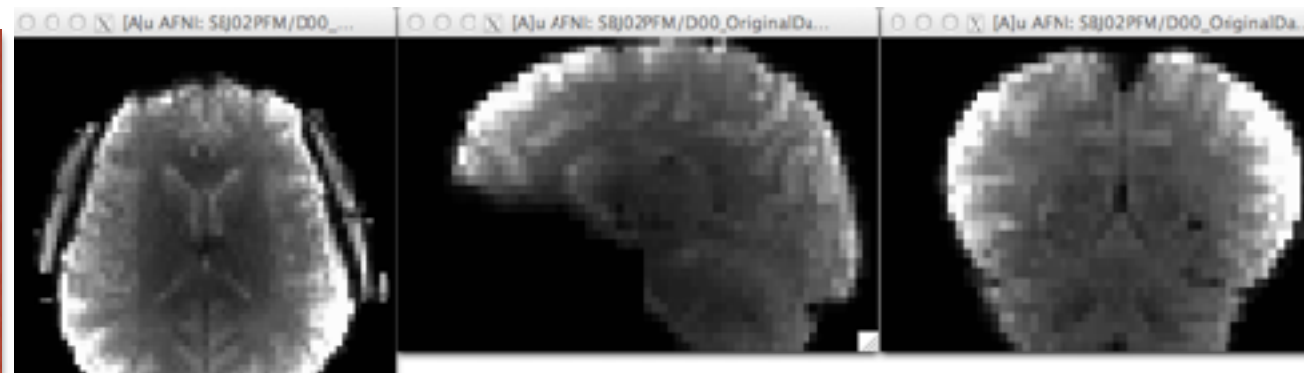


- Realignment does not fully compensate for motion-related signal changes. It cannot correct the data as if motion had never occurred.
- Slice-wise motion correction approaches are becoming increasingly effective for compensating within-volume motion , e.g. SLOMOCO (Beall and Lowe, 2014), using EEG-cap as motion sensor (Zotev et al., 2012),

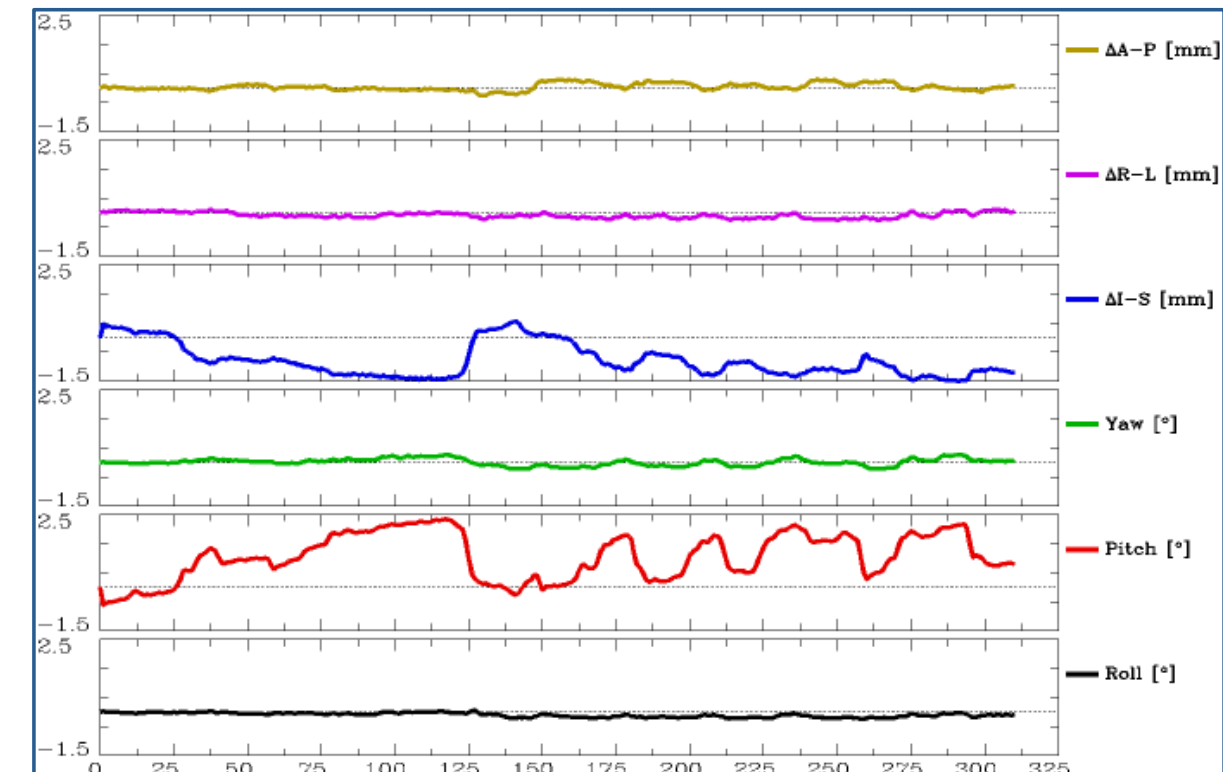
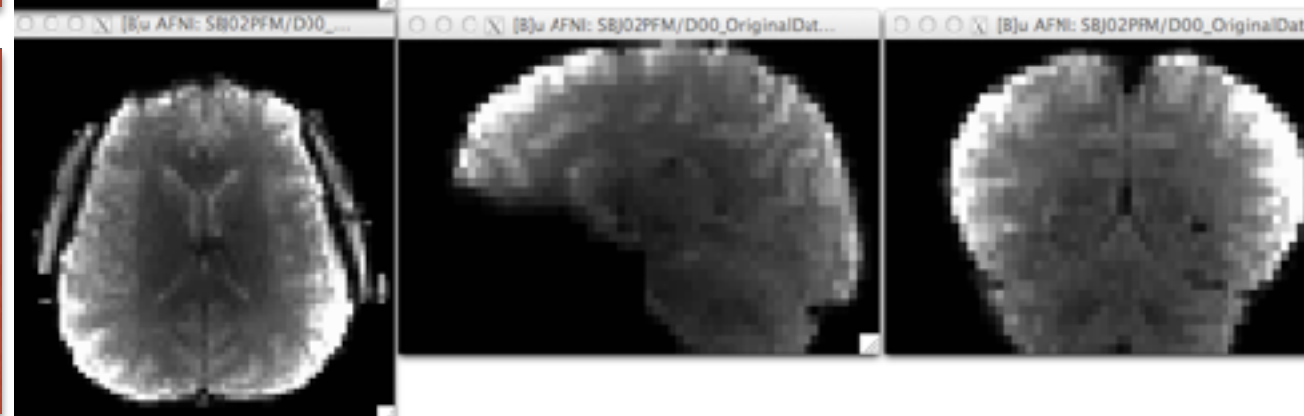
Compensation of motion effects: Volumetric realignment

- Translation ($\Delta x, \Delta y, \Delta z$) and rotation (yaw, pitch roll) to reference image

BEFORE CORRECTION



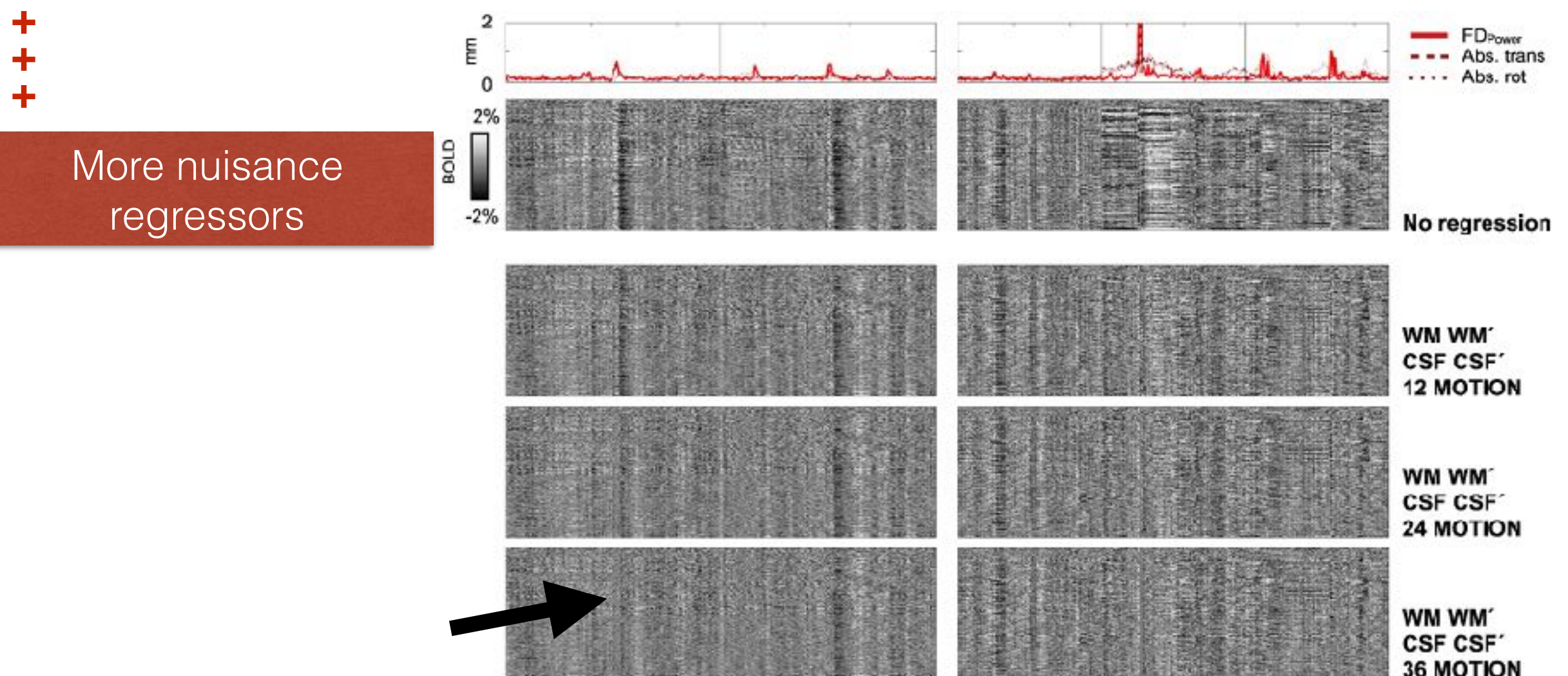
AFTER CORRECTION



- Realignment does not fully compensate for motion-related signal changes. It cannot correct the data as if motion had never occurred.
- Slice-wise motion correction approaches are becoming increasingly effective for compensating within-volume motion , e.g. SLOMOCO (Beall and Lowe, 2014), using EEG-cap as motion sensor (Zotev et al., 2012),
- Prospective motion correction (e.g. navigators or optical tracking systems) are also very effective ways of compensating motion occurring faster than the TR.

Compensation of motion effects: Volumetric realignment

- Realignment parameters: $R(t) = \{\Delta x, \Delta y, \Delta z, \text{yaw}, \text{pitch roll}\}$ → 6 regressors
- + the temporal derivatives: $R(t-1)$ → 12 regressors
- + the corresponding squares, i.e. $R^2(t)$ and $R^2(t-1)$ → 24 regressors
- + the second temporal derivative: $R(t-2)$ and $R^2(t-2)$ → 36 regressors



Compensation of motion effects: Volumetric realignment

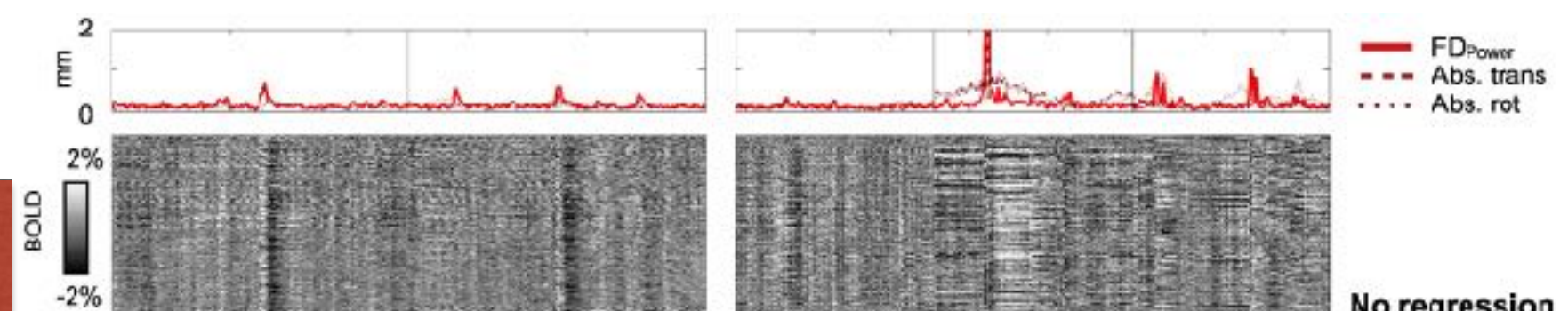
- Realignment parameters: $R(t) = \{\Delta x, \Delta y, \Delta z, \text{yaw}, \text{pitch roll}\}$ → 6 regressors
- + the temporal derivatives: $R(t-1)$ → 12 regressors
- + the corresponding squares, i.e. $R^2(t)$ and $R^2(t-1)$ → 24 regressors
- + the second temporal derivative: $R(t-2)$ and $R^2(t-2)$ → 36 regressors

+

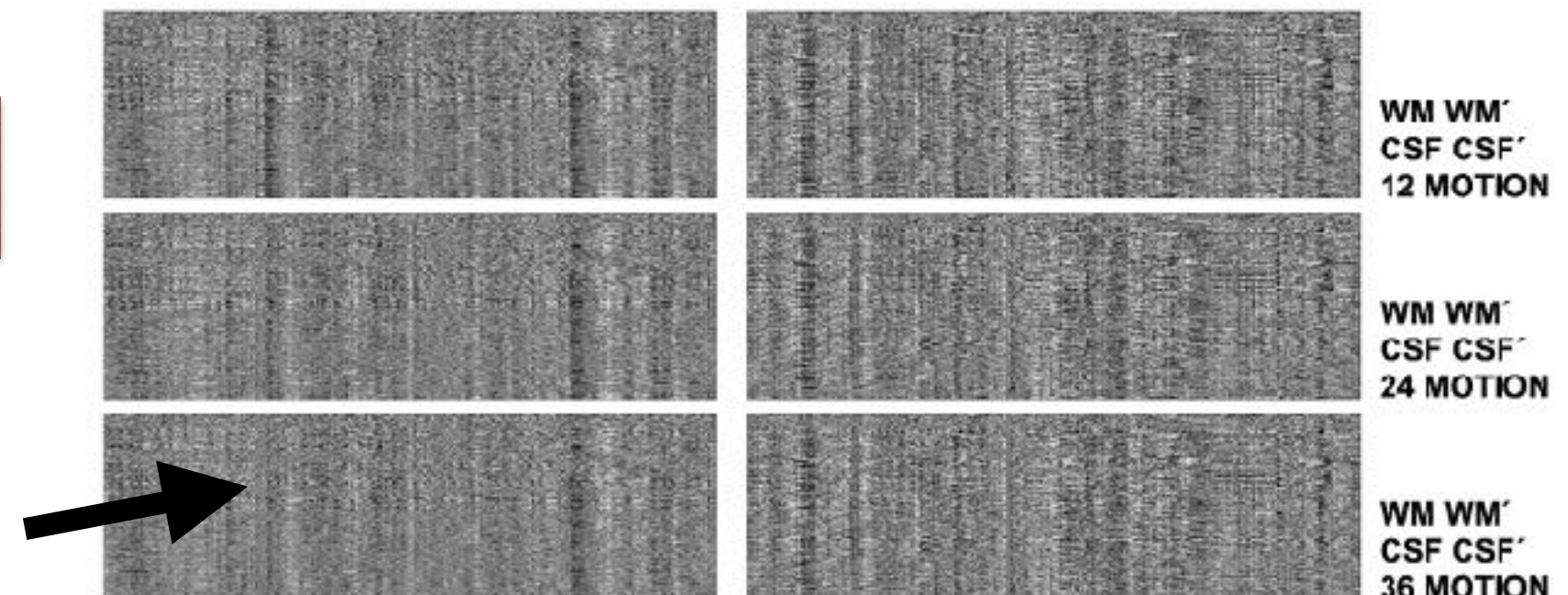
+

+

More nuisance
regressors



More loss of degrees of freedom



Compensation of motion effects: Volumetric realignment

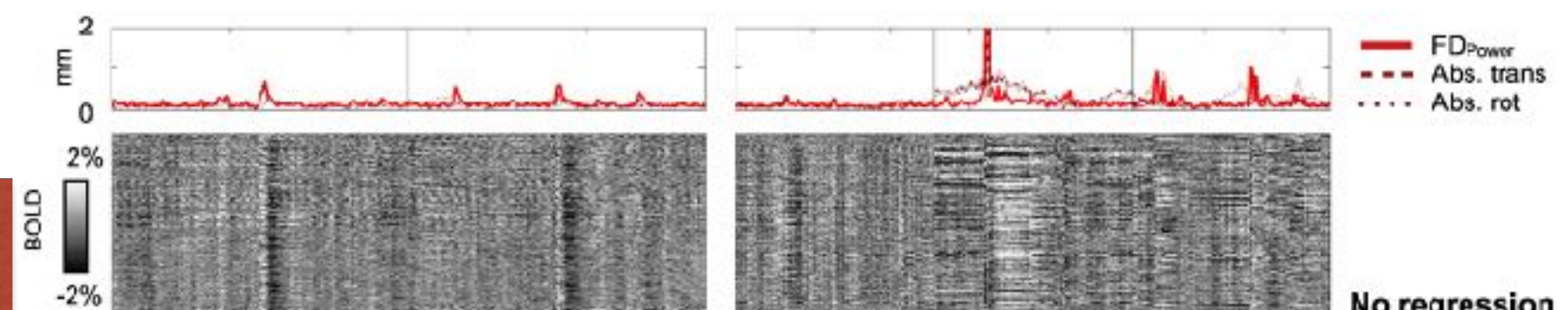
- Realignment parameters: $R(t) = \{\Delta x, \Delta y, \Delta z, \text{yaw}, \text{pitch roll}\}$ → 6 regressors
- + the temporal derivatives: $R(t-1)$ → 12 regressors
- + the corresponding squares, i.e. $R^2(t)$ and $R^2(t-1)$ → 24 regressors
- + the second temporal derivative: $R(t-2)$ and $R^2(t-2)$ → 36 regressors

+

+

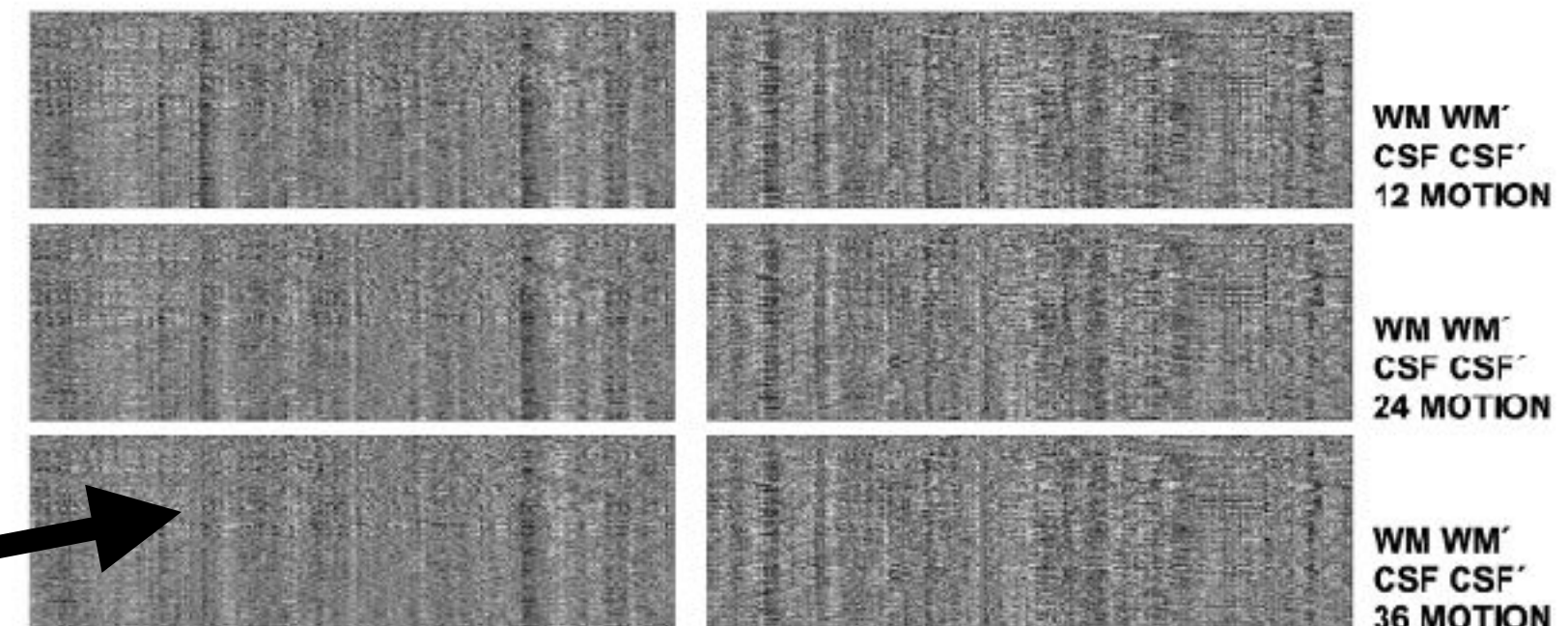
+

More nuisance regressors



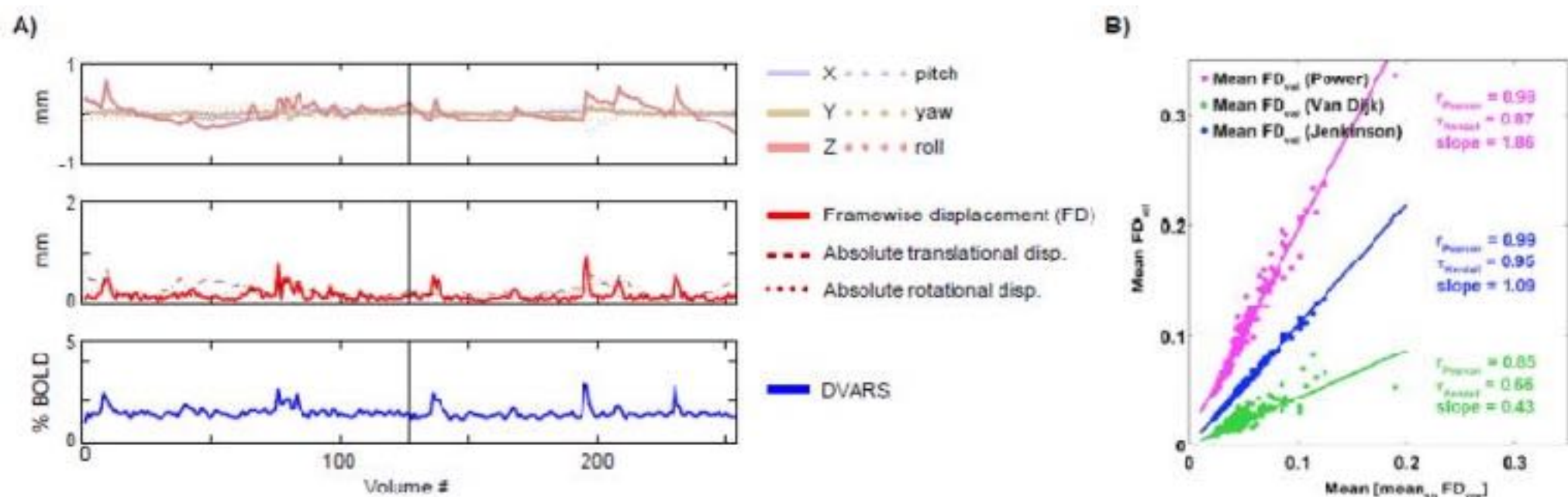
More loss of degrees of freedom

Less statistical confidence



Censoring and data interpolation

- **Censoring:** Nulling (or excluding) those scans with artefacts (e.g. due to excessive motion, hardware instabilities, etc.)
- Based on summary time courses computed from:
 - Realignment parameters: Framewise displacement (FD): **Multiple definitions.**
 - Directly from fMRI data
 - Number of spikes in the data (e.g. with 3dDespike function in AFNI)
 - DVARS: Root-mean square value of the differentiated fMRI signal

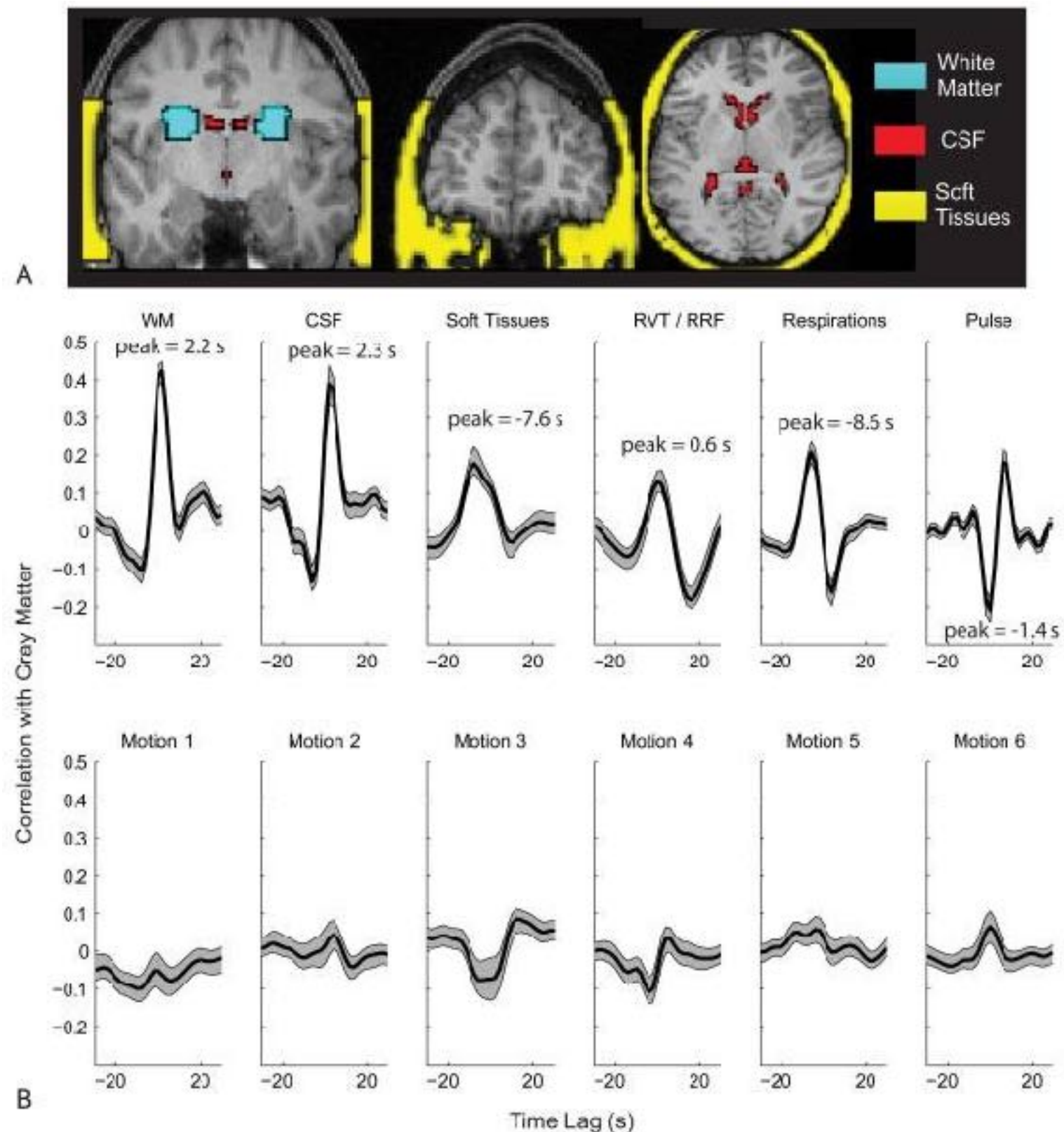


- **Interpolation:** Insertion of NEW data between scans affected by artefacts

Important to report methods used for censoring (criteria, threshold) and interpolation as well as the number of censored scans per subject or groups, and whether data was interpolated, zeroed, or nulled for subsequent analyses.

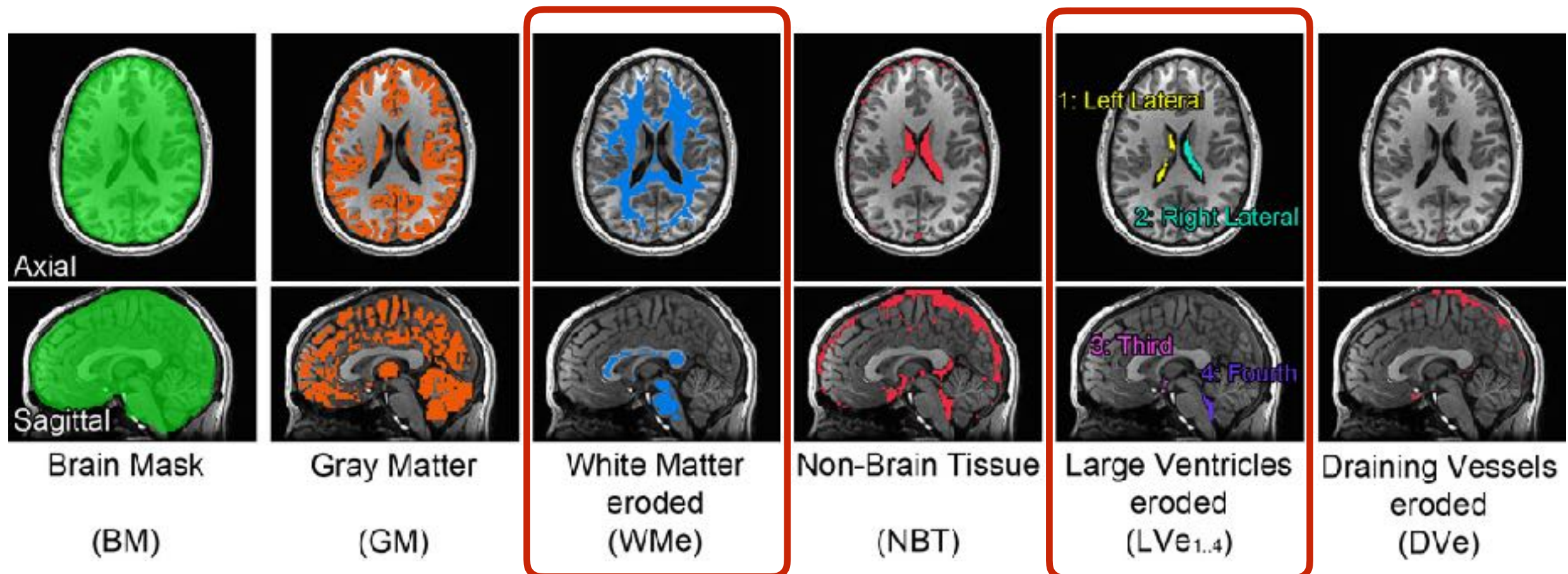
Phase-shifted Soft Tissue Regression (PSTCor)

- Lagged time series from:
 - white matter ROIs,
 - CSF from lateral ventricles
 - soft tissues (i.e. face, skull)
 - physiological signals
 - 6 realignment parameters.
- Optimal lags are chosen for maximum cross-correlation with average GM signal.



Component Based Noise Correction Method (CompCor)

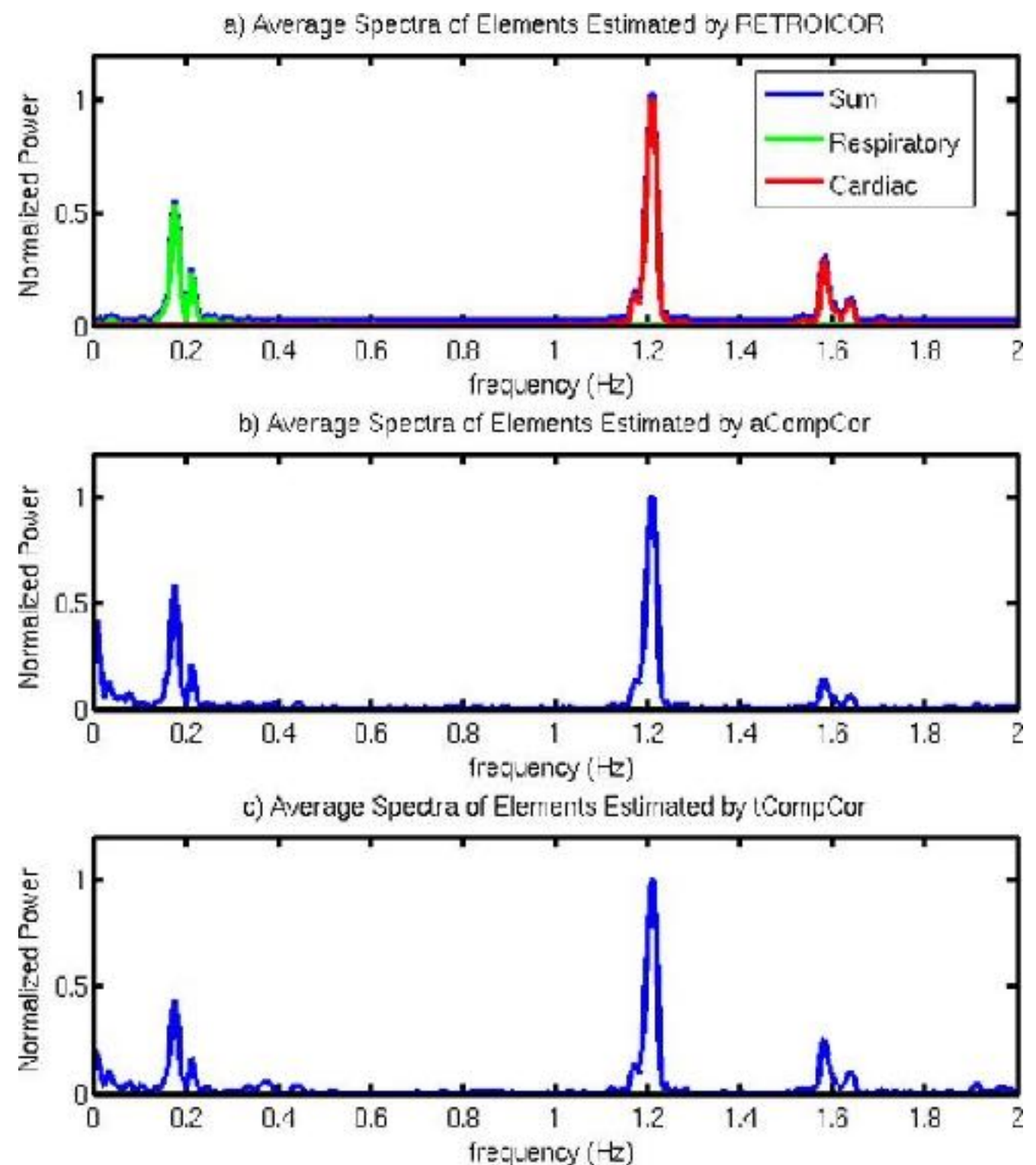
- Principal Components (PCs) explaining the highest variance from:
 - voxels with largest temporal standard-deviation (tCompCor)
 - voxels within eroded WM and ventricles CSF anatomical masks (aCompCor)
 - combination of both



Behzadi et al., (2007). A Component Based Noise Correction Method (CompCor) for BOLD and Perfusion Based fMRI. Neuroimage 37(1): 90-101.

Component Based Noise Correction Method (CompCor)

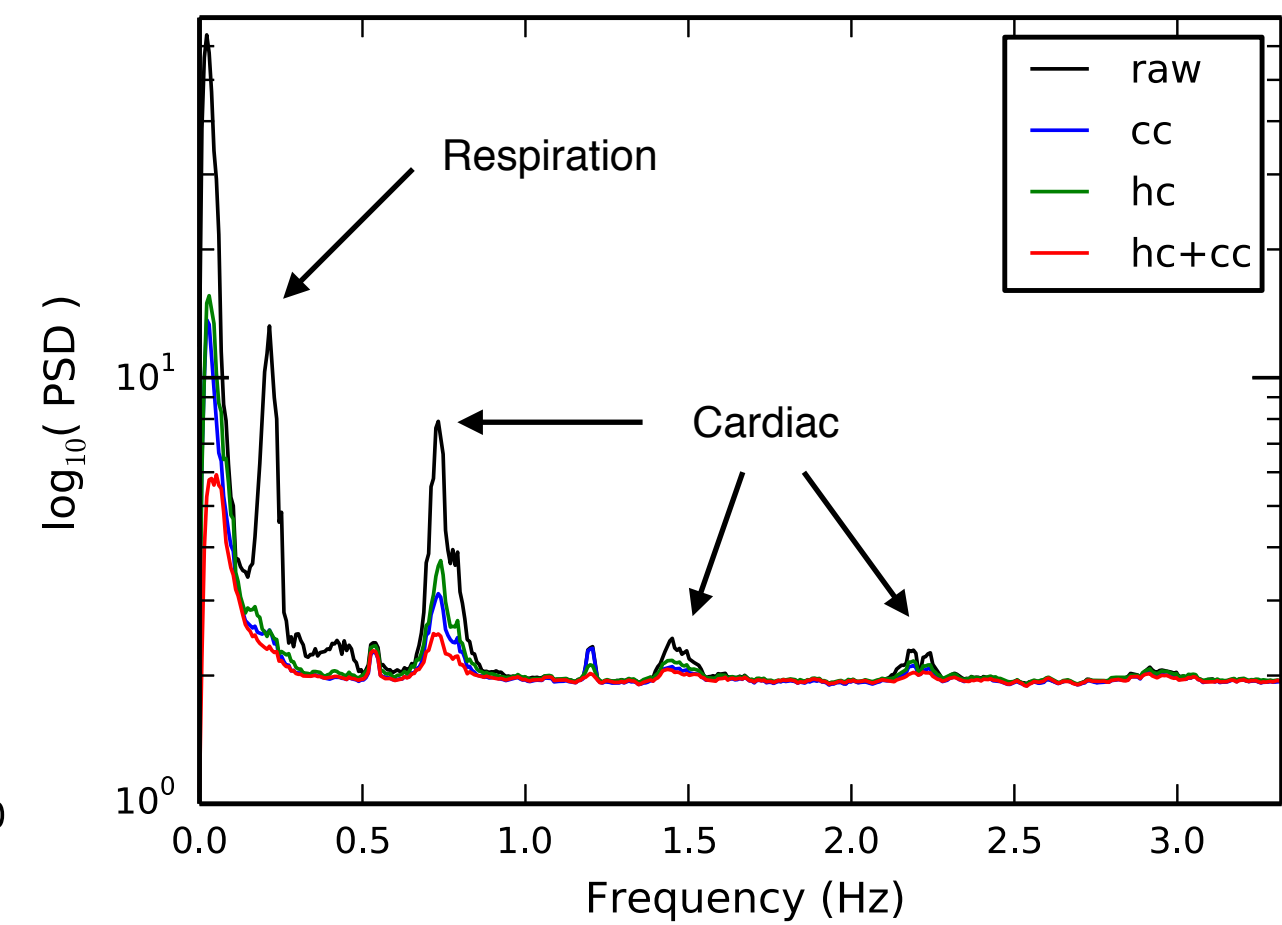
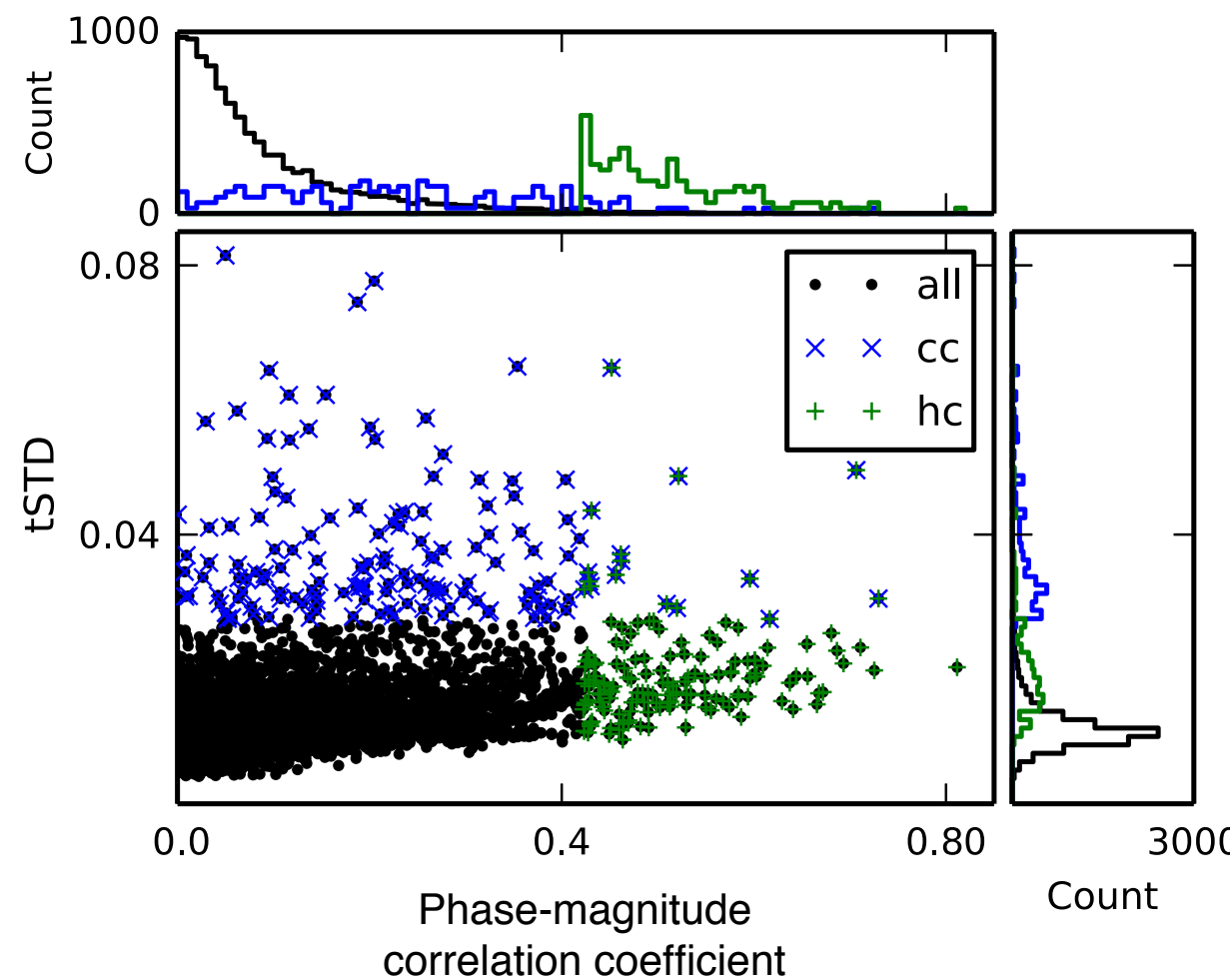
- Data driven approach: Only uses the fMRI data, as well as a anatomical segmentation in case of aCompCor
- It is able to account for physiological fluctuations without the need of external recordings.
- Determining the optimal number of PC is an open question (e.g. fixed number vs. % of variance) and the number depends on tissue.



Behzadi et al., (2007). A Component Based Noise Correction Method (CompCor) for BOLD and Perfusion Based fMRI. Neuroimage 37(1): 90-101.

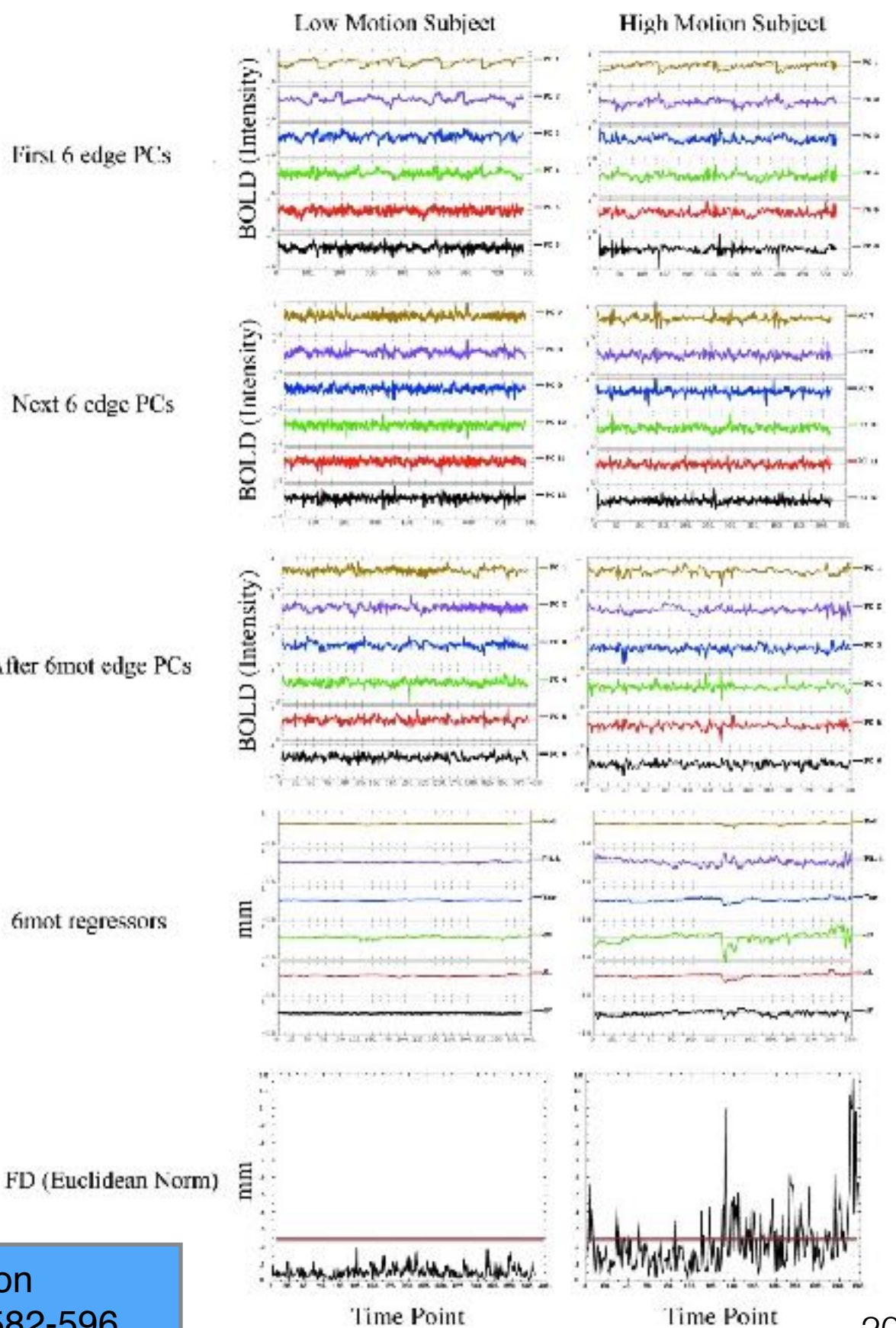
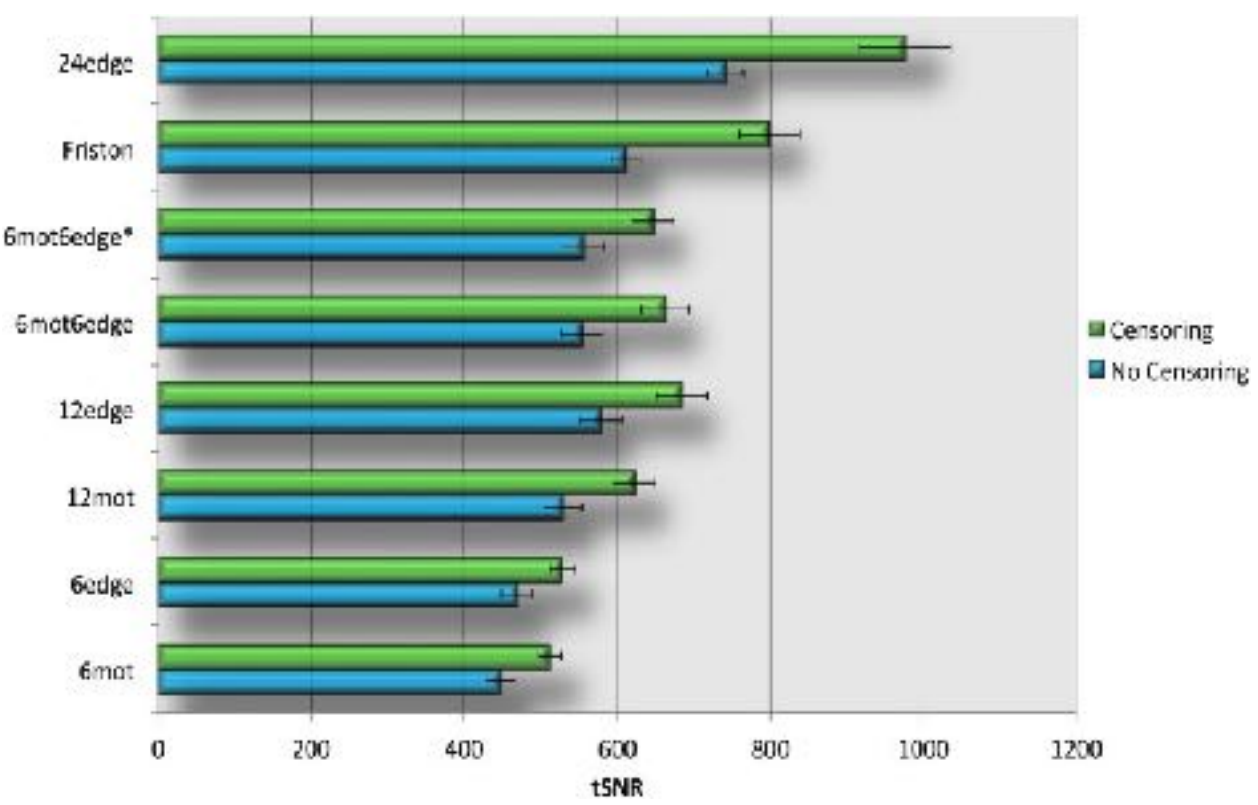
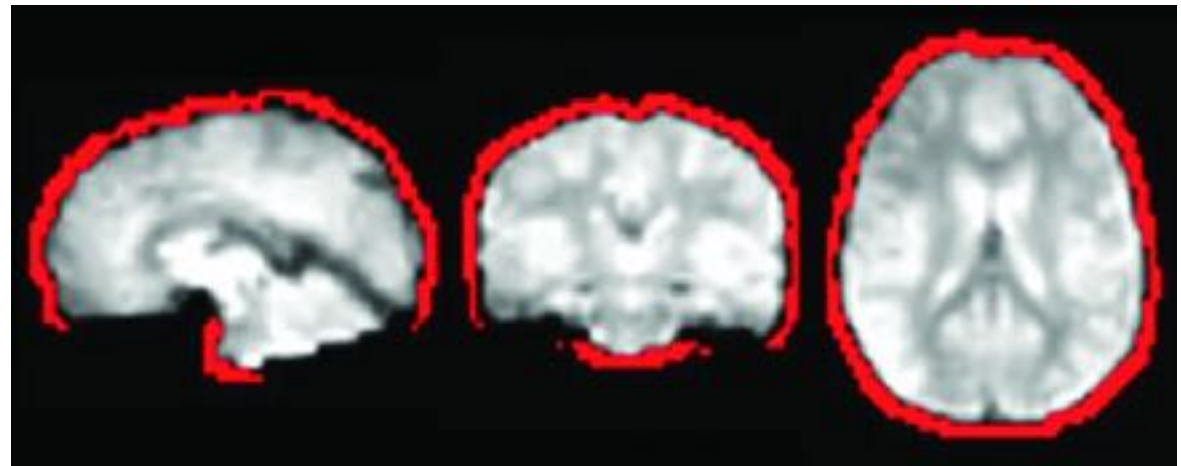
HighCor: PCA from phase-magnitude regression

- Principal components computed from voxels with high magnitude-phase correlation (HighCor) and/or high temporal standard deviation (tCompCor).
- Combination of Highcor and tCompCor further reduces temporal standard deviation, i.e. both sets of regressors account for different noises and artefacts.



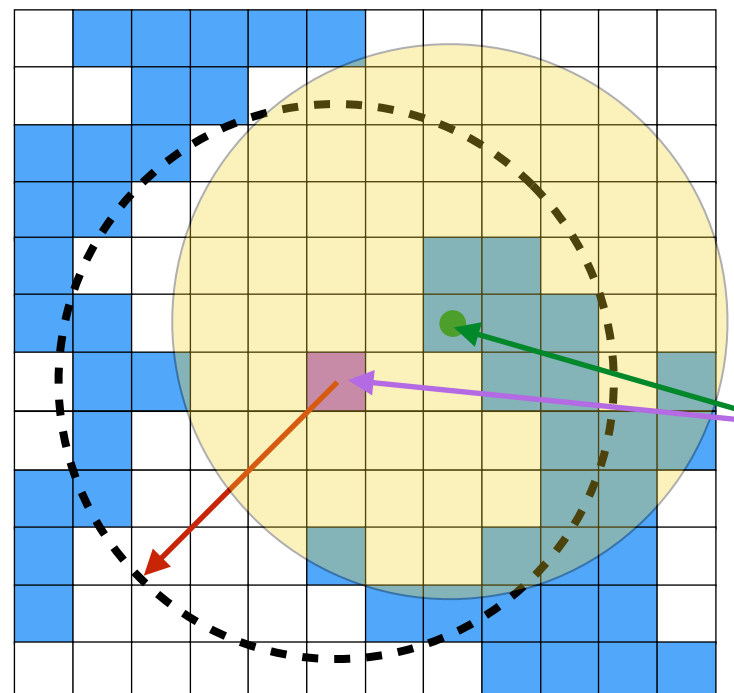
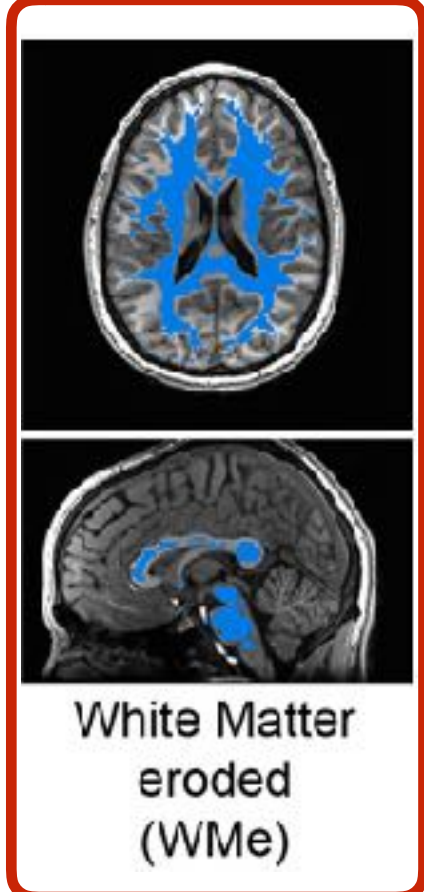
Edge Brain Voxels

- Nuisance regression employs the principal components with largest variance from voxels at the edges of the brain



Patriat et al., (2015). Using Edge Voxel Information to Improve Motion Regression for rs-fMRI Connectivity Studies. *Brain Connect.* 5(9): 582-596.

Anatomy-based Correlation Correction (ANATICOR)

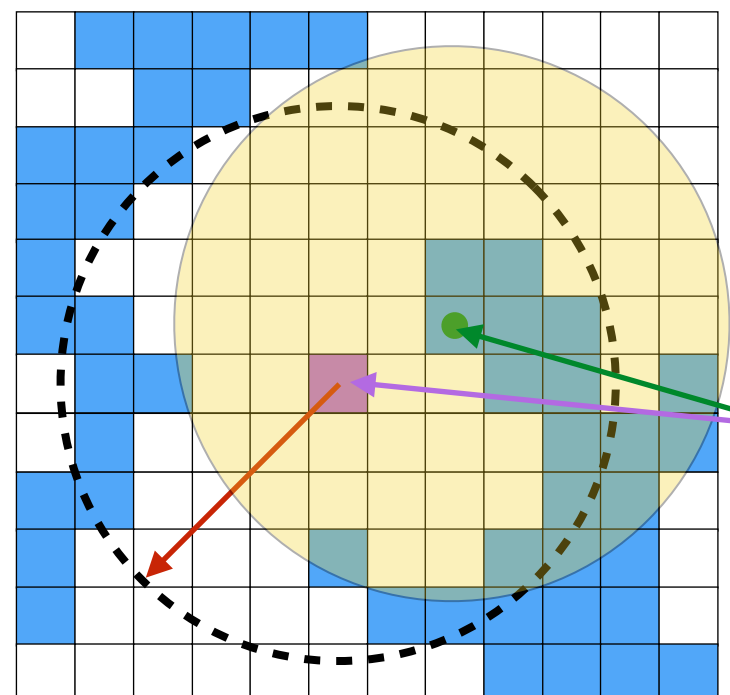
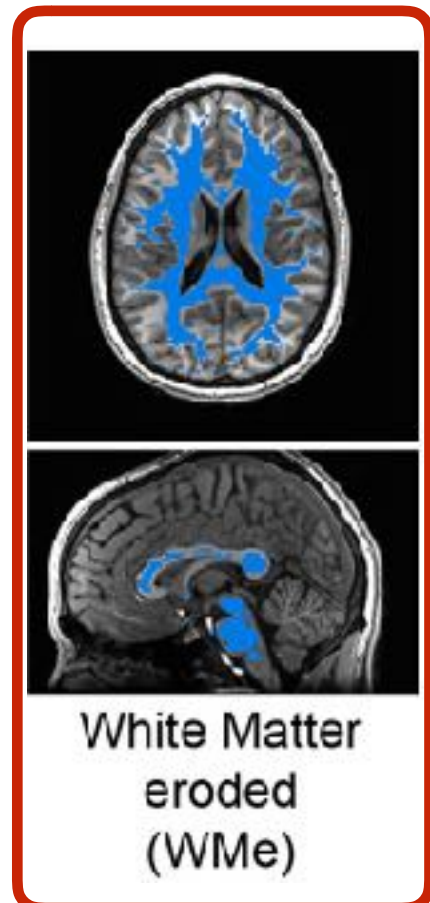


Average signal over
WMe voxels inside 20
mm radius

Voxel-dependent
nuisance regressors

Figure adapted from Box Cox (AFNI)

Anatomy-based Correlation Correction (ANATICOR)

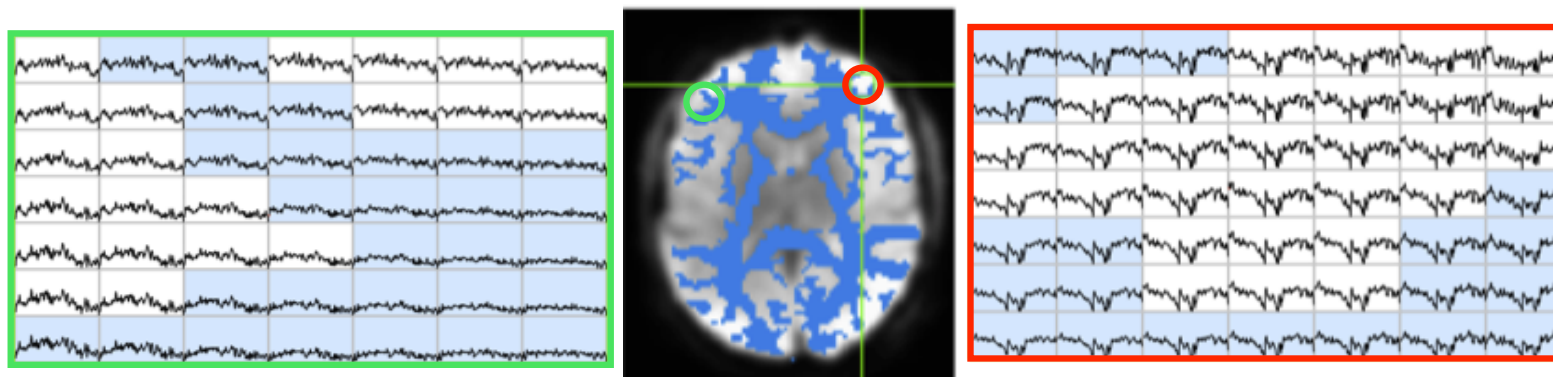


Average signal over
WMe voxels inside 20
mm radius

Voxel-dependent
nuisance regressors

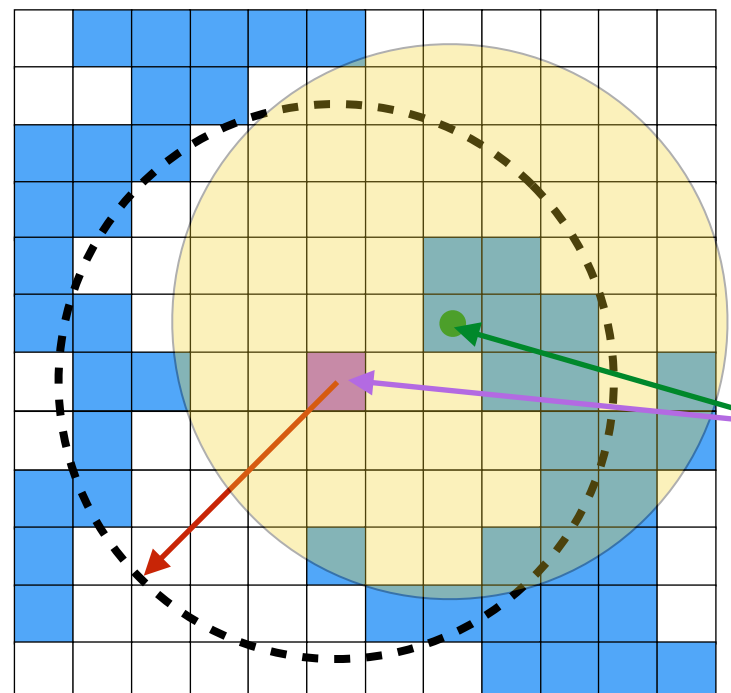
Figure adapted from Box Cox (AFNI)

LOCALIZED HARDWARE INSTABILITIES



Jo et al., (2010). Mapping Sources of Correlation in Resting State fMRI, with Artifact Detection and Removal. Neuroimage 52(2): 571–582.

Anatomy-based Correlation Correction (ANATICOR)

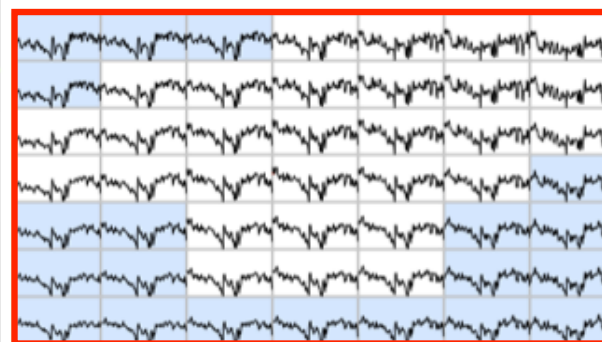
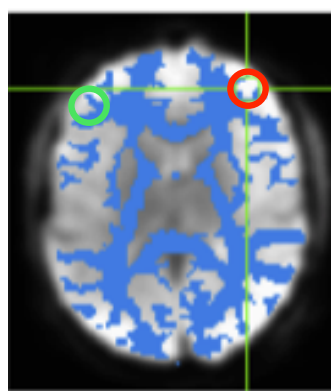
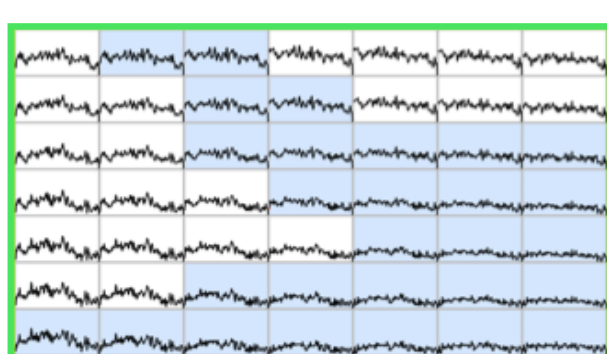


Average signal over
WMe voxels inside 20
mm radius

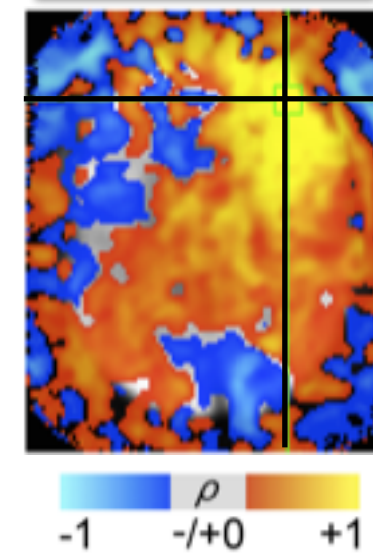
Voxel-dependent
nuisance regressors

Figure adapted from Box Cox (AFNI)

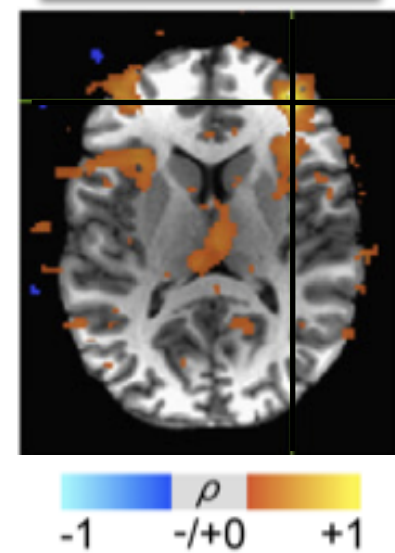
LOCALIZED HARDWARE INSTABILITIES



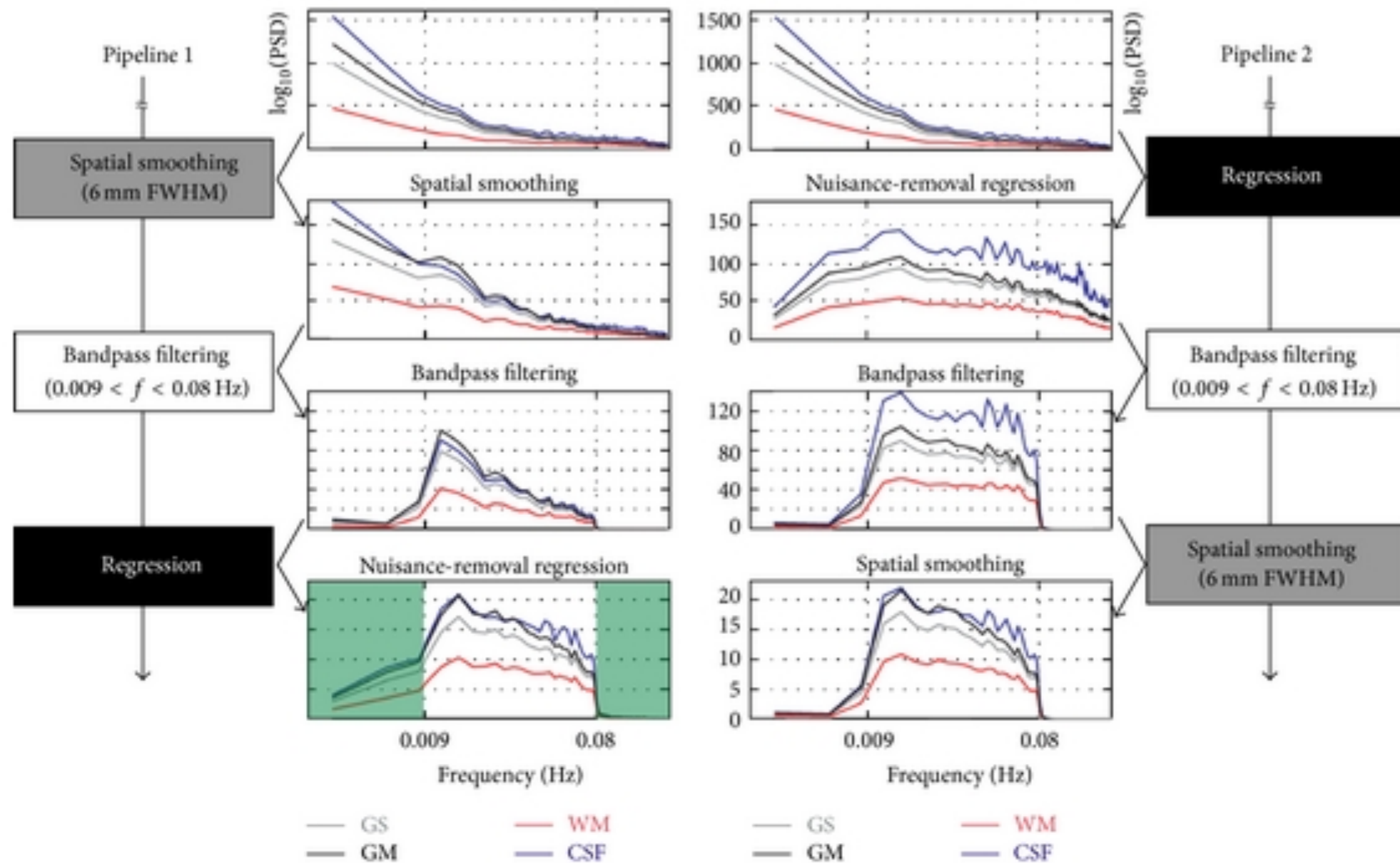
BEFORE
ANATICOR



AFTER
ANATICOR



All nuisance regression must be done in a single step!!

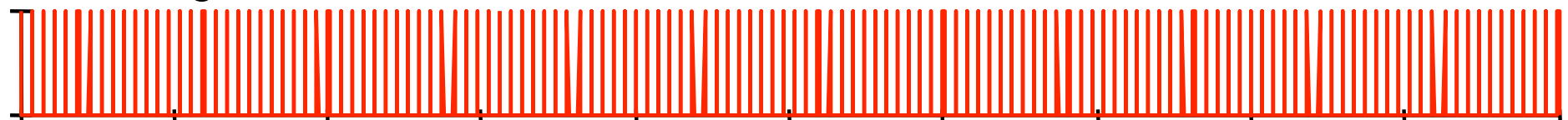


Group averaged power spectrum densities (PSD) of resting-state FMRI time series within brain tissues for each step in two different preprocessing orders. The improper processing order (pipeline 1) can reintroduce noise frequency components (signals of no interest) in lower frequency bands (Hz, the green-tinted area) and higher frequency bands

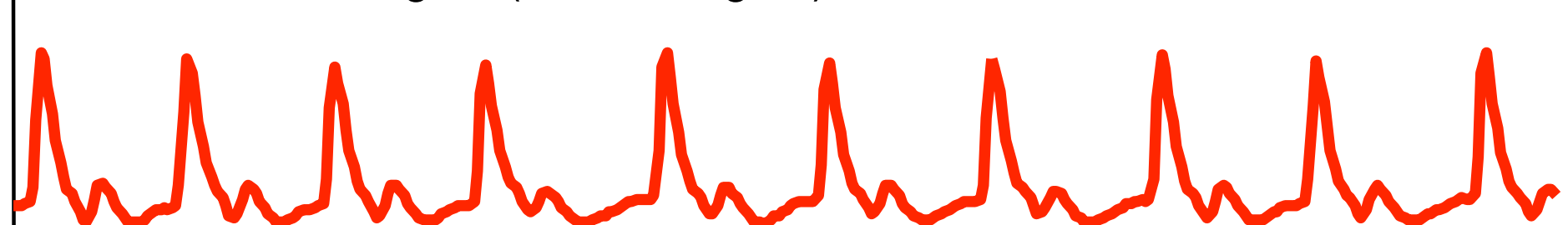
Denoising physiological noise with external recordings



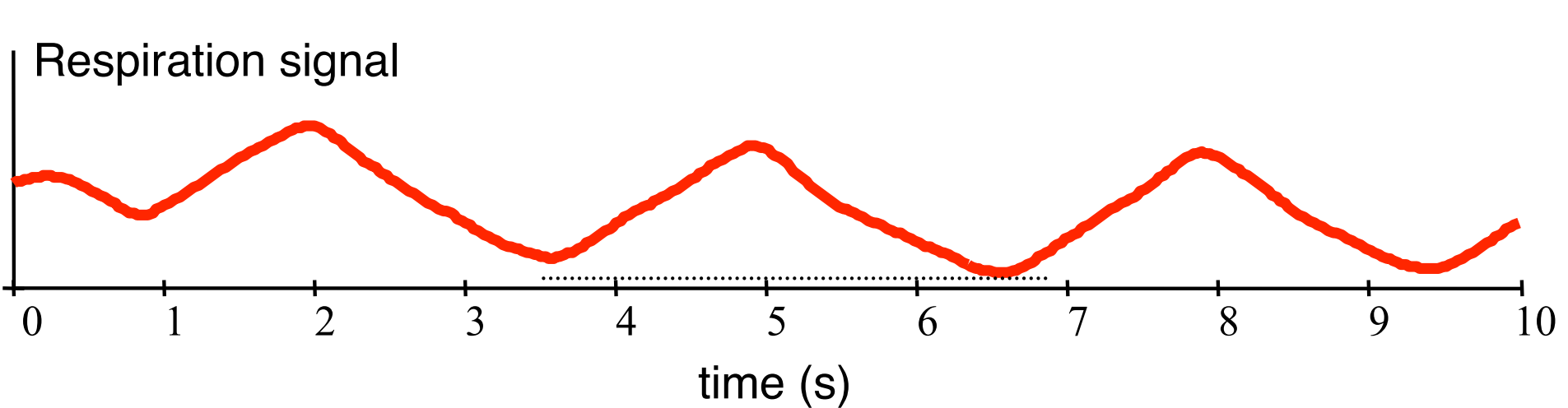
MR images



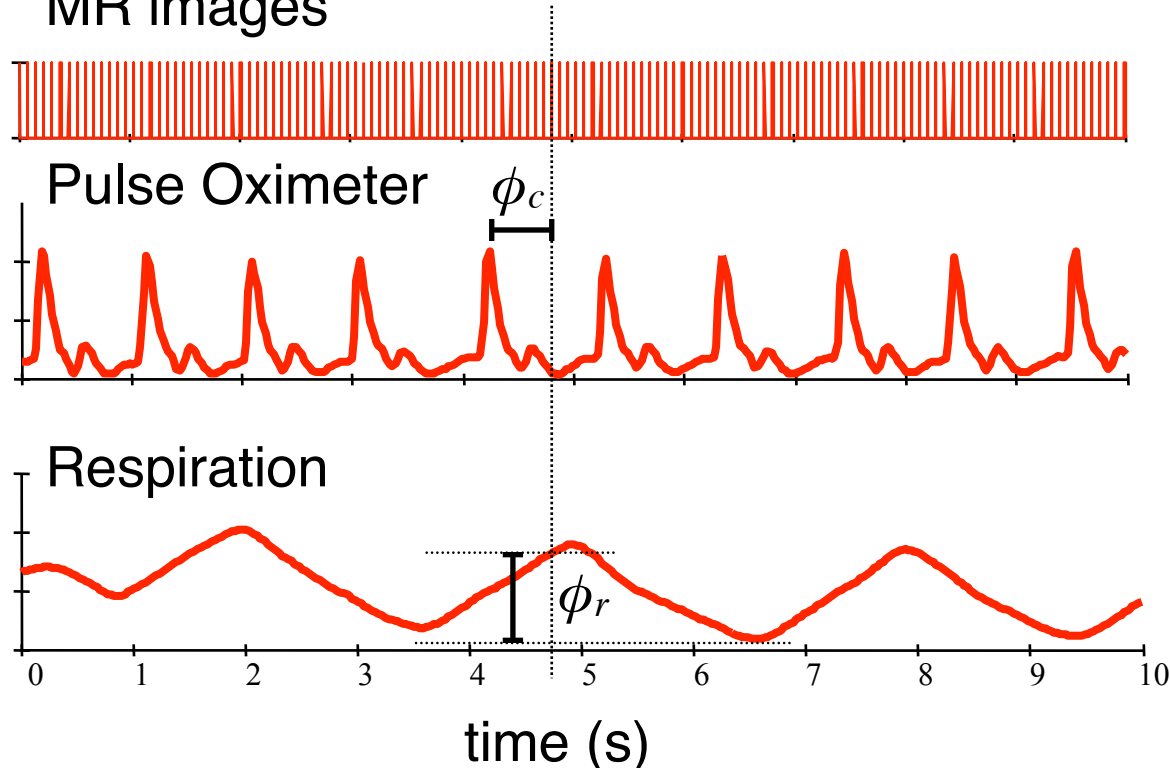
Pulse Oximeter signal (or ECG signal)



Respiration signal



MR images



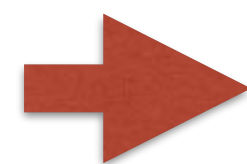
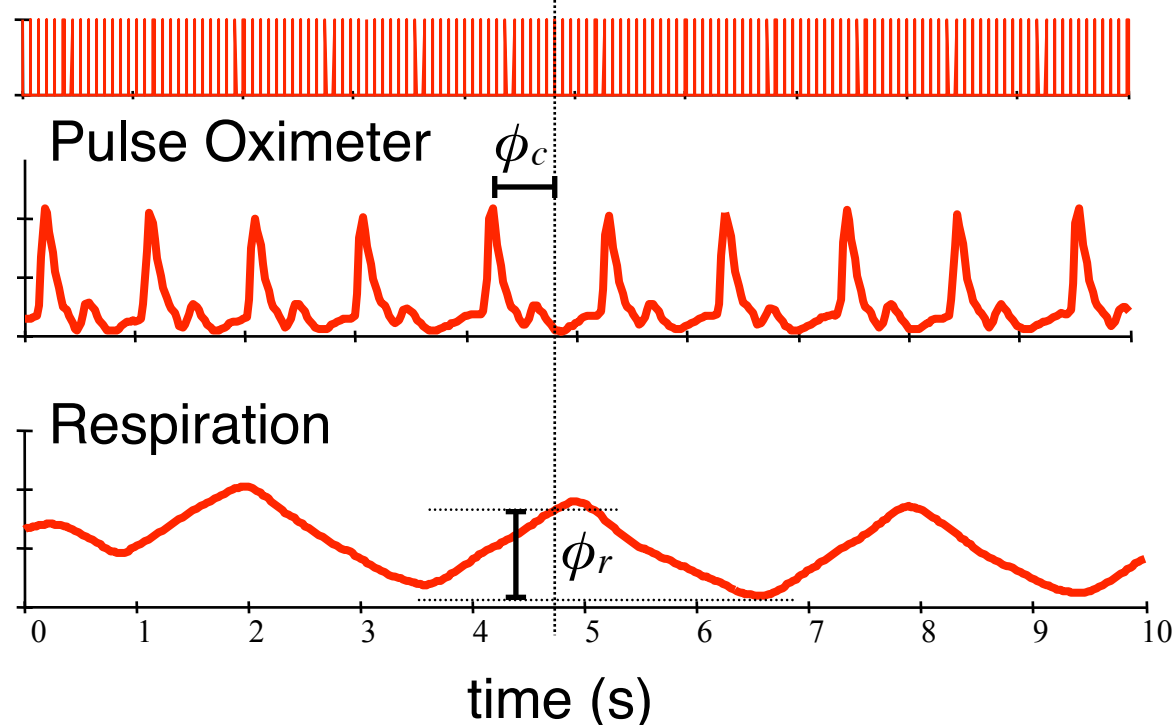
Figures courtesy of Rasmus Birn

$$\phi_c(t) = \frac{2\pi(t - t_1)}{t_2 - t_1}$$

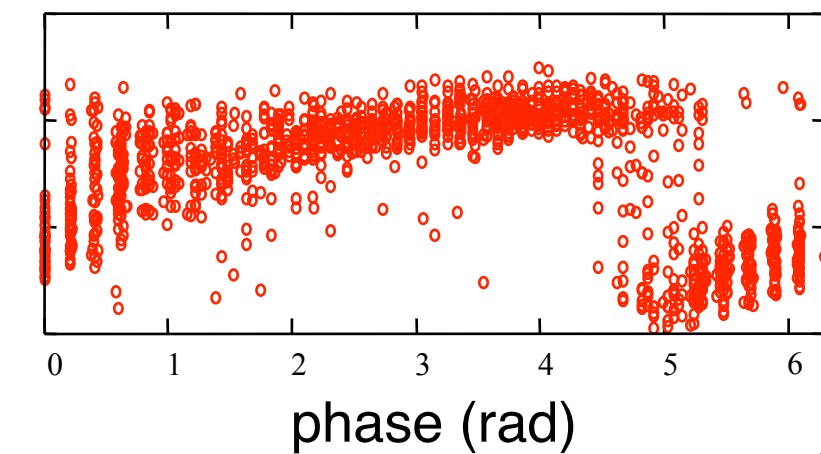
$$\phi_r(t) = \pi \frac{\sum_{b=1}^{\text{rnd}(R(t)/R_{max})} H(b)}{\sum_{b=1}^{100} H(b)} \text{sgn}\left(\frac{dR}{dt}\right)$$

RETROICOR

MR images



physio signal



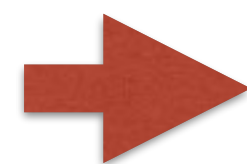
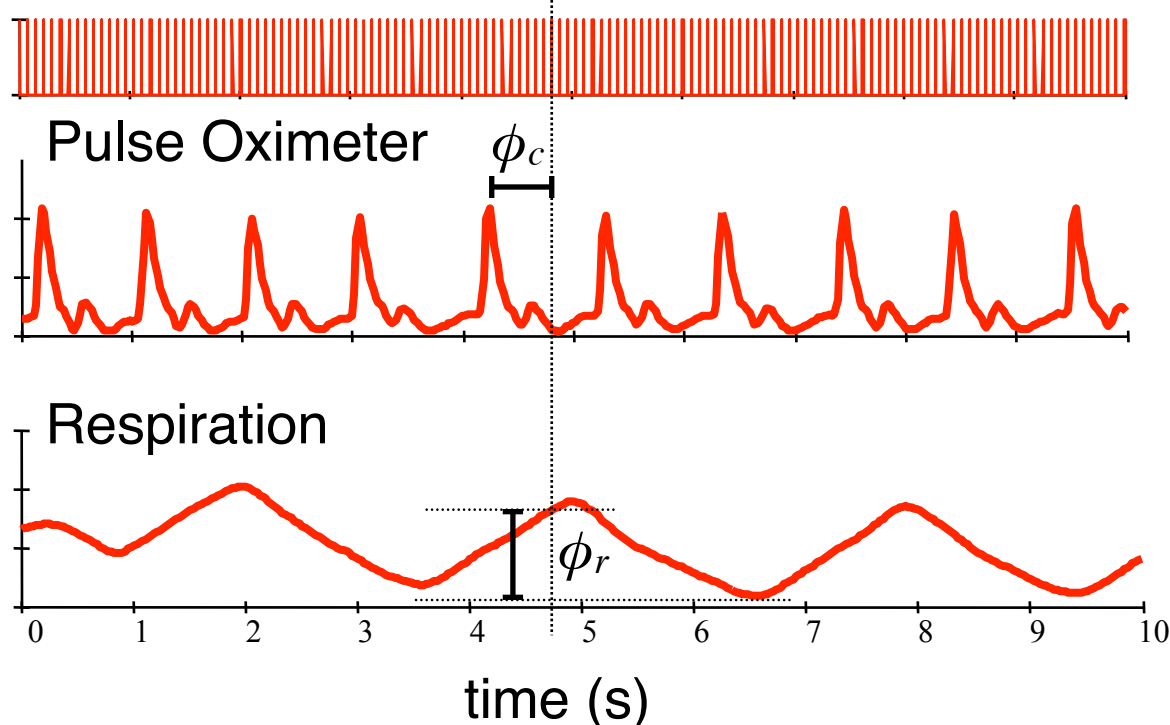
Figures courtesy of Rasmus Birn

$$\phi_c(t) = \frac{2\pi(t - t_1)}{t_2 - t_1}$$

$$\phi_r(t) = \pi \frac{\sum_{b=1}^{\text{rnd}(R(t)/R_{max})} H(b)}{\sum_{b=1}^{100} H(b)} \text{sgn}\left(\frac{dR}{dt}\right)$$

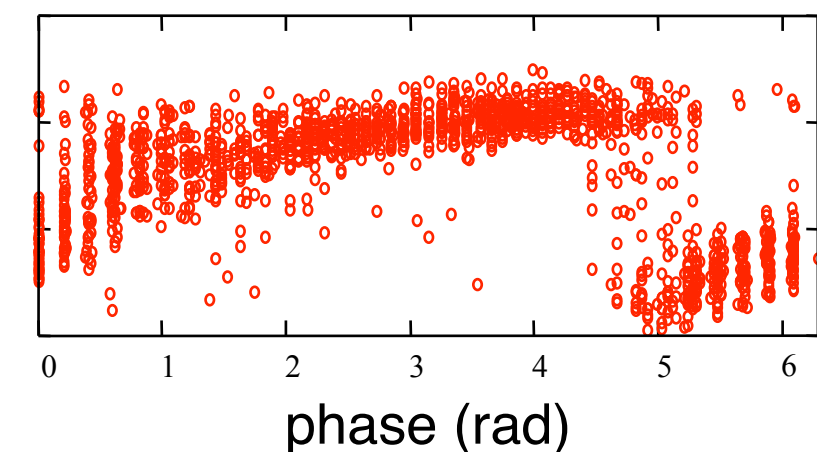
RETROICOR

MR images



Figures courtesy of Rasmus Birn

physio signal



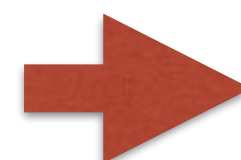
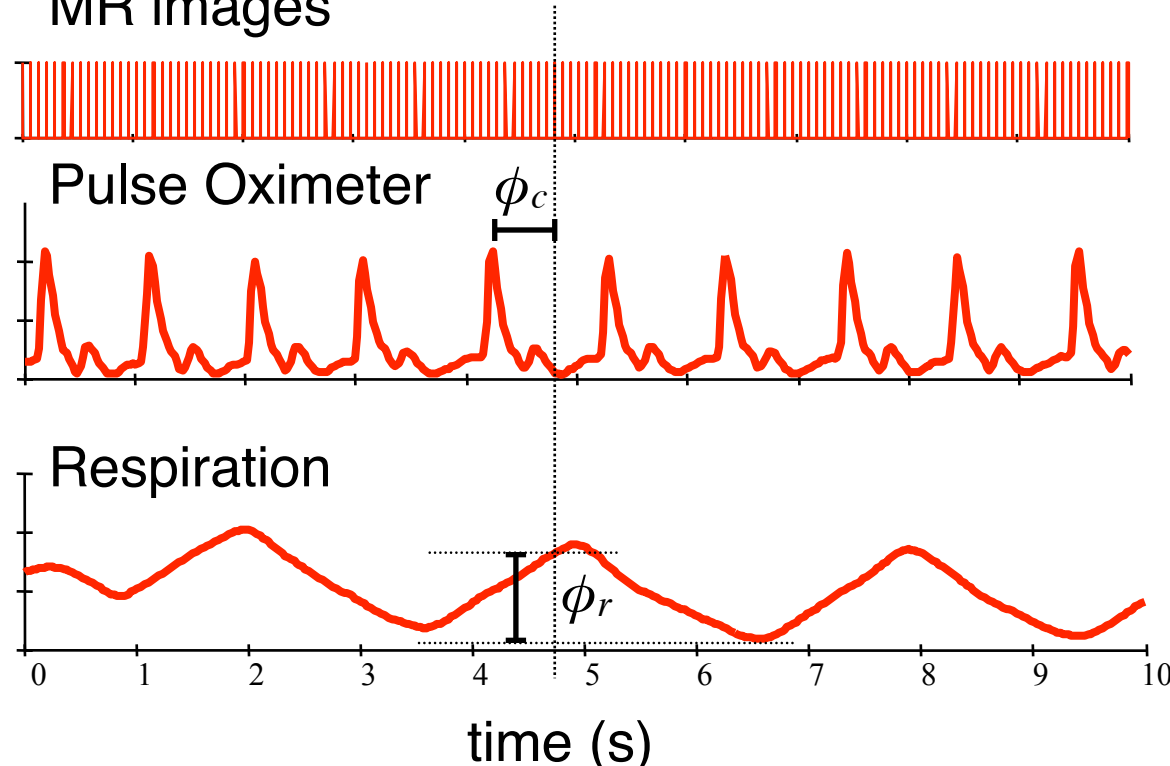
$$\phi_c(t) = \frac{2\pi(t - t_1)}{t_2 - t_1}$$

$$\phi_r(t) = \pi \frac{\sum_{b=1}^{\text{rnd}(R(t)/R_{max})} H(b)}{\sum_{b=1}^{100} H(b)} \text{sgn}\left(\frac{dR}{dt}\right)$$

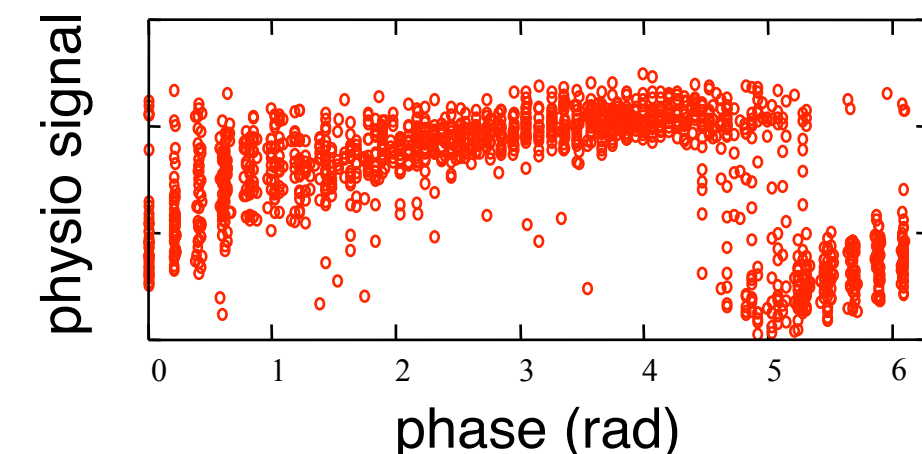
$$\left\{ \begin{array}{l} \cos(\phi_r) \\ \sin(\phi_r) \\ \cos(2\phi_r) \\ \sin(2\phi_r) \\ \cos(\phi_c) \\ \sin(\phi_c) \\ \cos(2\phi_c) \\ \sin(2\phi_c) \end{array} \right\}$$

RETROICOR

MR images



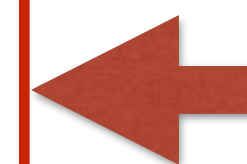
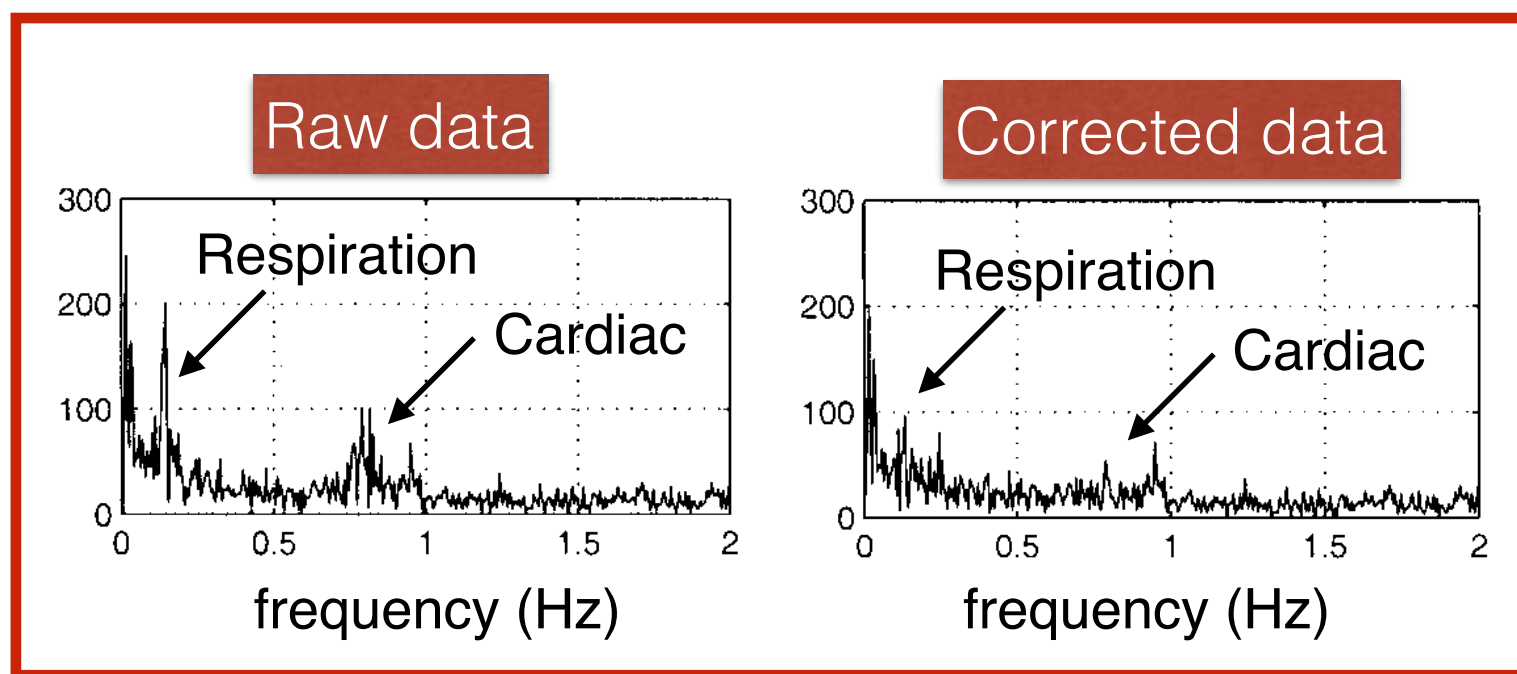
Figures courtesy of Rasmus Birn



$$\phi_c(t) = \frac{2\pi(t - t_1)}{t_2 - t_1}$$

$$\phi_r(t) = \pi \frac{\sum_{b=1}^{\text{rnd}(R(t)/R_{max})} H(b)}{\sum_{b=1}^{100} H(b)} \text{sgn}\left(\frac{dR}{dt}\right)$$

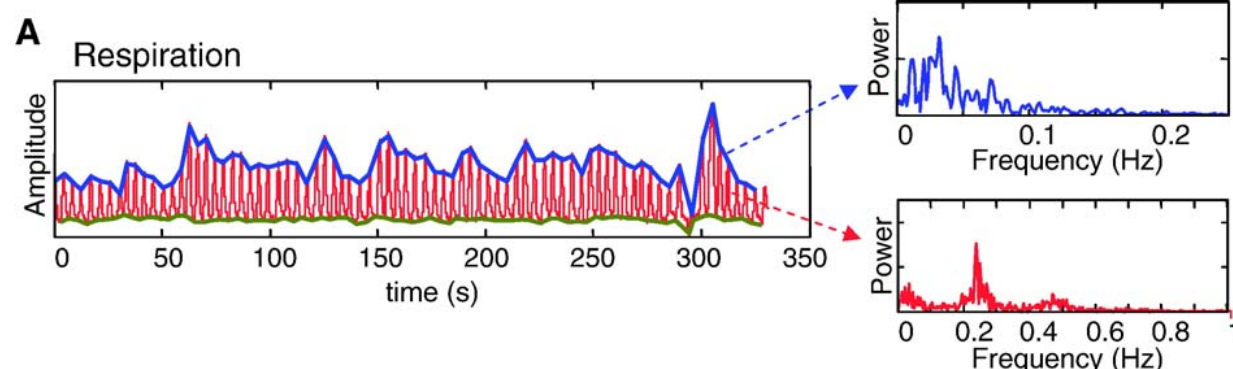
$$\left\{ \begin{array}{l} \cos(\phi_r) \\ \sin(\phi_r) \\ \cos(2\phi_r) \\ \sin(2\phi_r) \\ \cos(\phi_c) \\ \sin(\phi_c) \\ \cos(2\phi_c) \\ \sin(2\phi_c) \end{array} \right\}$$



Low frequency fluctuations in respiratory volume (RVT)

- Variations in respiratory rate can be reduced by regressing out changes in respiratory volume (RVT) that are assumed to correlate with fluctuations in arterial CO₂ concentrations.

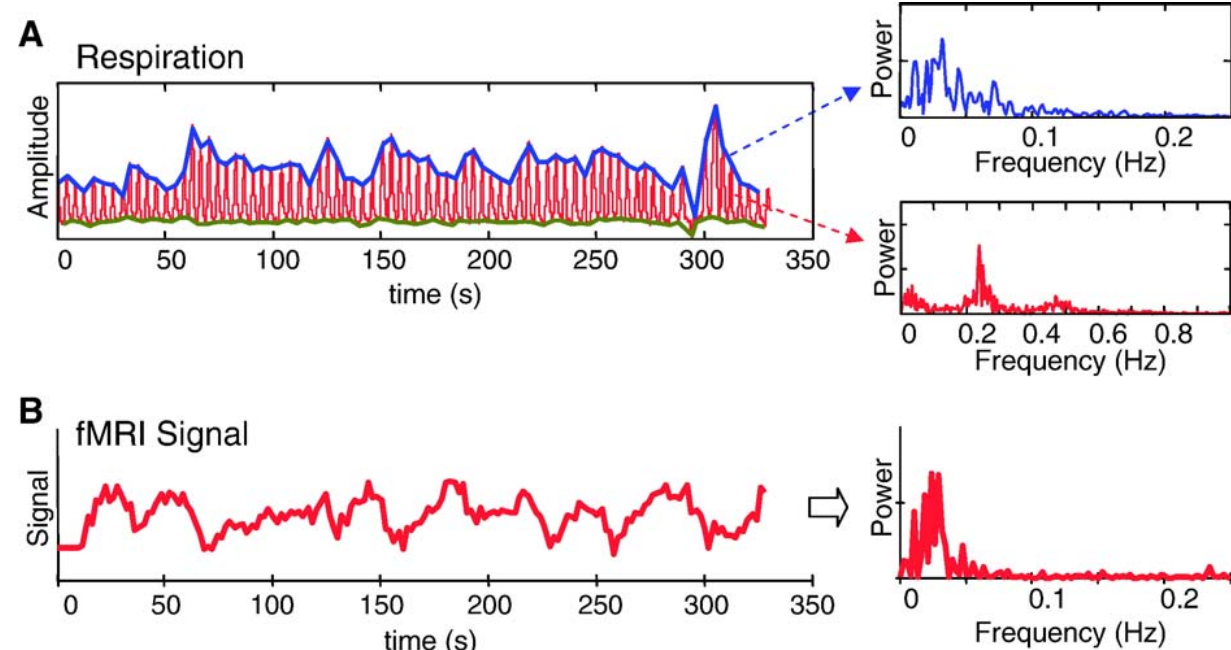
Regular Breathing



Low frequency fluctuations in respiratory volume (RVT)

- Variations in respiratory rate can be reduced by regressing out changes in respiratory volume (RVT) that are assumed to correlate with fluctuations in arterial CO₂ concentrations.

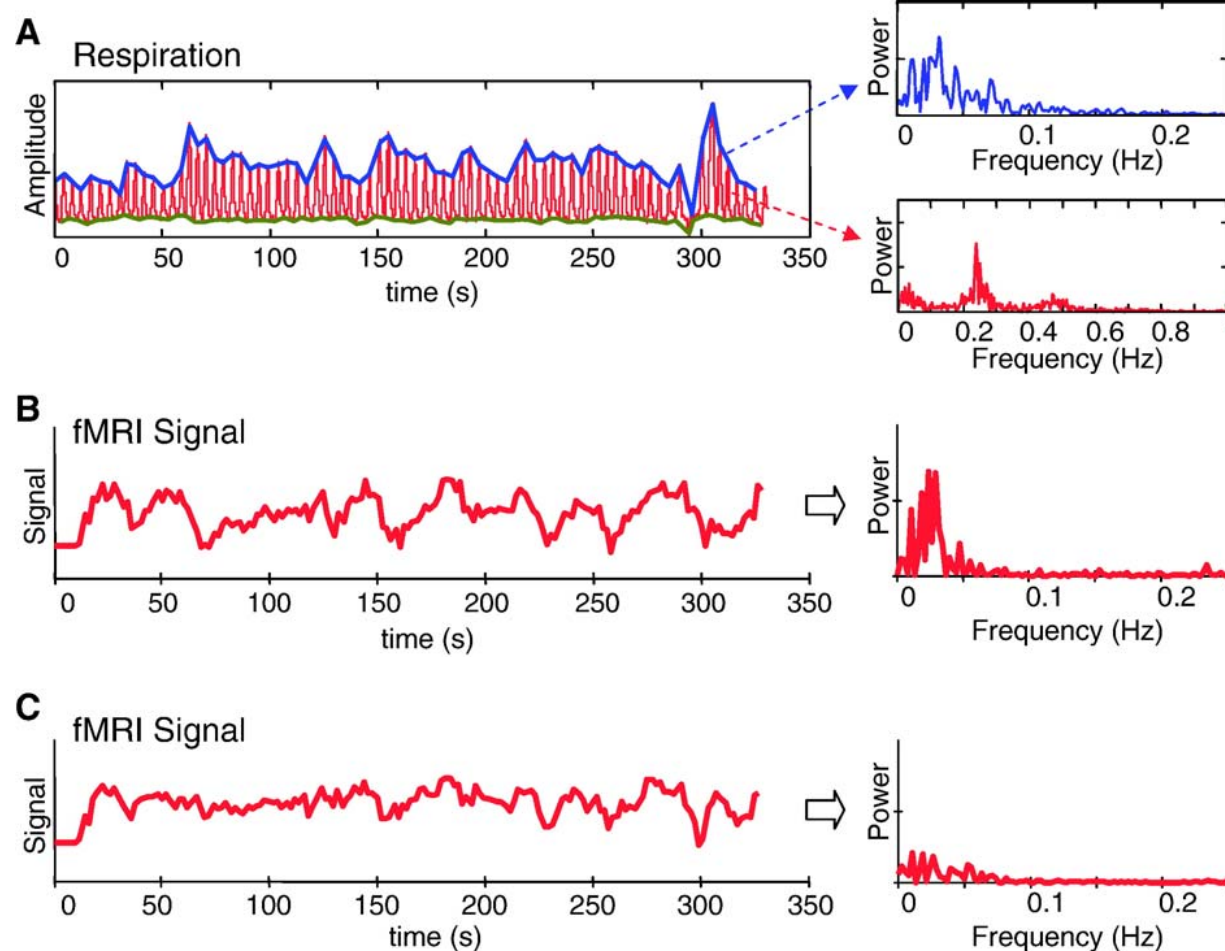
Regular Breathing



Low frequency fluctuations in respiratory volume (RVT)

- Variations in respiratory rate can be reduced by regressing out changes in respiratory volume (RVT) that are assumed to correlate with fluctuations in arterial CO₂ concentrations.

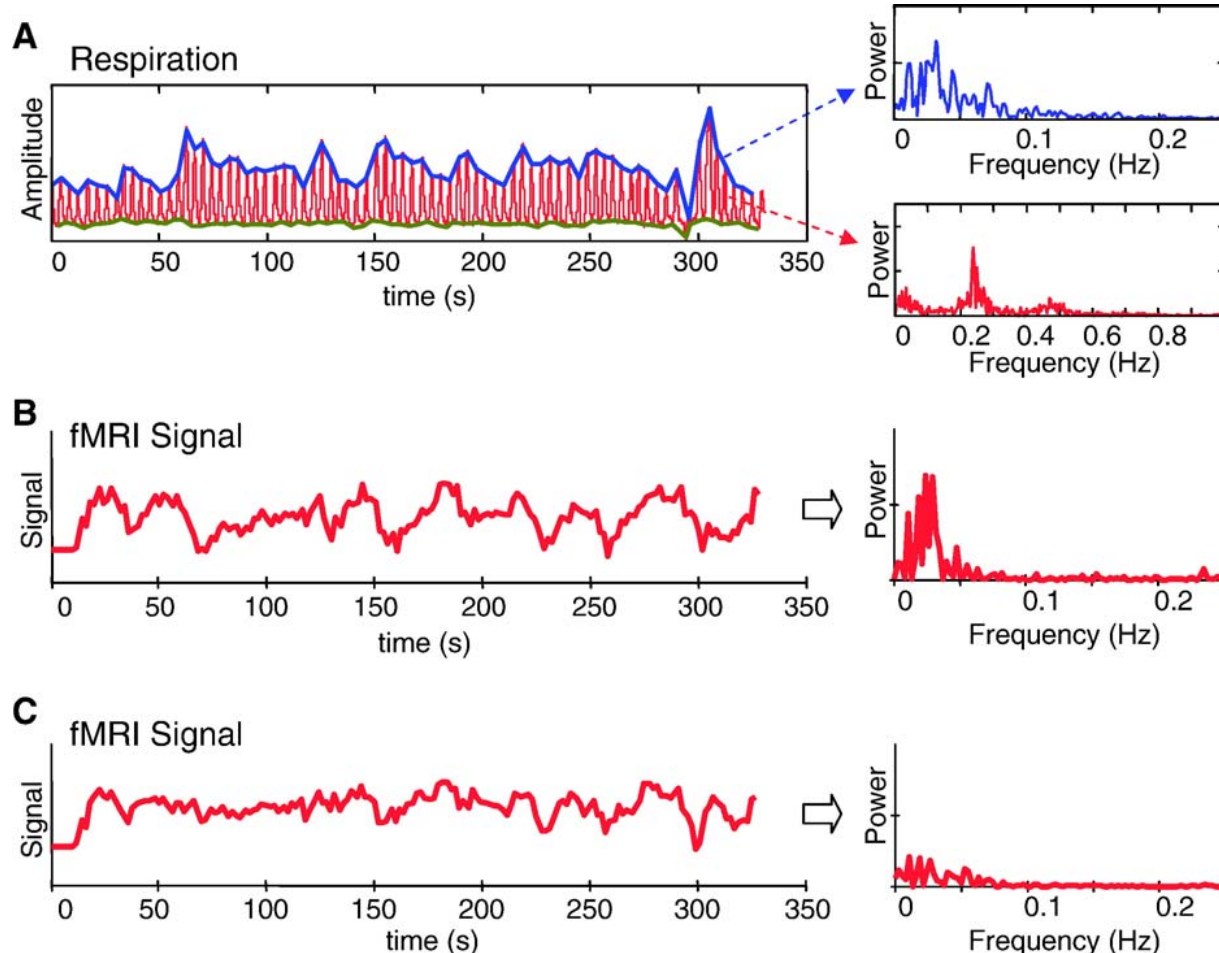
Regular Breathing



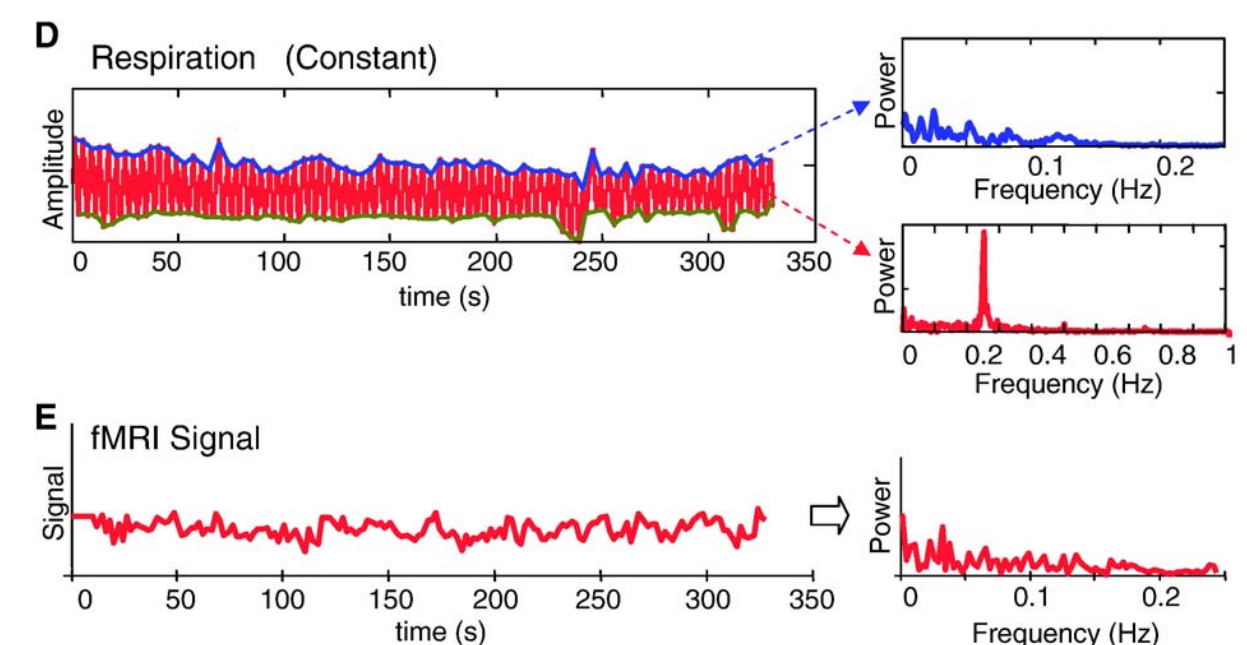
Low frequency fluctuations in respiratory volume (RVT)

- Variations in respiratory rate can be reduced by regressing out changes in respiratory volume (RVT) that are assumed to correlate with fluctuations in arterial CO₂ concentrations.

Regular Breathing

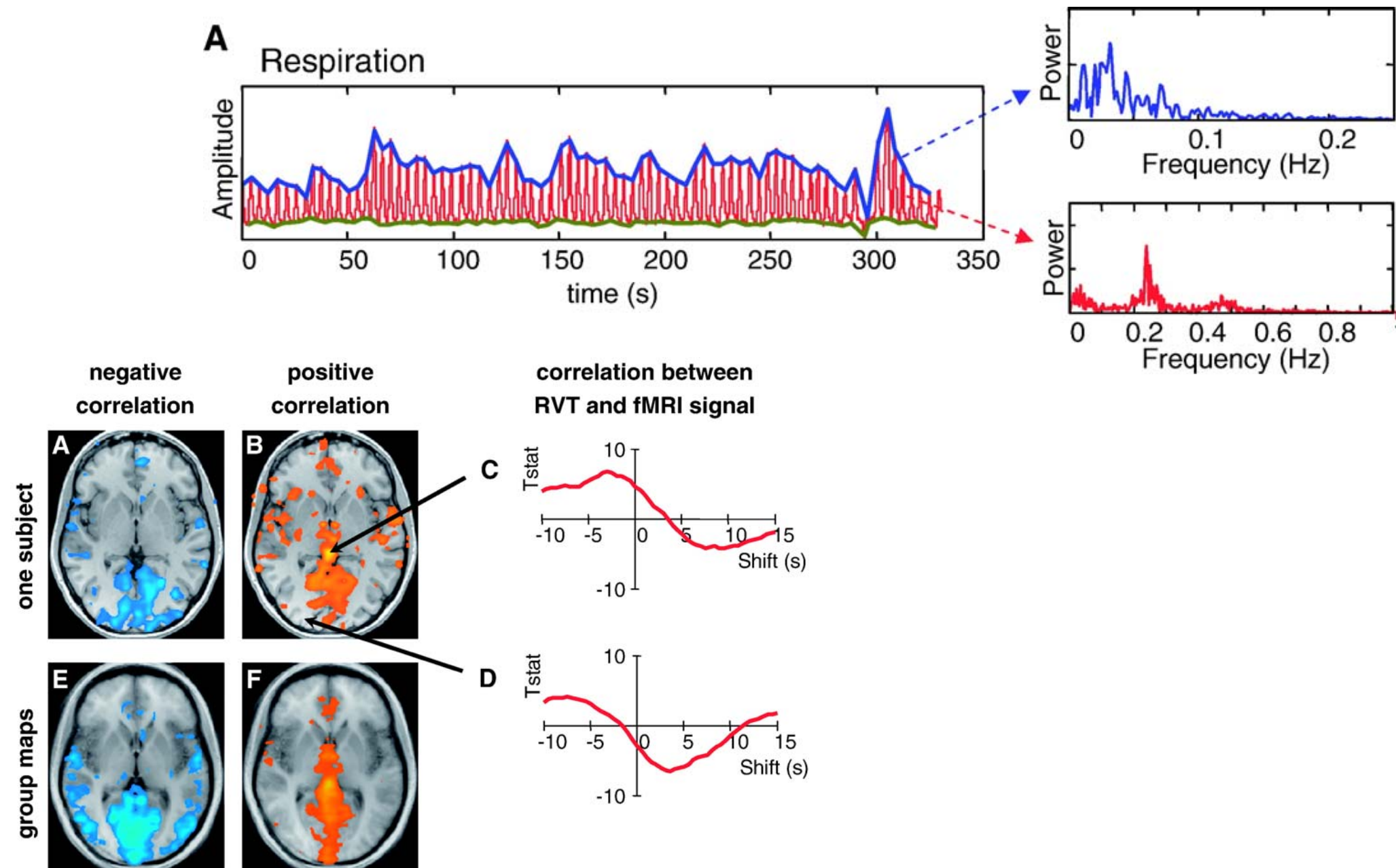


Constant Breathing



Low frequency fluctuations in respiratory volume (RVT)

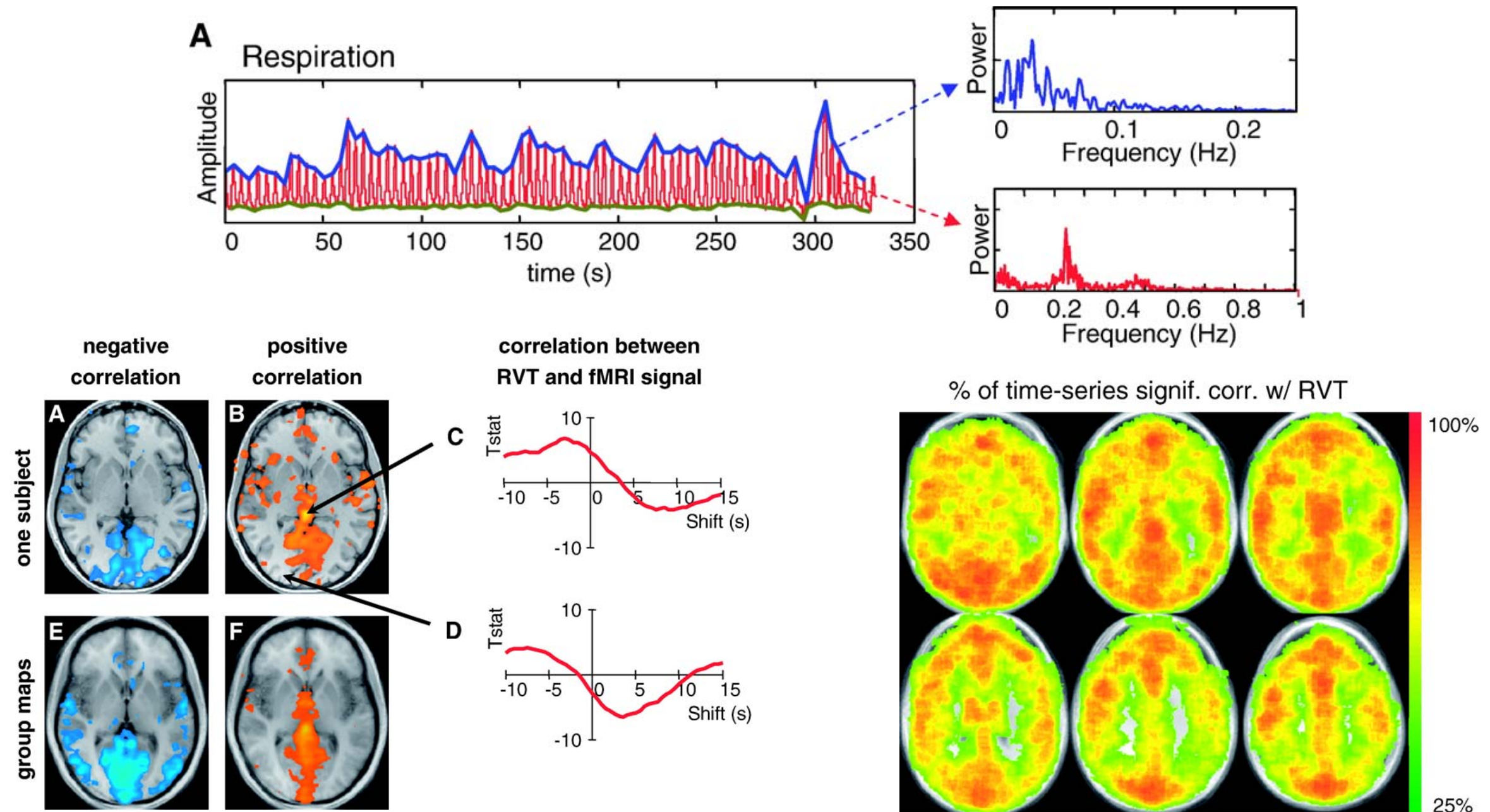
- The Respiratory Volume Time (RVT) is correlated with the average GM (or global) time series at multiple lags, and usually the two lagged RVT with maximum positive and negative correlation are used as nuisance regressors.



Birn et al. (2006). Separating respiratory-variation-related fluctuations from neuronal-activity-related fluctuations in fMRI. *Neuroimage* 31(4):1536–1548.

Low frequency fluctuations in respiratory volume (RVT)

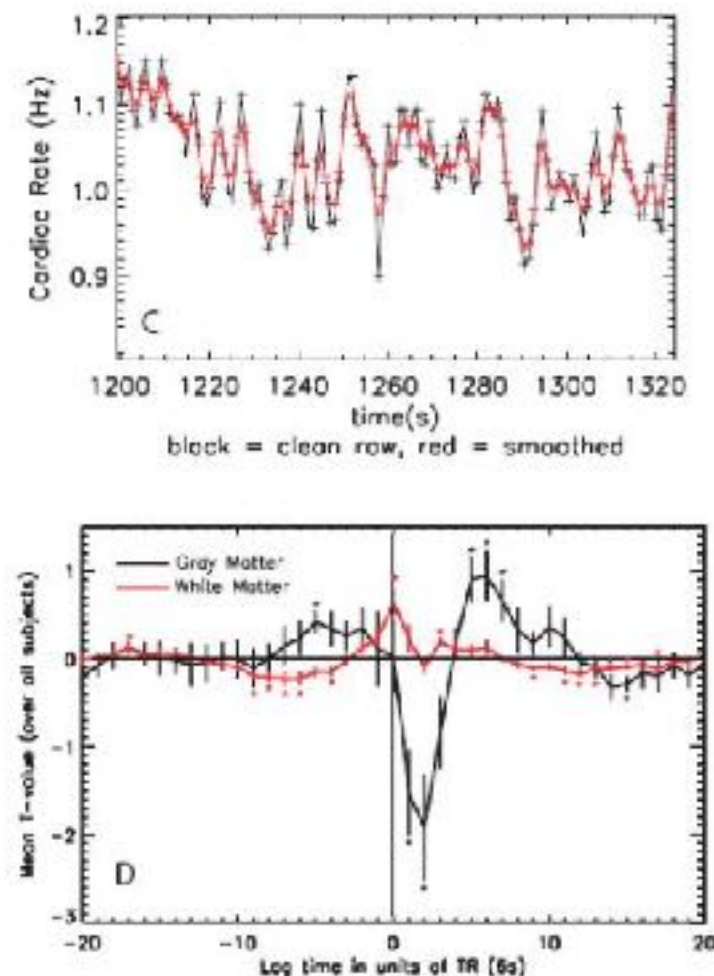
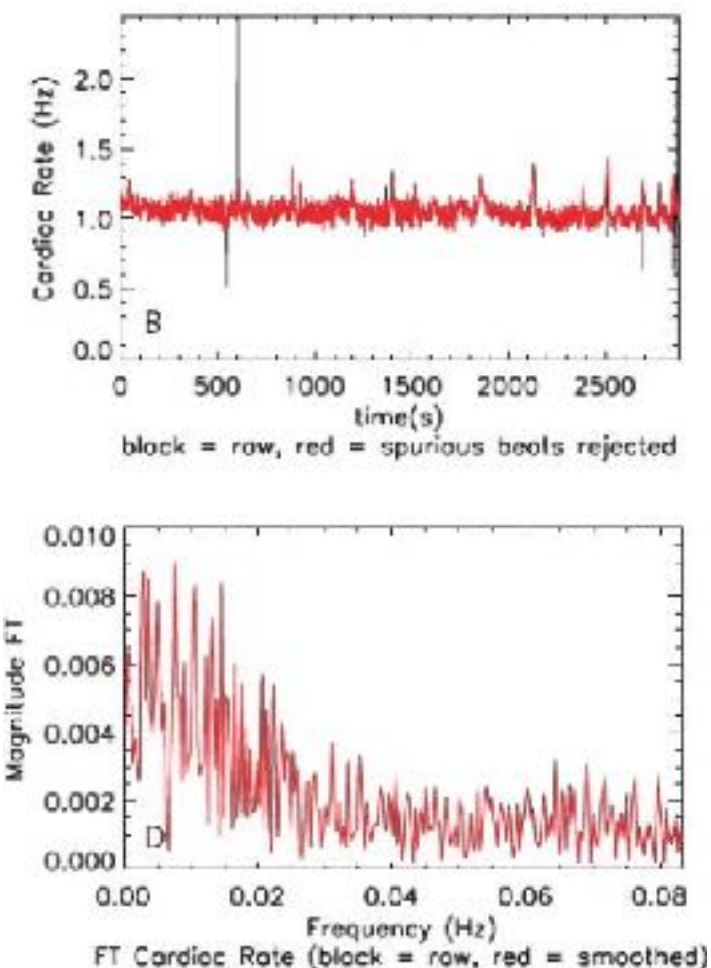
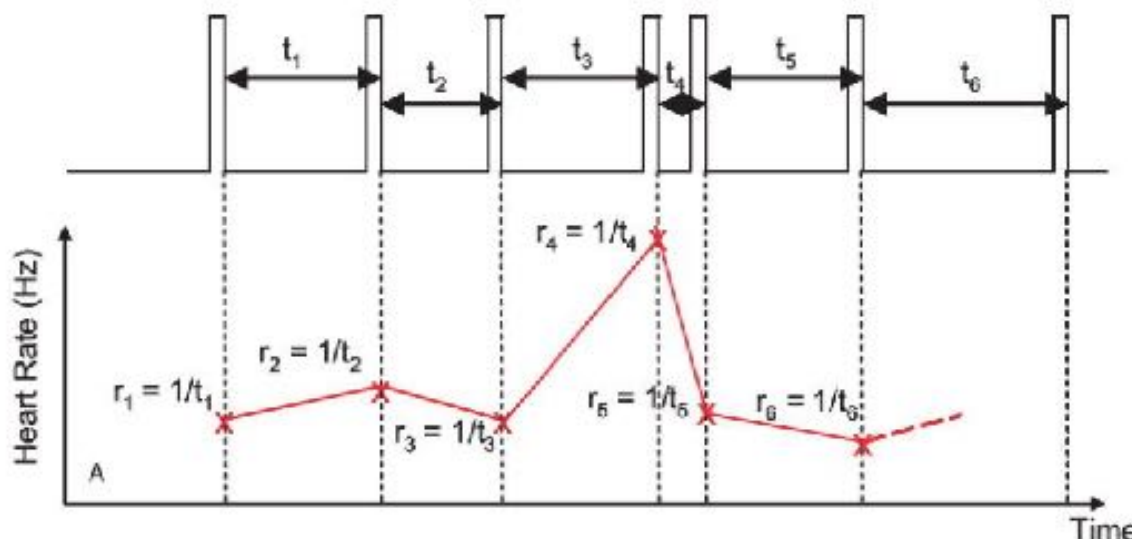
- The Respiratory Volume Time (RVT) is correlated with the average GM (or global) time series at multiple lags, and usually the two lagged RVT with maximum positive and negative correlation are used as nuisance regressors.



Birn et al. (2006). Separating respiratory-variation-related fluctuations from neuronal-activity-related fluctuations in fMRI. *Neuroimage* 31(4):1536–1548.

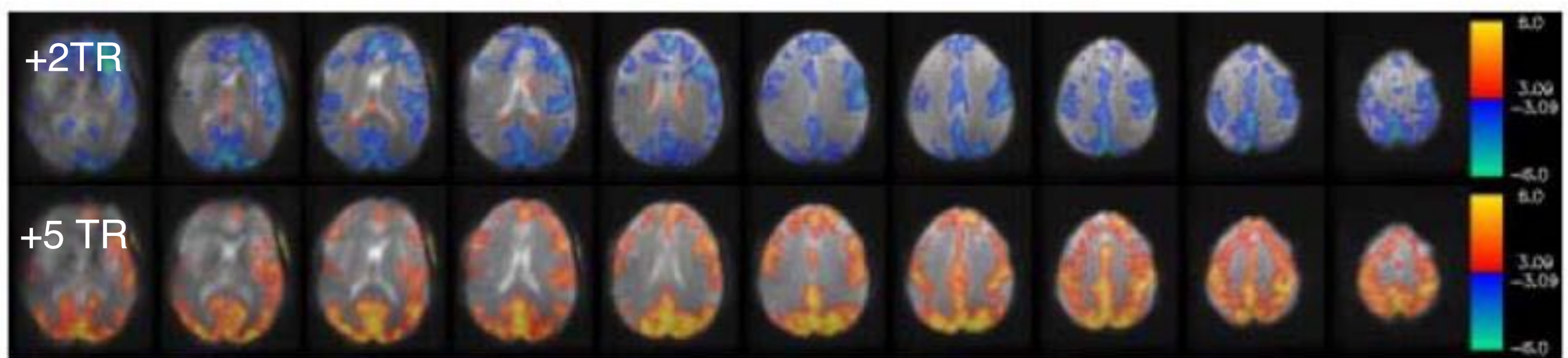
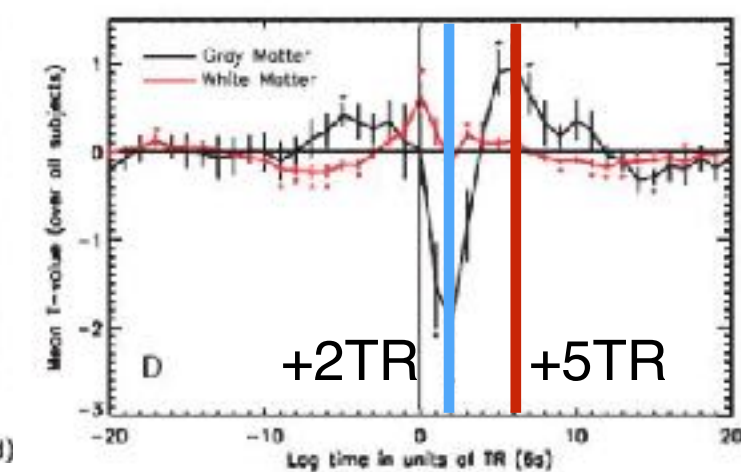
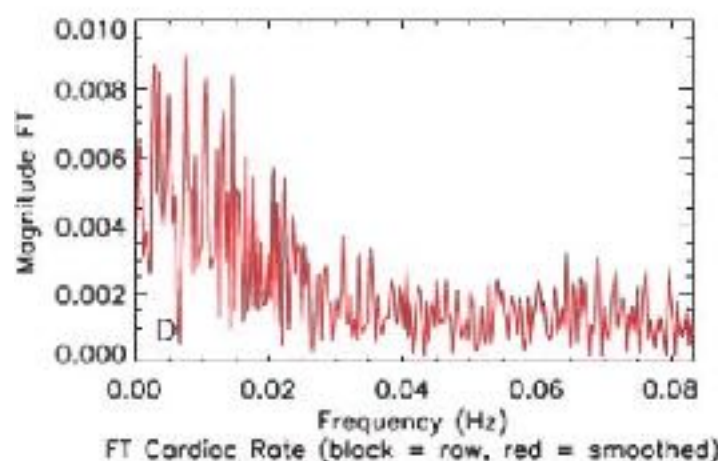
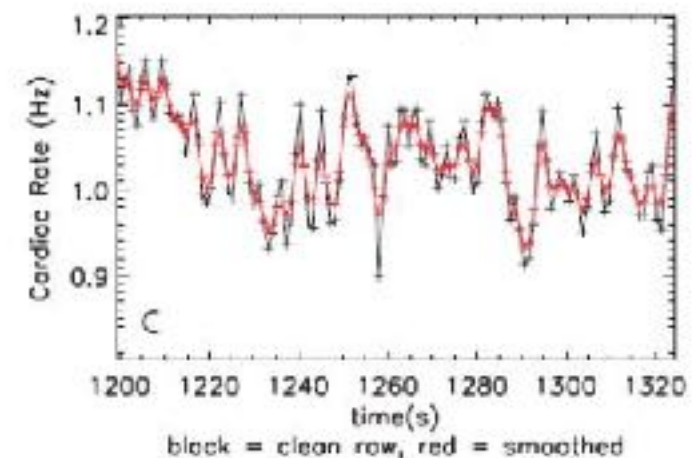
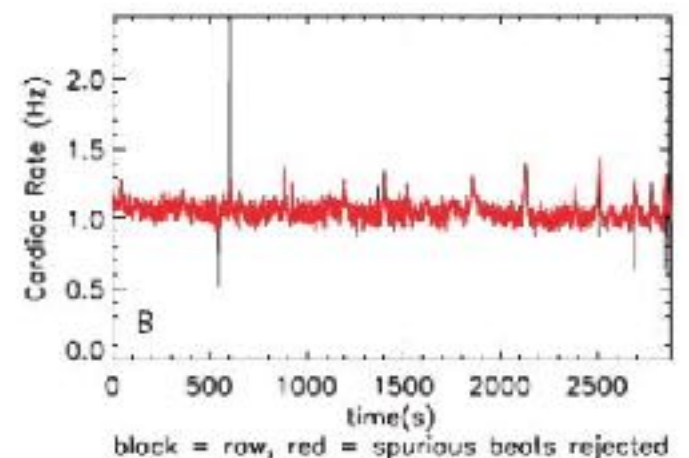
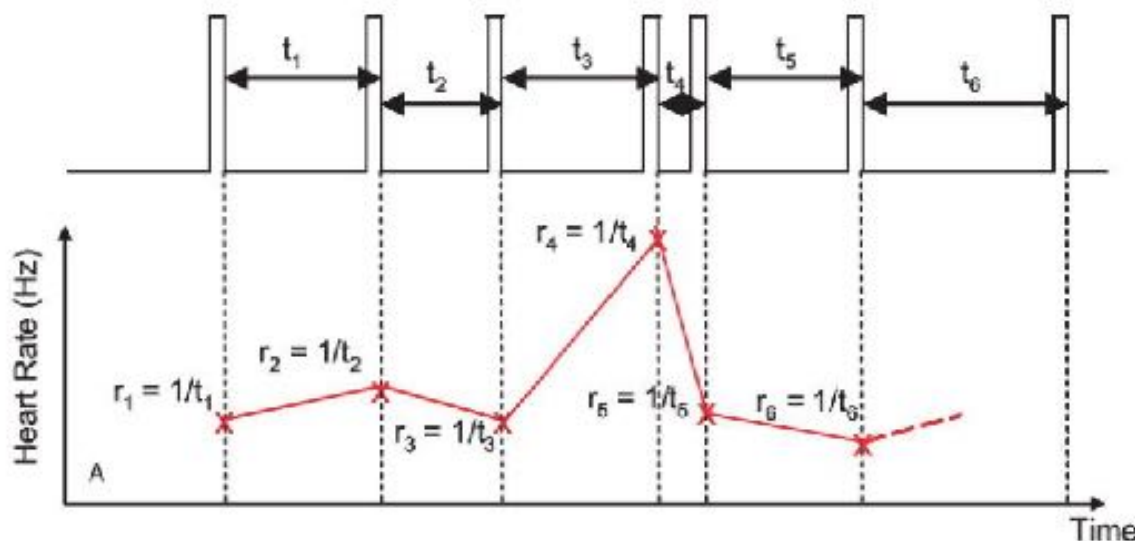
Low frequency fluctuations in cardiac rate (CR)

- Similar for variations in cardiac rate



Low frequency fluctuations in cardiac rate (CR)

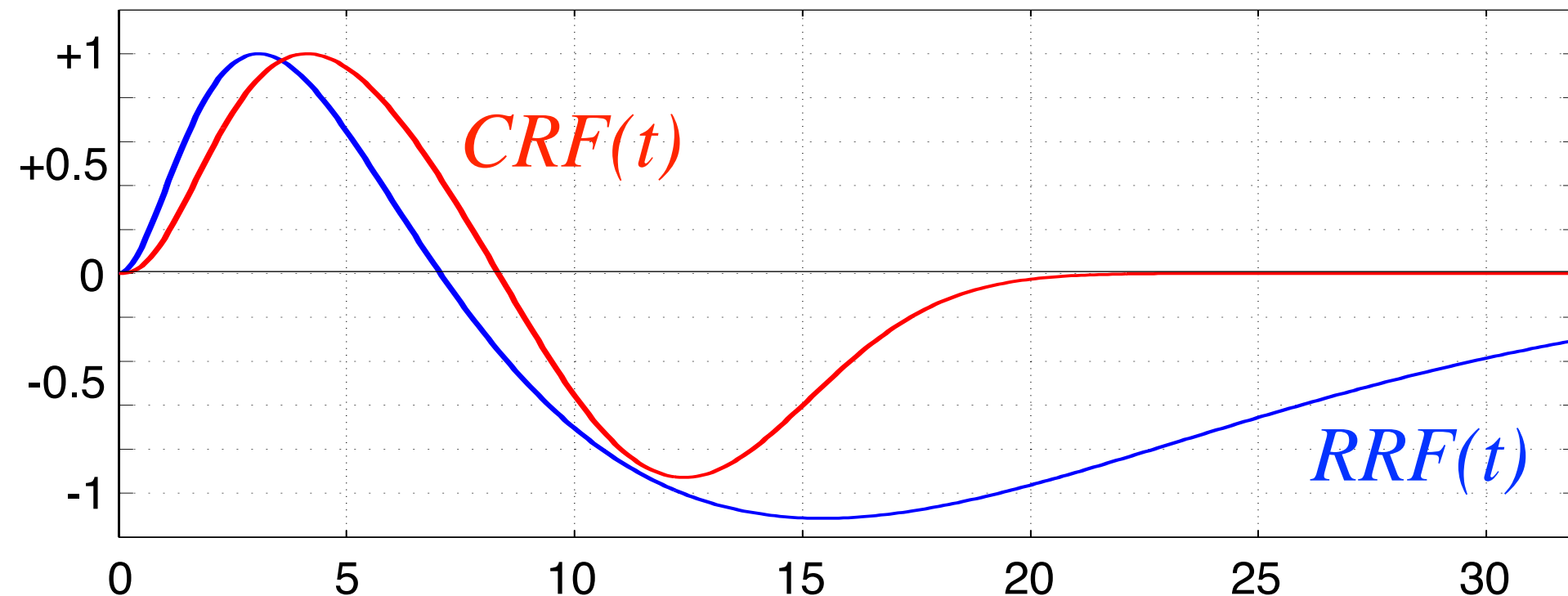
- Similar for variations in cardiac rate



Shmueli et al. (2007). Low frequency fluctuations in the cardiac rate as a source of variance in the resting state fMRI BOLD signal. Neuroimage 38(2):306-320.

Respiration and Cardiac Response Functions (RRF & CRF)

- Instead of fitting 2 lags of the respiratory volume (RV) and cardiac rate (CR) time series, deconvolve their responses from the fMRI signal.



$$RRF(t) = 0.6t^{2.1}e^{-t/1.6} - 0.0023t^{3.54}e^{-t/4.25}$$

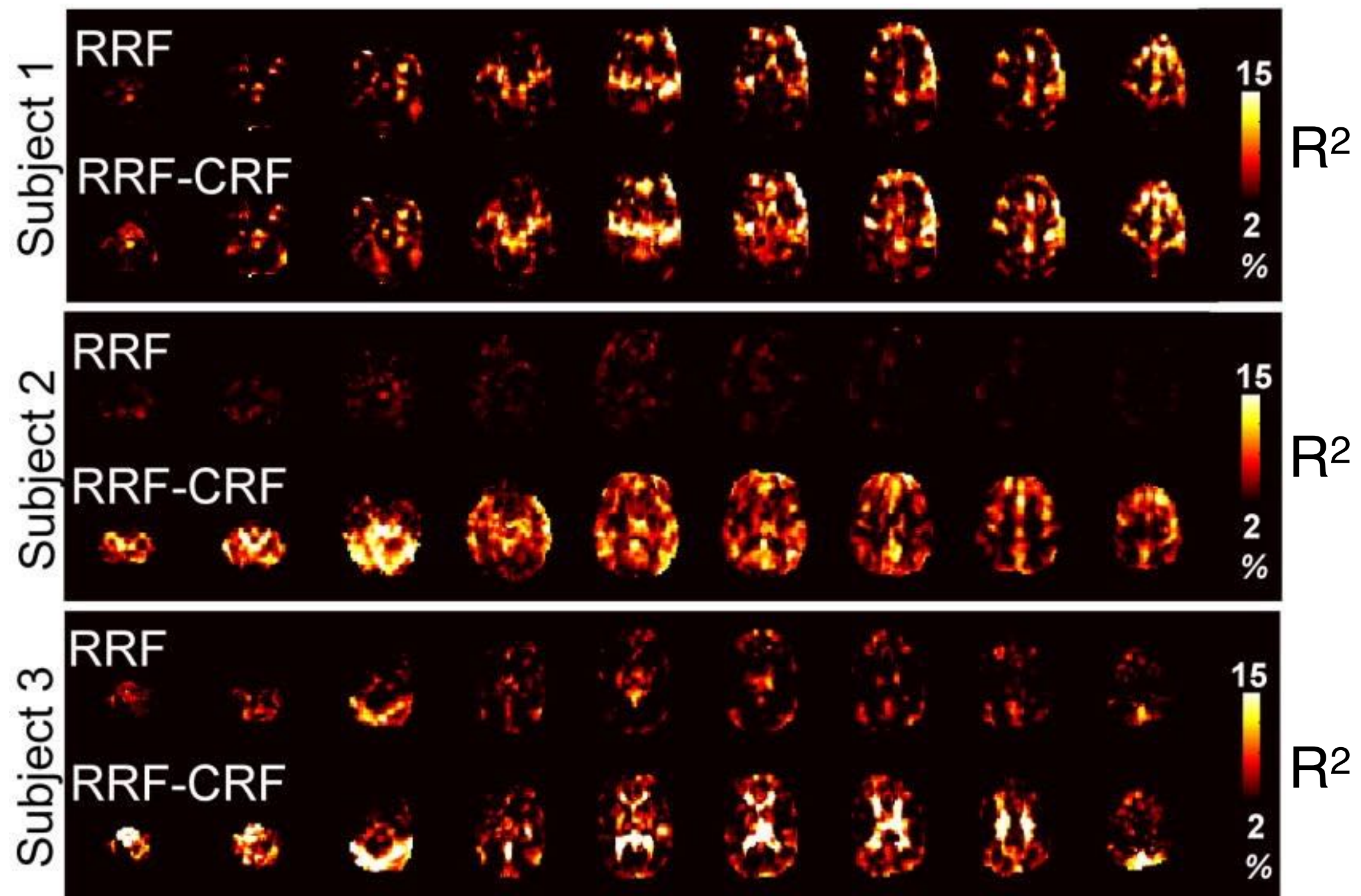
$$CRF(t) = 0.6t^{2.7}e^{-t/1.6} - \frac{16}{\sqrt{18\pi}}e^{-(t-12)^2/18}$$

$RRF(t)$ was initially estimated as the average response to brief breath-holding events

Birn et al. (2008). The Respiration Response Function: The temporal dynamics of fMRI signal fluctuations related to changes in respiration. Neuroimage 40(2):644-654.

Chang et al. (2009). Influence of heart rate on the BOLD signal: The cardiac response function. Neuroimage 44(3):857-869.

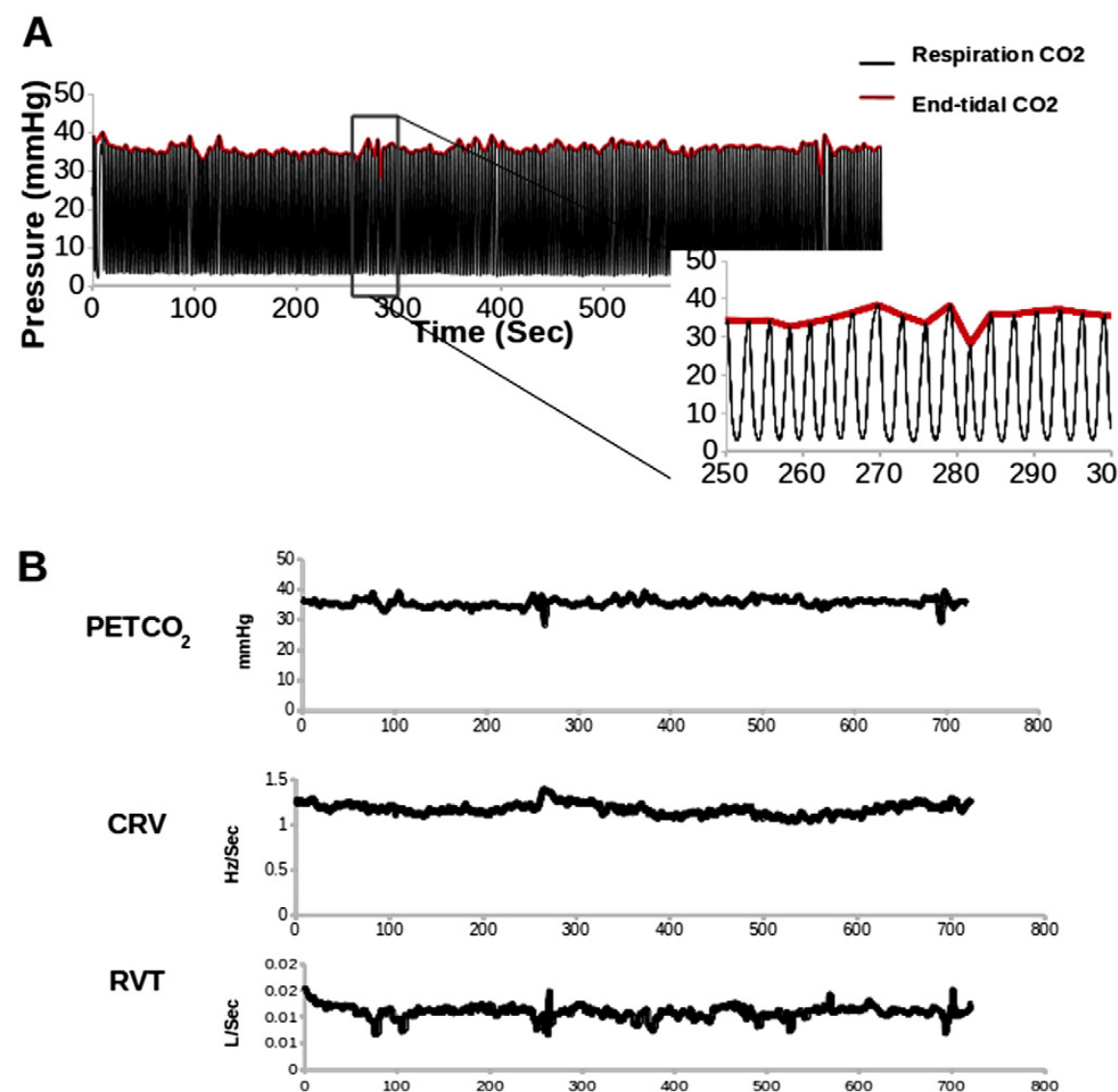
RVHRCOR: RVT^(*)RRF and CR^(*)CRF



Chang et al. (2009). Influence of heart rate on the BOLD signal: The cardiac response function. Neuroimage 44(3):857-869.

Modelling End-tidal CO₂ fluctuations

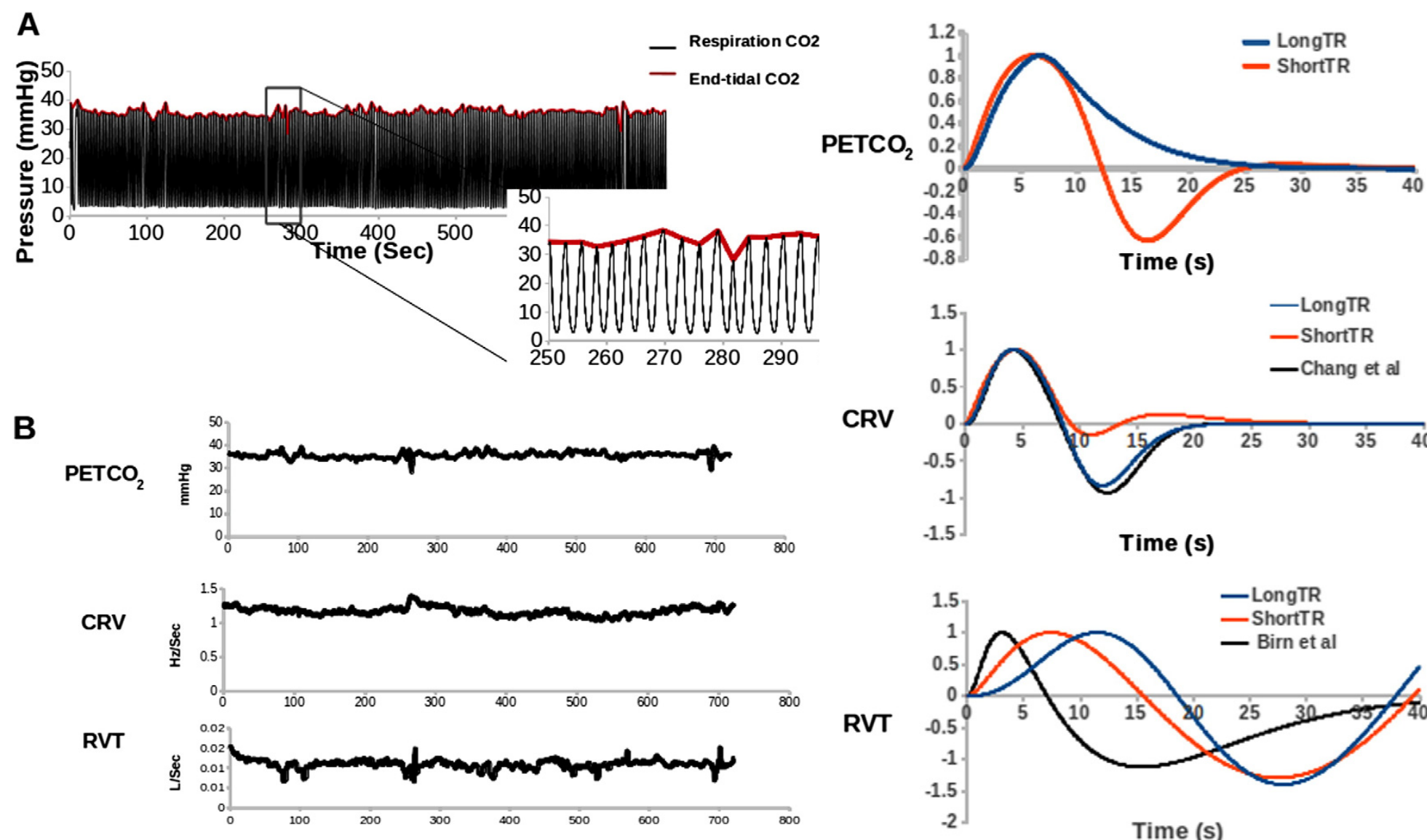
- End-tidal CO₂ (PetCO₂) measurements can also be recorded during fMRI experiments via a nasal cannula or face mask.



Golestani et al. (2015). Mapping the end-tidal CO₂ response function in the resting state BOLD fMRI signal: Spatial specificity, test-retest reliability and effect of fMRI sampling rate. Neuroimage 104:266-277.

Modelling End-tidal CO₂ fluctuations

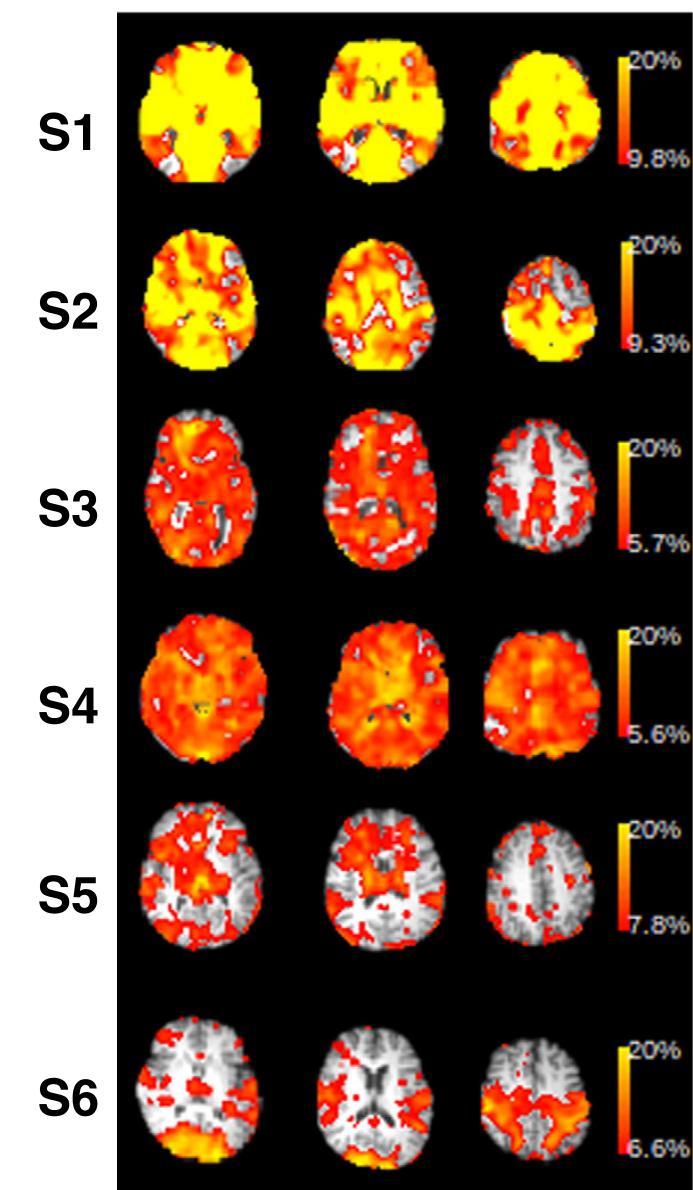
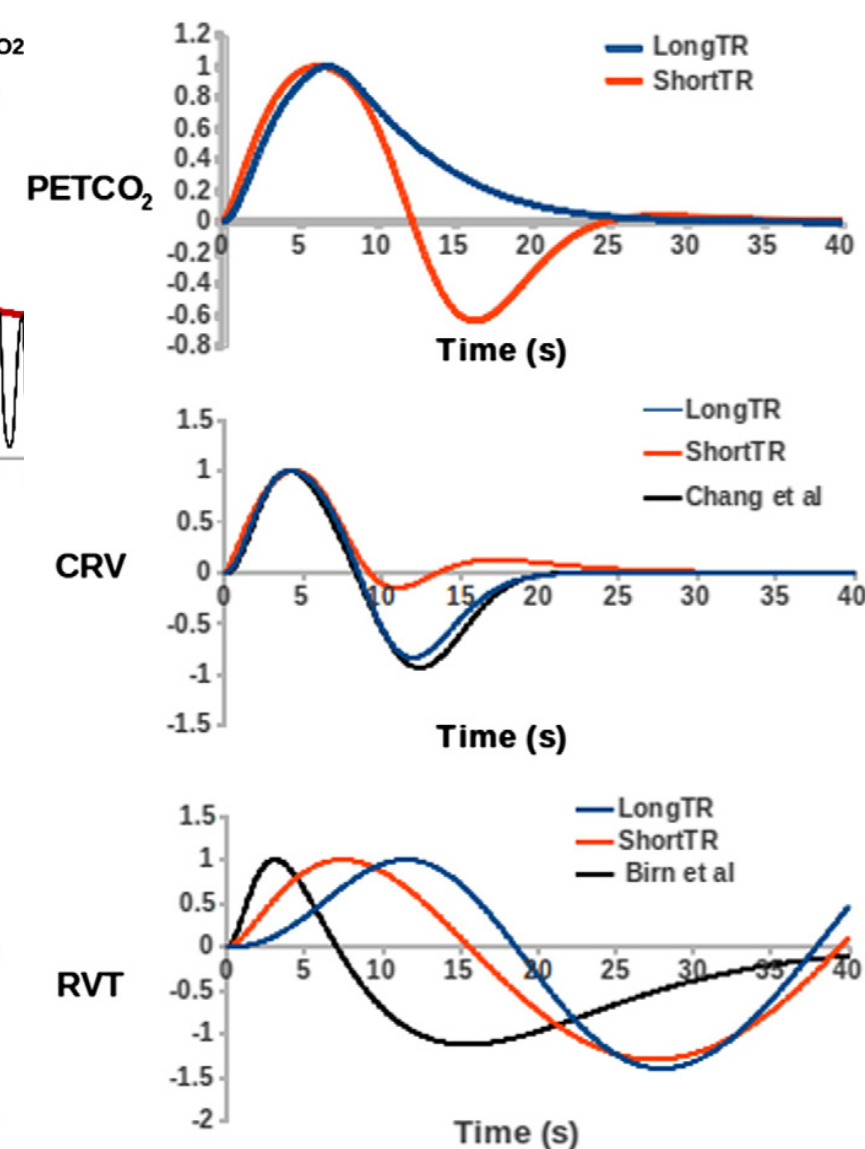
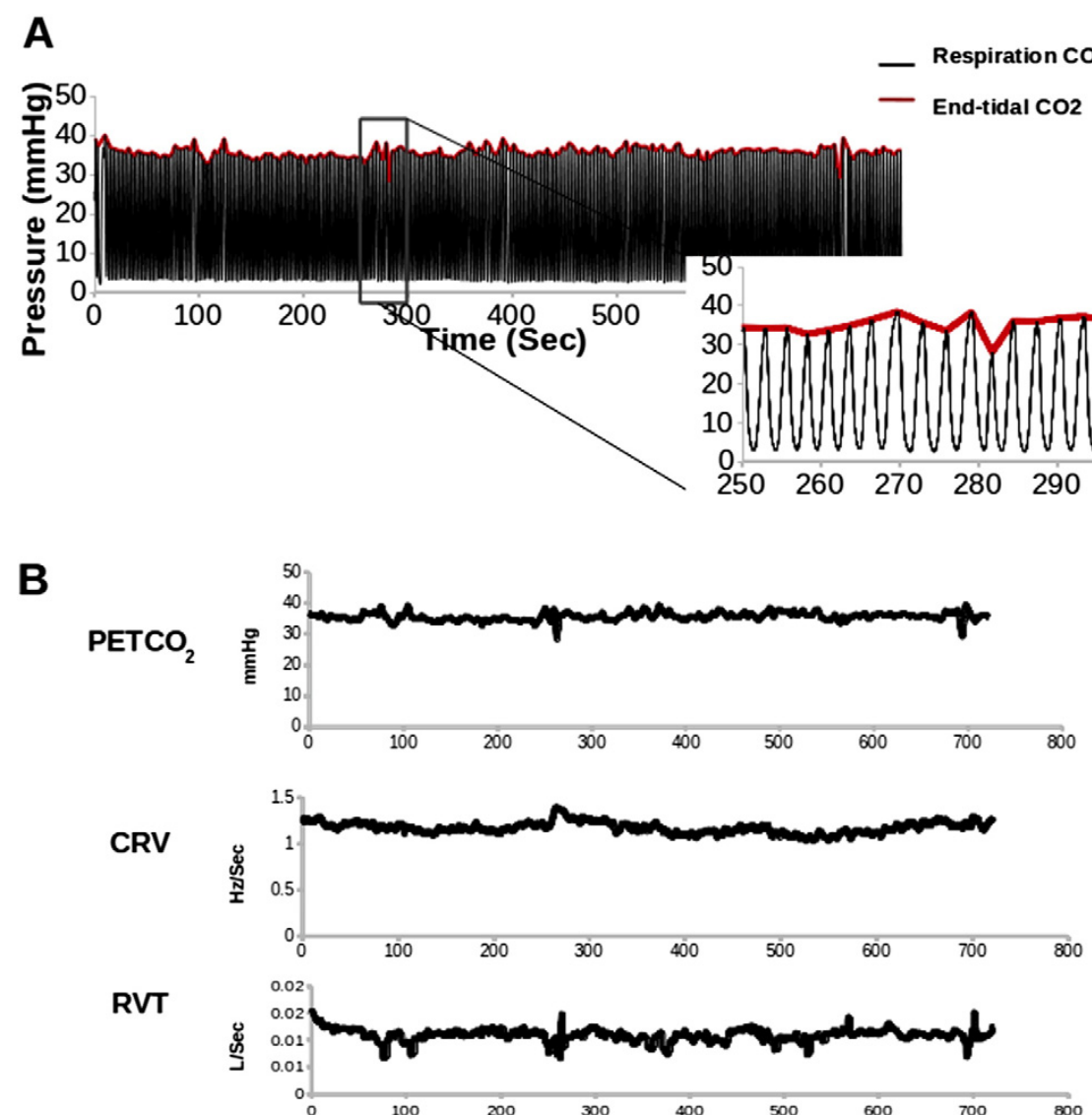
- End-tidal CO₂ (PetCO₂) measurements can also be recorded during fMRI experiments via a nasal cannula or face mask.
- The PetCO₂ response function can be estimated in similar fashion to the cardiac and respiratory response functions



Golestani et al. (2015). Mapping the end-tidal CO₂ response function in the resting state BOLD fMRI signal: Spatial specificity, test-retest reliability and effect of fMRI sampling rate. Neuroimage 104:266-277.

Modelling End-tidal CO₂ fluctuations

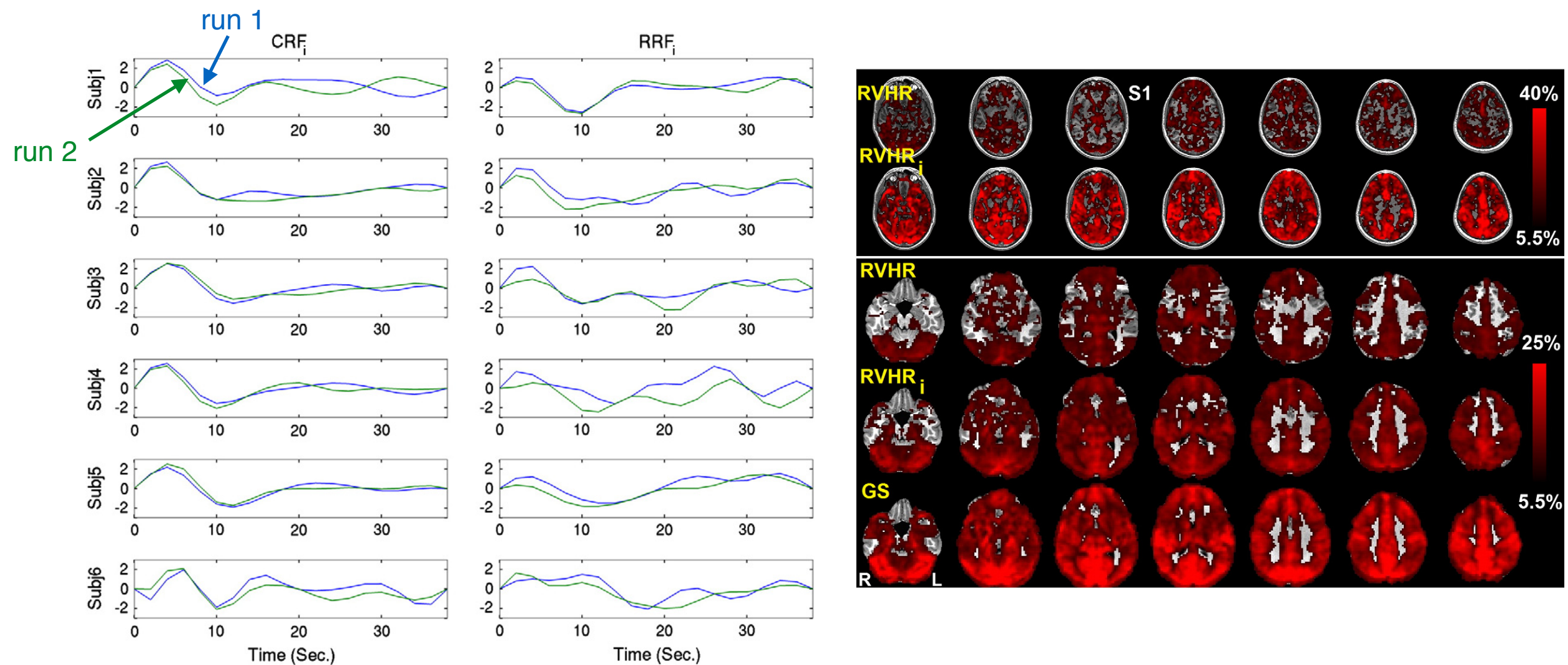
- End-tidal CO₂ (PetCO₂) measurements can also be recorded during fMRI experiments via a nasal cannula or face mask.
- The PetCO₂ response function can be estimated in similar fashion to the cardiac and respiratory response functions



Golestani et al. (2015). Mapping the end-tidal CO₂ response function in the resting state BOLD fMRI signal: Spatial specificity, test-retest reliability and effect of fMRI sampling rate. Neuroimage 104:266-277.

Subject-specific physiological response functions

- The RRF and CRF were computed as the average physiological responses across subjects; yet, utilizing these responses, however, does not warrant for intra-subject variations in physiological response, particularly for clinical cases.
- Derive the RRF and CRF from the global or average GM signal since we are in the physiological noise regime (thermal noise is averaged across voxels).



Falahpour et al. (2013). Subject specific BOLD fMRI respiratory and cardiac response functions obtained from global signal. Neuroimage 72:252-264.

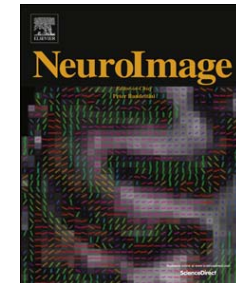
Take home message

- **fMRI is very noisy.** The BOLD effect due to neuronal activity is only 2-5% of the mean amplitude and the signal is corrupted by multiple noise components.
- **Denoising is critical for both task and resting state fMRI.** Numerous techniques are available for denoising the BOLD fMRI signal.
- Motion-related signal changes and physiological noise fluctuations are usually the main targets for denoising.
- There is no 'best' method for preprocessing and denoising, but there are incorrect methods.

Take home message

- **fMRI is very noisy.** The BOLD effect due to neuronal activity is only 2-5% of the mean amplitude and the signal is corrupted by multiple noise components.
- **Denoising is critical for both task and resting state fMRI.** Numerous techniques are available for denoising the BOLD fMRI signal.
- Motion-related signal changes and physiological noise fluctuations are usually the main targets for denoising.
- There is no 'best' method for preprocessing and denoising, but there are incorrect methods.

ALWAYS LOOK AT THE DATA!!
(BEFORE AND AFTER PREPROCESSING)



Methods for cleaning the BOLD fMRI signal

César Caballero-Gaudes^{a,*}, Richard C. Reynolds^b

^a Basque Center of Cognition, Brain and Language, San Sebastian, Spain

^b Scientific and Statistical Computing Core, National Institute of Mental Health, National Institutes of Health, Department of Health and Human Services, USA

ARTICLE INFO

Keywords:

BOLD fMRI
Denoising methods
Motion artifacts
Physiological noise
Multi-echo
Phase-based methods

ABSTRACT

Blood oxygen-level-dependent functional magnetic resonance imaging (BOLD fMRI) has rapidly become a popular technique for the investigation of brain function in healthy individuals, patients as well as in animal studies. However, the BOLD signal arises from a complex mixture of neuronal, metabolic and vascular processes, being therefore an indirect measure of neuronal activity, which is further severely corrupted by multiple non-neuronal fluctuations of instrumental, physiological or subject-specific origin. This review aims to provide a comprehensive summary of existing methods for cleaning the BOLD fMRI signal. The description is given from a methodological point of view, focusing on the operation of the different techniques in addition to pointing out the advantages and limitations in their application. Since motion-related and physiological noise fluctuations are two of the main noise components of the signal, techniques targeting their removal are primarily addressed, including both data-driven approaches and using external recordings. Data-driven approaches, which are less specific in the assumed model and can simultaneously reduce multiple noise fluctuations, are mainly based on data decomposition techniques such as principal and independent component analysis. Importantly, the usefulness of strategies that benefit from the information available in the phase component of the signal, or in multiple signal echoes is also highlighted. The use of global signal regression for denoising is also addressed. Finally, practical recommendations regarding the optimization of the preprocessing pipeline for the purpose of denoising and future venues of research are indicated. Through the review, we summarize the importance of signal denoising as an essential step in the analysis pipeline of task-based and resting state fMRI studies.

More than 300 references